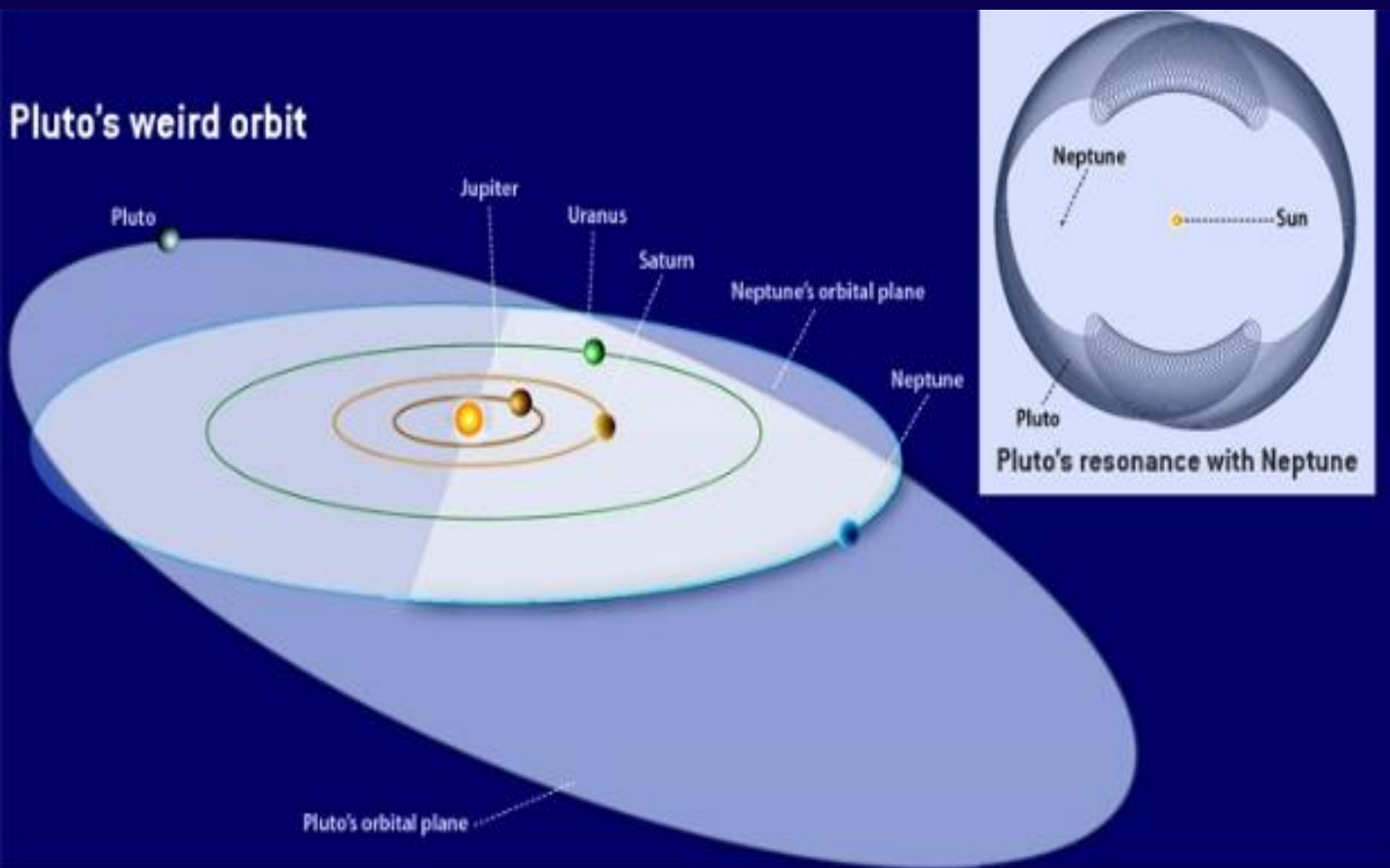


**ISSN 0970-5953**

**Volume 36. No. 4**

**October - December 2020**

# **PHYSICS EDUCATION**



**[www.physedu.in](http://www.physedu.in)**

**Volume 36, Number 4****In this Issue**

- ❖ **Solar System: A Historical Perspective and a Deeper Look** 11 Pages  
Shilpa Mehta
  - ❖ **Low-Cost Experiment to Measure the Speed of Light** 06 Pages  
Faraz Mehdi and Kiran M. Kolwankar
  - ❖ **Fractals in Leaves- An Interdisciplinary Project for Undergraduates** 11 Pages  
Nishanth P., Prasanth P., Reshma P and Udayanandan K. M.
  - ❖ **Learning Density Matrix with the help of Exercises** 10 Pages  
Reshma. P, Prasanth. P, Nishanth. P and K. M. Udayanandan
  - ❖ **Simulation of Vibrational Spectrum of Diatomic Molecules Using Morse Potential by Matrix Methods in Gnumeric Workheet** 15 Pages  
O.S.K.S Sastri, Aditi Sharma, Shikha Awasthi, Anil Kachi and Lalit Kumar
  - ❖ **Some Issues in Teaching Landau Diamagnetism** 10 Pages  
A. Reshma, B. Prasanth, C. Sreeraj and D. K. M. Udayanandan
  - ❖ **Designing of Digital Processing System Using ADS1115 and Arduinouno** 10 Pages  
Sreenath Nair, Snehal Vataliya, Devansh Desai and D. P. D. Lele
  - ❖ **Govind Swarup (1929 – 2020); The Dominant Force in Radio Astronomy in India Since Early Sixties.** 08 Pages  
V Balasubramanian and S Ananthakrishnan
-

---

# Solar System: A Historical Perspective and a Deeper Look

Dr. Shilpa Mehta

Professor, ECE, SoE  
Presidency University Bangalore, India

shilpamehta1.official@gmail.com,  
shilpamehta@presidencyuniversity.in

*Submitted 22-09-2020*

## Abstract

Almost every one of us has read the names of Solar System Planets in our school days. But we mostly stop there – we know them just as a series of names. In recent past, many space exploration agencies like the NASA, ESA, ISRO and others have sent numerous probes to study and understand our family of planets, and we are also looking for other galaxies, stars and exoplanets. In this review paper, I will concentrate on the planets in our solar system. We have big and small planets, Terrestrial planets, Ice Giants and Gas giants, the lost planets and the dwarf planets. Pluto, which was recently removed from our list of planets and demoted into being just a dwarf one, is one special case to be referred here. Giant Moons like the Ganymede are large enough to be called dwarf planets too. In this paper, we will try to understand the planets size, their atmosphere, the weather and seasons on various planets and the reason behind such variations, their Moons, and distances in our system. The paper will use images from NASA and other agencies which are in public domain for the sake of better understanding of what we are referring to. It aims at a little closer view into the members of the solar family of heavenly bodies.

---

Keywords: The Solar System, The Astronomical Unit, Ice giants, Gas Giants, Failed planet, Failed star, Trojans.

## 1. Introduction

Traditionally humans have been peering into space and wondering about the universe and the cosmos for many eons. The planets of the solar system till planet number six, viz. Saturn have been known for ages. The latest ones discovered by modern science after the advent of Galilean telescopes are Uranus and Neptune. While everyone knows about the names of our family of solar system planets, most are unaware of the intricacies of the latest findings by various probes sent out to space by various agencies. This paper is not about any new research, it just attempts to bring the planets closer into our perspective and know a little more about them than their names and their sequential positions in the system. After this paper, the reader will know a little more than the string of names of solar system planets. Let's take a Deeper look. This paper will use pictures and images which are available on the Web, with credits as available.

## 2. Literature Review – The Parameters of study

Before delving into each planet, let us tabulate the main points to begin our exploration. The first important parameter we consider here is the axial tilt, which causes the seasons on planets [1]

Table 1: Axial Tilt or Obliquity - The Angle between Rotational Axis and Orbital Axis

Courtesy Wikipedia

Body	Sun	Mercury	Venus	Earth	Moon**	Mars	Jupiter	Saturn	Uranus	Neptune	Pluto##
Axial tilt (degrees)	7.3	0.03	177.36 or -2.34	23.4	6.68	25.2	3.13	26.73	97.8 Or -82.2	28.32	122.53 Or -57.47

\*\* Moon refers to the Earth’s Moon – the body well observed by us in the night sky. It is not a planet but included for its interest

## Pluto has been recently removed from the list of planets as it does not satisfy criteria 3 [2] for planets, which is the clearing of its orbit

The tilt of the axis has a direct impact on the seasons of a heavenly body. The more the tilt, the more will the poles go into extremes. The above table shows two special cases of tilt – Uranus and Venus (actually Pluto also but Pluto is not considered a planet any more). When we discuss the particular planet, we will see the effects of these strange tilts.

Another important parameter for the study of a planet is the relation between the rotational and the orbital period. We will tabulate the data here and discuss the effects when we discuss the particular planet. As any planet or satellite rotates or spins on its axis, stars apparently move around its axis. The time taken by the stars to move apparently go around once is the *sidereal day* for the planet. Similarly, due to the same spin, the Sun also appears to go around the sky, and this is called the *synodic day*. The sidereal and synodic periods usually match but not always. [3] The negative sign for Venus, Uranus

and Pluto indicate that they spin in a *retrograde* direction, making it appear as if the Sun rises in the west and sets in the east. If a planet or Moon move in their orbit in the same direction their primary spins, then the *revolution* is *prograde*, else *retrograde*. Similarly if the spin direction is opposite to the direction of its orbit around its primary then the *spin* is said to be *retrograde*. [4] This happens when the axial tilt is between 90 and 180 degrees.

The distance from the Sun to Earth will be an important unit for us to be able to visualize the planetary distances. As we know, light takes about 8.32 minutes to reach the Earth from the Sun, the speed of light being about 300,000 Km per second. Hence, the distance of the sun is about 150 million Km from the Earth, and this distance is labelled as the *AU or Astronomical Unit*.

Table 2: Comparison of Sidereal and Synodic Rotation Periods (Values are approximate)

Body	Mercury	Venus	Earth	Moon**	Mars	Jupiter	Saturn	Uranus	Neptune	Pluto ##
Sidereal Period	58.6 Earth days	243 Earth days	23 hr 56 min	27.322 Earth days	1.04 Earth days	9 hrs. 55 min	About 10 hrs. 32 min	About 17 hrs. 14 min	About 16 hrs. 6.6 min	- 6 Earth days 9.17 hrs.
Synodic Period = Solar "Day"	175.9 Earth days	116.75 Earth days	24 hrs	29.53 Earth days	24 hrs. 39 min	9 hrs. 55 min	About 10 hrs. 32 min	About 17 hrs. 14 min	About 16 hrs. 6.6 min	- 6 Earth days 9 hrs. 17.0 min

Table 3: Orbital periods in the Solar System compared to Sidereal Rotation periods

Planet	Mercury	Venus	Earth	Mars	Jupiter	Saturn	Uranus	Neptune	Pluto
Rotation Period	58.6 Earth days	243 Earth days	0.99 Earth days	1.04 Earth days	0.41 Earth days	0.45 Earth days	0.72 Earth days	0.67 Earth days	6.39 Earth days
Revolution Period (sidereal)	87.97 Earth days	224.7 Earth days	365.26 Earth days	1.88 Earth years	11.86 Earth years	29.46 Earth years	84.01 Earth years	164.79 Earth years	248.59 Earth years

The orbital period defines the year on that planet, and the above table shows all planets' rotational and orbital periods [5] (even though rotational periods were already shown in table 2) are tabulated together because the two together decide the duration of time the one side of the planet will face towards/ away from the Sun.

Apart from these, the other factors of interest in planets study are the mass, radius, density, atmosphere chemicals, the prevalent temperature ranges, the escape velocity, and so on. The data can be found at a number of sources, one tabulation may be found on [6]

### 3. The Planets

The planets names and their sequence order are already well known, now we will look into some other interesting facts like, their Orbit, rotation, tilt, Seasons, Climate, and Weather and so on one by one.

#### 3.1 Mercury:

Mercury, which is the nearest planet to the Sun, and has been explored by multiple Earth agencies which are involved in space exploration. It is just 0.39 AU away from our Star (the Sun) and is a Sun scorched planet. The first probe which went there was the Mariner 10. It flew by Mercury thrice during 1974 and 1975 and mapped about half the surface. It also discovered the thin atmosphere there and detected a magnetic field. Later, the craft "Messenger" went into Mercury orbit in 2011, and completed mapping of the surface in 2013. Bepi Colombo is planned to enter orbit around Mercury in 2022. [7] Mercury has quite a strange day year cycle. It revolves around its orbit in about 88 Earth days, while it rotates about its axis in approximately 58 Earth days. So, about 176 Earth days is 2 sidereal years on Mercury and 174 Earth days is 3 mercurial days. What would be the effects of this? Well, for one thing, 3 days on Mercury is equivalent to 2 years there. [8] A very weird thing caused by this is that, even though the planet rotates once in 58 days, but due to the slow orbital speed, the actual Sunrise does not occur once per spin, because by the time the rotation gets

completed from the last Sunrise, the orbital position has shifted so much that the previously risen Sun has not still set. The actual Sunrise on the small planet happens only once in 180 Earth days, i.e. once in a mercurial year. Because of this special relation between the rotational and orbital periods, during the mercurial day, to a hypothetical observer on Mercury, the Sun apparently stops in the sky, retraces its path, and then moves on its normal east west direction. This retrograde motion is just an apparent one, the actual direction of spin is still the same, but for that duration the orbital speed exceeds the spin speed.

It is also the smallest planet in the solar system, slightly larger than our Earth Moon (excluding the demoted Pluto). It is a terrestrial one, with almost no atmosphere, and no Moons. Further, the surface is full of craters, as all the impacts craters are preserved on Mercury due to the extremely thin atmosphere. The side of the planet which faces the Sun (for a very long time indeed) gets superheated to about 430 degree Celsius, while the side facing away quickly cools down to a freezing minus 180 degrees Celsius. With these extremes in temperature, it appears impossible that Mercury could ever support life. One interesting fact about the name, both the metal Mercury and the Planet Mercury derive their names from The Messenger god Mercury from Mythology, Planet Mercury because it runs so fast and Element Mercury because at normal ranges of temperature on our Earth, the metal is liquid and runny. It is very dense, and the core is about 80% of its diameter, and 55% of its volume, and the outer shell including mantle and crust is hardly 450 miles thick. Its extremely thin mantle has been a point of great discussions. Some scientists propose the theory that long back Mercury either hit some huge object or was hit by another and the collision made it lose almost all its mantle. Another interesting fact is that the Sun appears 2.5 to 3 times larger there than on Earth, because it is so much nearer to the Sun. Mercury has a very strong magnetic field too.

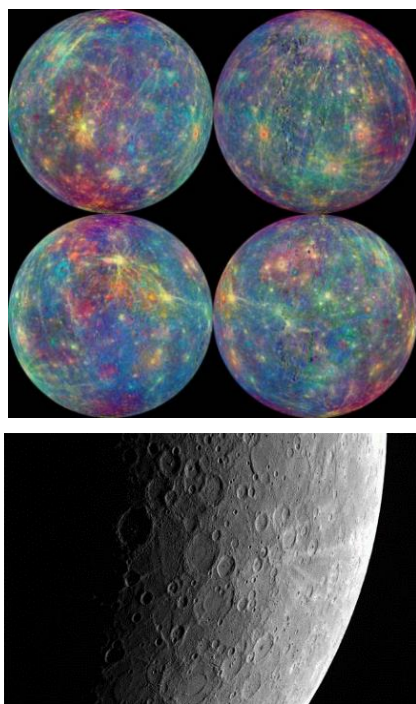


Figure 1: (a) Images of Mercury from NASA's MESSENGER craft (b) An image of Craters on Mercury (scaled)

<https://www.space.com/11952-latest-photos-Mercury-nasa-messenger-probe-part2.html>  
Courtesy space.com

### 3.2 Venus

Venus is named after the Roman Goddess, and is often called the evening star/ morning star. Being on an inner orbit than Earth, it never ventures too far from the Sun in our observations. Venus is also a terrestrial (rocky) planet and has the densest atmosphere among the four rocky ones – the atmospheric pressure on Venus is much higher than the pressure on Earth – which may be compared to the pressure a kilometer undersea on Earth. But the atmosphere is 96% Carbon Dioxide (also known as the greenhouse gas) and hence Venus is like a furnace, its mean temperatures are around 500 degree centigrade. Plans for sending crafts there are hindered by the hostile environment there. It rains Sulphuric acid there (though the rain vaporizes in the intense heat long before it hits the surface), so a likely visitor wishing to see the “Goddess of Beauty” (the name implies this) can take a pick between burning by the high temperature and acid rain, or getting crushed to death by the extreme pressures!

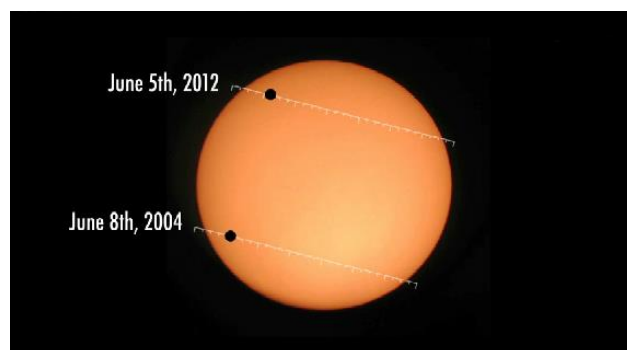
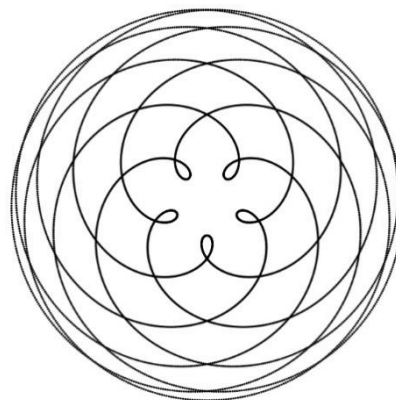


Figure 2: (a) The Pentagram of the Venus (b) The transit of Venus across the Sun in 2004 and 2012

Venus has an axial tilt of almost 180 degree – that means its rotation (spin direction) appears to be opposite to other sister planets, and its rotation is extremely slow. It takes about 243 days to complete one retrograde rotation (i.e. opposite to the Sun spin, and apparently the Sun rises in the west and sets in the east) while it takes about 224 days to orbit around the Sun. This means the year is shorter than the day there. Because of this ratio of Earth orbital period to Venusian orbital period, it takes about 13 apparent rounds of Earth while the Sun makes about 8 rounds if an imaginary observer looks down at the solar system from the top keeping Earth stationary. It traces a beautiful path called the pentagram of Venus [9] as shown in figure 3 below. The Venus eclipses the Sun similar to the Moon eclipsing the Sun, but being so far away, it appears like a tiny dot on the huge star in the background.

### 3.3 Our Earth and Earth's Moon

As we are almost all aware of the general information about the Earth, I will not say anything about our home planet here. We

already know our rotational and orbital periods, our tilt, seasons, atmosphere and mean temperatures etc. I would only say this - Earth and Venus were twins, and then Venus became hell with the Carbon Di Oxide mounting in the atmosphere. Our environmentalists are begging us to reduce Carbon Di Oxide emissions, let us not wait till we turn into Venus. Our Moon is believed to have broken away from Earth itself after a giant impact, whereby the debris thrown into space slowly coalesced together to form the Moon. The Moon is tidally locked to Earth, in the sense, it's rotational and revolution periods are same, hence the same face of the Moon is always visible from the Earth, while the other side always faces away from us. Hence we see only one side of the Moon. The below image shows Earth rise as seen from our Moon.



Figure 3: Earthrise pictures from the Moon: Earth shows similar growing and decreasing phases on Moon as Moon shows from the Earth: Courtesy Apollo 8 Images from NASA and Japanese Kaguya spacecraft

### 3.4 Mars

The red planet is the last one among the terrestrials in the solar family. It is followed by the rocky *asteroid belt*. Numerous probes have been sent to Mars, including Mariner 4 and Viking. Evidence of liquid water flows in earlier eons has been found and the polar caps on Mars still have water ice. The planet appears reddish due to the presence of iron Oxide on its surface. Olympus Mons with a height of about 21 to 27 Km towers high and is assumed to be the tallest in the planets in the Solar system (By comparison our own Mt Everest is under 9 Km above sea level) (Actually Rheasilvia on the

asteroid Vesta is bigger, but we are counting planets only).

Mars has the most Earth like seasons among all terrestrial planets. It has two known well known Moons, Phobos and Deimos, but apart from these Moons, it hosts multiple Mars Trojan which are captured asteroids that apparently orbit Mars like a Moon. (In fact our own Earth also sports at least one Earth *Trojan* though most people are unaware of it) Mars lost its Magnetosphere about 4 billion years ago, and as a result solar winds pull away the atoms from the atmosphere and its atmosphere is extremely thin, the pressure being about 1% of Earth. Martian temperatures range from about -143 to +30 degree Celsius.

Mars is followed by the asteroid belt, which has small and large bodies of irregular shape orbiting the Sun between the orbits of Mars and Jupiter. The asteroids in the belt are assumed to be a failed planet. Scientists are of the opinion that, left alone it might have formed a planet. But the mighty gravity of the Gas Giant Jupiter did not allow it to coalesce into a planet.

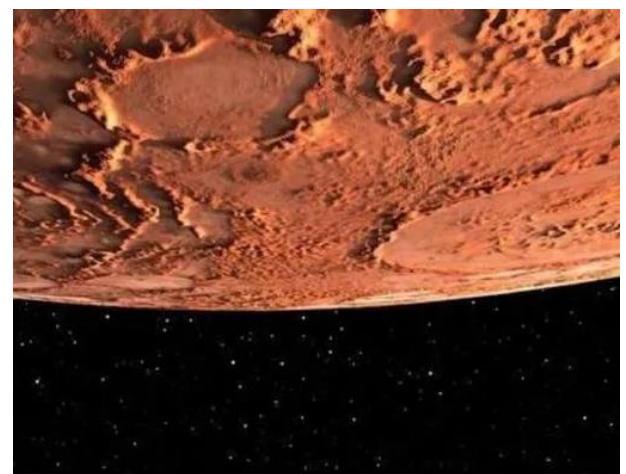
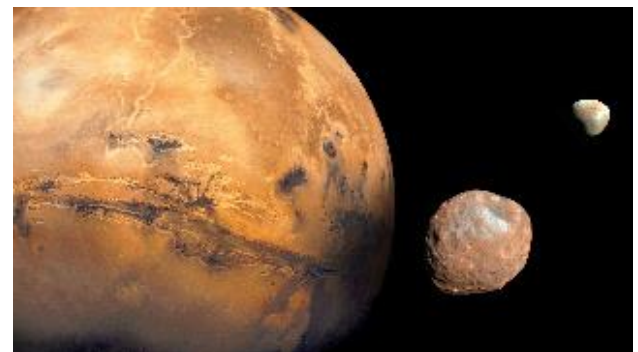


Figure 4: Mars and its Moons

### 3.5 Jupiter

Jupiter is the “Big Brother” in the solar system. While the Sun encases 99% of the total mass in the solar system, Jupiter dominates the planets by a huge margin. It is the first gas giant, as the first 4 planets are rocky ones. Pioneer 10 was the first craft visiting there. It was the first to tell us that Jupiter’s magnetic tail itself is nearly 800 million Km long. Jupiter is so huge that it could host about 1300 Earths inside it. And it is so massive that its mass is more than twice that of all other planets combined mass. If it was 80 times more massive, it would have been a star – in fact sometimes Jupiter is called the failed star. It is aptly named after the Greek God Zeus. [10] The gravity there is twice that on Earth, so if one weighs 50 of any standard units here, we will be 100 same units there.

It hosts 79 satellites but notable among them are 4 large Moons - viz. Io, Europa, Ganymede and Callisto. These Moons were the first of the heavenly bodies seen orbiting anything other than the Earth, and gave support to the Copernicun theory that everything does not go around the Earth. Ganymede is even larger than Mercury and Pluto. Io is tidally locked to Jupiter (just like our own Moon to Earth) and hence shows only one face to Jupiter, and it is the most volcanically active body in our system. Europa is highly reflective and has a very smooth surface as it is water ice. It is believed that below this frozen surface huge oceans of liquid water exist, and exploration missions are planned to find out if they hide life. Jupiter also sports at least 3 rings. Its atmosphere is mostly Hydrogen and it has the strongest magnetic fields in the solar system, much stronger than Earth, and it has radiations strong enough to damage even heavily shielded probes and space-crafts. Despite its giant size, it spins so fast that it completes one rotation in about 10 hours. But the year is much longer, about 12 Earth years. But the axis is almost perpendicular to the orbital plane (tilts just 3.5degrees) so there is hardly any seasonal variation. The most well-known feature of Jupiter is its Giant Red Spot which is actually an anticyclone raging on Jupiter from centuries.

The red spot itself is so wide that about 3 Earths would disappear into it side by side. It is believed that the core is almost nonexistent, the giant planet has 90% Hydrogen and 90% Helium, just like a young star.

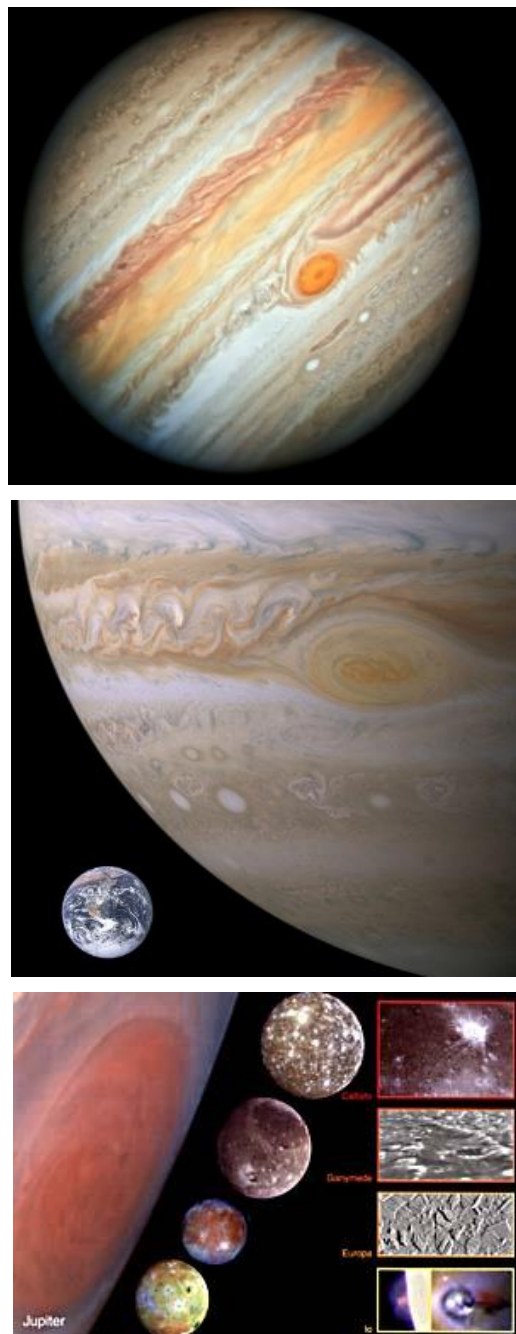


Figure 5 (a) Jupiter (b) The size of Earth compared to the Giant Red Spot on Jupiter (c) The size of the four largest Moons of Jupiter compared to its Red Spot

### 3.6 Saturn

Saturn is an absolutely fascinating sight in the night time sky. A gas giant like Jupiter, its size

is second to only Jupiter in our system. It has 9 times the Earth's diameter (i.e. the volume will be about 729 times of Earth) but it is only 95 times as massive as us. Hence the density is very low, in fact it has such a low density that if there was a big enough bathtub filled with water, Saturn would float in water due to low density. Winds of up to 1800 Kmph rage there. It is the king of Moons, with 82 established ones, of which Titan has a real atmosphere. Once again has a maximal concentration of Hydrogen (96.3%) and Helium (~3.5%), though it has some ammonia, methane, and ethane also. The North Pole has a fascinating hexagonal pattern, while the South Pole has a vortex – the eye of a storm. It allows us a window to look inside to a certain depth within the atmosphere. Notably, Saturn has the most spectacular system of rings among all planets. The Cassini orbiter captured beautiful view of the rings and sent it to enthral us. The rings extend from 6630 to 120700 kilometers outwards from the equator, but are extremely thin. The average thickness is about 20 meters, which may be about as tall as a double storied house around us – which will be sharper than a razor blade if we scale down a model of Saturn to the size of a football. The Phoebe ring travels retrograde around the planet, along with the Moon with the same name. [11] Smaller Moons act like shepherds, not allowing the rings to fizzle inwards or outwards. Planets till Saturn are observable even without powerful telescopes, so planets till Saturn were already well known to various cultures and find a place in mythological literature of almost all ancient civilizations.

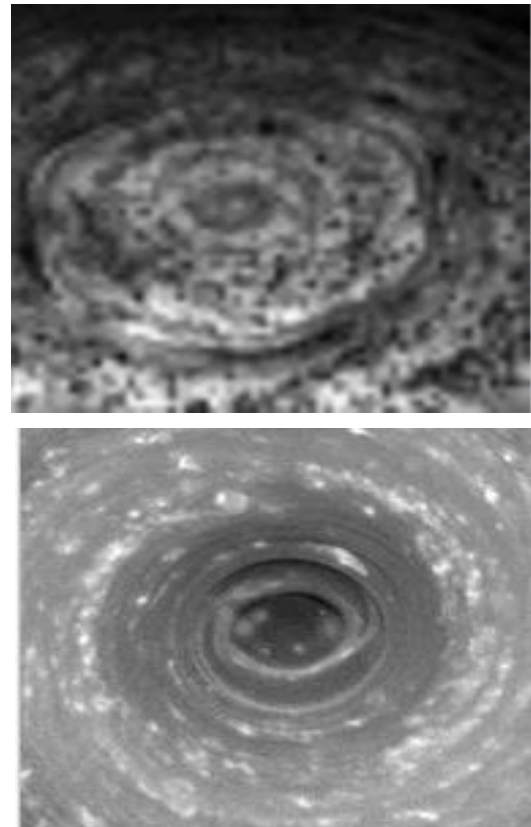


Figure 6 (a) Saturn shadow on its rings captured by the Cassini (b) The hexagonal pattern on North Pole of Saturn (c) The “EYE” or vortex on the South Pole

### 3.7 Uranus

Uranus is a relatively recent discovery, being the first of the ice giants. After the era of Galilean telescopes, these far off planets could be closely observed by humans, which are not mentioned in early literatures. It can actually be seen without telescopes also, but even though it was known earlier, it was mistaken to be a distant star because of its dimness and slow orbit. William Herschel, a British astronomer is believed to have first realized that it is not a star (in 1781), and he actually named it after the King George the III, but the tradition of naming planets after Greek and Roman gods prevailed and it was finally renamed as Uranus. [12, 13] Uranus has a dramatic tilt, and its axis almost points at the Sun. While all other planets spin like tops on their orbital planes, Uranus appears to roll on its side. It has a tilt of about 98 degrees, so that the poles face the overhead Sun for almost half its orbital period, and away from the Sun for the other half. [14] On our Earth,

the equator gets overhead Sun, while poles receive slanting Sun. Equator on Uranus receives slanting Sunrays, even though at those distances the Sun is a tiny light in the sky, not like the Sun we see from Earth. And the orbital period is huge (about 84 Earth years), so the seasons (due to the tilt) are extreme seasons. So huge is the variation, that when Voyager 2 photographed it in 1986 (it was a Uranus winter when observed), it was dubbed as the “most boring and sluggish planet” compared to Neptune with its raging storms. But when the 2014 missions saw the summer storms there and it was unbelievable that there could be so much contrast in the two images generated. But the rotation period is quite short, just about 17 hours. It has 27 known Moons and 13 known rings. The rings are also on the side along the equator, which is the reason Scientists believe that the strange tilt could not have been caused by a single giant hit (which would have left the ring system separated from the equatorial plane) but by more than one smaller hits. It appears blue green in the night sky due to atmospheric Methane, Hydrogen and Helium rich atmosphere.

### 3.8 Neptune

Neptune was found after Uranus, The story of its recognition is quite interesting. It was actually discovered twice, but not labeled correctly as a planet the first time around. When telescopes were made, far off planets came into our view. In fact Mr. Galileo Galilei is believed to have observed and noted it in his notes, but as it moves so slowly relative to Earth, he believed it to be a star. Due to its little observable movement, he thought it is a faint star nearby compared to others so that it apparently shifts. Galileo was then (1612 and 1613) observing the four large then known Moons of Jupiter. He recorded a nearby faint star, not present in any modern catalogues. [15] Unfortunately for him, he did not note down or recognize or declare it as a planet, he thought it was a star. The realization that it is a planet came much later.

Uranus as studied in the previous section is a giant, though earlier thought of as a sleepy

drowsy one. When human observers started studying Uranus, various observatories started tracking its theoretical and practical orbits. It was soon observed that a lot of deviation from the expected path as per Newton’s laws of gravity (as per the then known bodies) was present. Some bright minds realized the possibility of hitherto unknown planet and mathematical work indicated the mass, position and orbit. Urbain Le Verrier discovered it with his pen on paper, he predicted exactly where it would be based on mathematics, and telescopic observations at the Berlin Observatory confirmed the existence on September 23–24, 1846. The actual “seeing” was done by Johann Gottfried Galle who was assisted by Heinrich Louis d'Arrest, working from Verrier's calculations. [16], [17]

Neptune and Uranus both are ice giants, though Neptune is much larger. It is 4 times the diameter of Earth, and applying the cubed volumes, about 64 Earths can be fitted into it, but still it rotates once in about 16 hours. The distance from the Sun is a whopping 4.5 billion kilometers, the orbital period is much larger – about 165 Earth years. It is believed to have a small rocky core while the fluid mass is mostly methane, ammonia and water. The atmosphere has mostly Hydrogen, Helium and Methane. It has 14 known Moons and 5 known faint rings. It is the windiest of our system, typical wind speeds of 2000kmph are assumed to be common. (The most powerful and devastating storms of Earth have seen peak winds of about 400kmph for a comparison) The average temperature is taken to be about -214 degrees Celsius. Just like Jupiter’s red spot, Neptune also has a lingering storm - giant dark spot roughly the size of Earth. It radiates out much more energy than it receives from the Sun. Some scientists believe and state that it may rain diamonds on both Uranus and Neptune, as the super pressures would extract carbon from methane and crush it into diamonds.

There is one notable thing about Triton - the largest among the Moons of Neptune – it orbits Neptune in a retrograde fashion, implying it travels in a direction opposite to Neptune’s spin. This has caused lots of space conspiracy

theories and science fiction movies – saying Triton [18] is not actually a Moon but is an alien spaceship in orbit to study the solar system for some alien civilizations. Scientists feel that it is actually a Kuiper belt object which was somehow captured by the gravity of Neptune in one of its near passes.

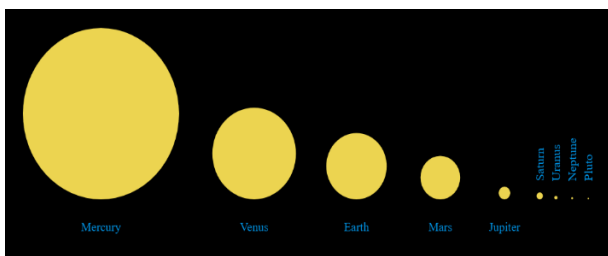
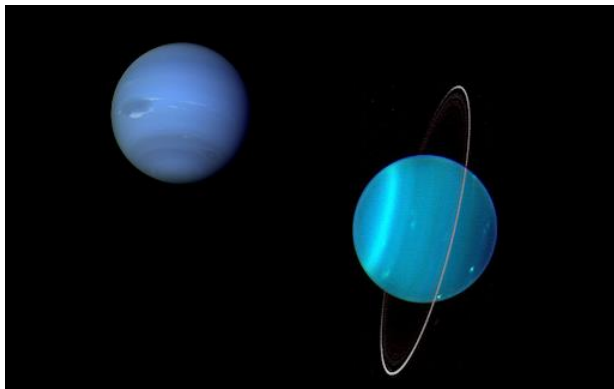


Figure 7: (a) Uranus and Neptune in one frame (not to scale) – notable are the rings of Uranus showing the almost rolling position (b) The Sun apparent size in the sky as seen from the Planets and Pluto

### 3.9 Pluto, the Dwarf Planet

Pluto was considered a planet till very recently. It was the ninth major body from the Sun and orbits further after Neptune. Even so, Due to the elliptic orbits, even though Neptune is the 8th and Pluto is the 9th (earlier) in orbit, Pluto sometimes nearer the Sun than Neptune [19]. Pluto has been relegated from its earlier classification of a planet to a Dwarf one because, while it satisfies the first two conditions to be a planet, it does not satisfy the third one. [20] The conditions are that (a) the body should be going around the parent star (b) it should be massive enough to reach hydrostatic equilibrium (i.e. be spherical) (c) it should have cleared its orbit of all debris – i.e in that orbit it should have above 95% mass.

Unfortunately for Pluto, there is the moon with almost 50% of its own weight, so it does not satisfy the third condition. Beyond the orbit of the gas giant Neptune, all known objects are called Kuiper belt objects, and Pluto is the largest Kuiper belt object.

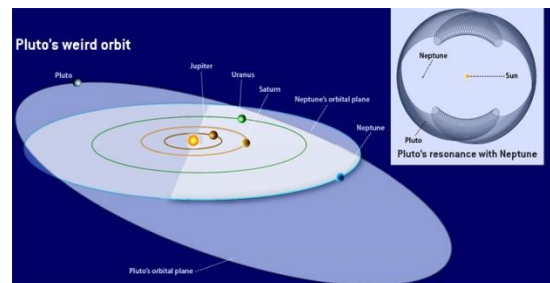


Figure 8: The Orbit of Pluto compared to other planets and the picture of Pluto captured by the New Horizons Spacecraft.

The Kuiper Belt [21] begins at the outer edge of Neptune’s orbit (about 30 AU from the Sun) and extends o about 1000 AU. We need to remember that one AU is the distance from the Sun to our Earth, which is approximately 150 million Km. The icy objects composing the Kuiper Belt are believed to be the remnants left over from the formation of the solar system. Just like Jupiter prevented the formation of the asteroid belt into a planet, similarly Neptune probably prevented the Kuiper belt from the same fate. There are tens of thousands of objects greater than 100Km in the belt, while trillions of smaller objects populate the pace. Numerous icy comets with long duration orbits originate here.

Beyond the Kuiper belt is the OORT cloud [22]



- [8] <https://spaceplace.nasa.gov/all-about-Mercury/en/>
- [9] <https://johnCarlosbaez.wordpress.com/2014/01/04/the-pentagram-of-Venus/>
- [10] <https://nineplanets.org/Jupiter/>
- [11] Mankovich, Christopher; et al. (17 January 2019). "Cassini Ring Seismology as a Probe of Saturn's Interior. I. Rigid Rotation". *The Astrophysical Journal*. 871
- [12] <https://www.space.com/45-Uranus-seventh-planet-in-Earths-solar-system-was-first-discovered-planet.html>
- [13] <https://nineplanets.org/Uranus/>
- [14] <https://solarsystem.nasa.gov/planets/Uranus/overview/>
- [15] <https://www.space.com/6941-theory-galileo-discovered-Neptune.html#:~:text=History%20books%20tell%20us%20that,of%20Melbourne%20physicist%20David%20Jamieson>
- [16] Adams, J.C.; MA, FRAS; Fellow of St Johns College, Cambridge (1846). "On the Perturbations of Uranus (p. 265)". Appendices to various nautical almanacs between the years 1834 and 1854 (reprints published 1851) (note that this is a 50Mb download of the pdf scan of the nineteenth-century printed book). UK Nautical Almanac Office, 1851. Retrieved 2008-01-23.
- [17] <https://web.archive.org/web/20150924073920/http://www.planetarium-berlin.de/pages/hist/WFS-History.html>
- [18] <https://solarsystem.nasa.gov/Moons/Neptune-Moons/triton/in-depth/>
- [19] <https://airandspace.si.edu/exhibitions/exploring-the-planets/online/solar-system/Pluto/orbit.cfm>
- [20] <https://www.loc.gov/everyday-mysteries/item/why-is-pluto-no-longer-a-planet/#:~:text=Answer,neighboring%20region%20of%20other%20objects.%E2%80%9D>
- [21] <https://solarsystem.nasa.gov/solar-system/kuiper-belt/overview/#:~:text=Where%20is%20the%20Kuiper%20Belt,50%20AU%20from%20the%20Sun>
- [22] <https://space-facts.com/oort-cloud/#:~:text=The%20Oort%20Cloud%20is%20an,comets%20that%20have%20been%20observed>
- [23] <https://voyager.jpl.nasa.gov/mission/interstellar-mission/>

#### *About the Author*

#### **Dr Shilpa Mehta**



Dr Shilpa Mehta is currently the Professor and Head of the ECE department in the School of Engineering, of Presidency University Bangalore. She is also heading the EEE Department. She has and experience of 28 years and has worked in various teaching and research positions from 1992 till date. She holds a B.E degree in Electronics Engineering (Gold Medalist) and M.E degree in Digital Techniques and Instrumentation. She has done her Doctorate from JNTU Andhra Pradesh in 2014.

# Low-cost experiment to measure the speed of light

Faraz Mehdi<sup>1,2</sup> and Kiran M. Kolwankar<sup>2</sup>

<sup>1</sup> Department of Physics, University of Mumbai, Santa Cruz (E),  
Mumbai 400 098, India

<sup>2</sup> Department of Physics, Ramniranjan Jhunjhunwala College, Ghatkopar (W),  
Mumbai 400 086, India

farazmehdi786@gmail.com, Kiran.Kolwankar@gmail.com

*Submitted 15-11-2020*

## Abstract

In this paper, we demonstrate a low-cost method to measure the speed of light. It uses instruments which are readily available in any undergraduate laboratory in a developing country and some components which are inexpensive. The method is direct as it measures the time of flight of the LASER beam and easy to implement. It will allow students to verify the finite value of the speed of light first hand. It can be part of the undergraduate syllabus as a regular experiment or a demonstration experiment.

jects, was difficult at those times and, even now, it poses a barrier among the young students studying science. As a result, it would be of interest to have an experiment in which the students can themselves measure the speed of light directly and verify that it is finite.

There are different ways to estimate the speed of light but most of them are either hard to perform in the given time, e.g., the experiments consisting of a rotating mirror based on the principle proposed by Fizeau and Foucault, or they are too expensive e.g., the use of pulsed LASER to measure the speed of light. There are commercially available set-ups for undergraduate laboratories but they cost usually in several lakhs of rupees. We present here an experiment which measures the time of flight of a modulated laser beam over a distance. Given the instruments like an oscilloscope (or a DSO), power supplies and a signal generator, which are readily available in any undergraduate lab-

---

## 1 Introduction

Light travels exceedingly fast. This lead to the belief among the earlier researchers that it travels with infinite speed. To fathom the fact that it travels with finite speed, though very large as compared to the everyday ob-

oratory, the other components cost less than 500 INR.

There are also indirect ways to measure the speed of light. One example consists of detecting nodes created by the standing waves formed by the microwaves in a microwave oven in the form of blackened spots on, say, a piece of paper and then estimating the speed of the radiation using known frequency. This is not a direct way in the sense that it involves another concept and, moreover, the microwaves are not visible leading to lesser impact.

The need for a pedagogical experiment for direct estimation of the speed of light was realised more than 50 years ago [1, 2, 3, 4]. As the technology evolved over time, these experiments too [5, 6, 7, 8, 9, 10, 11, 12, 13]. Most of these experiments involved a light source with modulated intensity which is allowed to travel some distance and the speed of light is estimated from the phase shift between the waveform detected at the source and at the end of the beam. A lamp, which was used in the initial set-ups, was replaced by LED, then a pulsed laser or a diode laser. Our aim was to design the experiment using instruments easily available in a typical undergraduate laboratory in a developing country and all the set-ups available in literature fail in this criterion for one or more reasons. For example, we can not use LED as the source of light as, in that case, distance travelled is small and then one needs to use very high frequency ( $> 50\text{MHz}$ ). Such signal generators are not

common. But the diode lasers are not at all expensive these days using which one can allow the beam to travel a longer distance thereby reducing the frequency to around 300 kHz. The set-up described in [13] turns out to be very close to ours but there the authors have used an advanced oscilloscope and some video analysis using computers which is not the case in our experiment.

In the next section we describe our experimental set-up in detail. Then in the section 3, we discuss our measurements and in 4 we discuss the results. Finally, we end by some concluding remarks in 5

## 2 Experimental set-up

The block diagram of the experimental set-up is shown in the figure 1. We are using a red 5mw diode LASER module as source of light. It is powered by a square-wave generator at a frequency of around 300-400 kHz. This particular frequency range is chosen because we already know the value speed of light and we also know the distance we are allowing the light to travel. Hence we expect the time delay in hundreds of nanoseconds and to get a better measurement of the time-delay in this range on oscilloscope with more precision, the frequency should be in the range taken. This range can be changed depending upon the distance light is allowed to travel.

The modulated light from the LASER falls on a thin glass slab which splits the

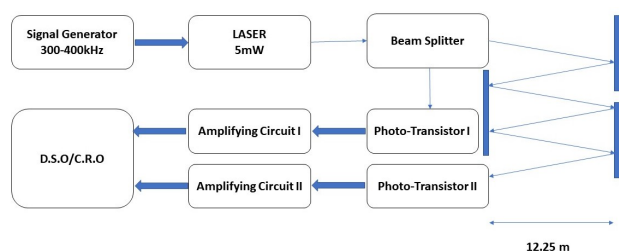


Figure 1: The block diagram

beam into a reflected and a refracted part. The reflected light falls on a photo-transistor which is then connected in series with a resistance (as shown in the fig 2) and the voltage across the resistance gives the required signal. This signal from the receiver is weak and has noise. So to remove the noise and amplify the signal the two ends of the resistor are connected to the amplification and noise cancellation circuit (see fig 2). For the amplification of the signal we use a high-speed Op-Amp (LM318J) in non-inverting amplifier mode with a gain of 30. Since we are working with high frequencies (of the order of 300kHz) the Op-Amp also generates noise of high frequencies (in MHz). To remove this high frequency noise along with the 50Hz background noise coming from the mains, we connected the output of the Op-Amp to a band-pass filter allowing only the frequencies from 1kHz to 500kHz to pass and thus improving the signal to noise ratio. This signal is then observed on C.R.O or D.S.O for the measurement.

The refracted part of light falls on a mirror (placed at sufficiently large distance

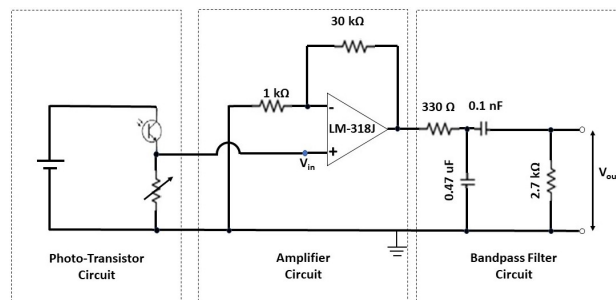


Figure 2: The circuit diagram

so that the time delay of the signals can be observed on the C.R.O./D.S.O.) and gets reflected back near the experimental set-up to fall on a convex lens which converges it on the second photo-transistor with identical amplification and noise-cancellation circuit as that of the first photo-transistor. Then the output is observed on the second channel of the C.R.O. or D.S.O. To increase the distance travelled, it is possible to have several reflections from the mirrors at the farther end. This arrangement of multiple reflections allows us to take the readings for several distances.

### 3 MEASUREMENT

We observe the signals from both the photo-transistors corresponding to reflected and refracted beam. The refracted beam travels more distance than the reflected one and hence will take more time which results in the shifting of its waveform towards right on the time axis and a difference between the peaks of the two signals can be observed. The speed of light is then measured by tak-

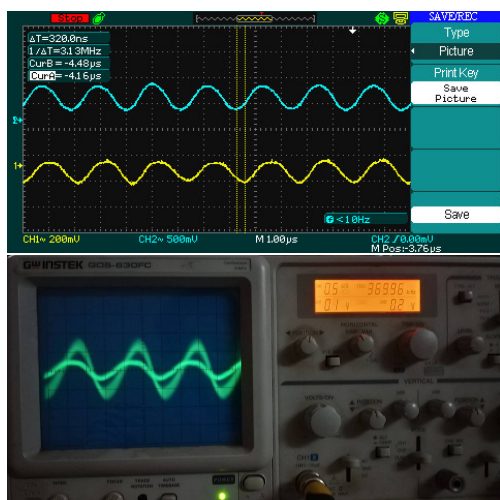


Figure 3: Image of the DSO and oscilloscope screen demonstrating the delay in two waveforms

ing ratio of the excess distance travelled by the refracting light and this time difference between the peak. This delay can be observed even on a simple CRO which immediately confirms the finiteness of the speed of light. It also yields a value of the speed of light which is quite close to the actual value. For more accurate results, we use a DSO and take readings for several distances as described below.

Our first measurement was for zero relative distance as for 0 distance ideally there should be no time difference and any observed time difference would correspond to time-lag in the two receiver circuits. We observed that both the waveforms coincided so there was no observable time-lag in the two receiver circuits. Then different measurements were made by changing the position of the mirror and also by using more mirrors leading to multiple reflections.

An example of the waveform that we see is depicted in Fig. 3 We see that, though we have given a square wave power supply to the laser, the waveform is more near to a sinusoidal waveform. This happens because the higher frequencies get filtered out at the laser and/or at the photo-transistors. This is a result of their finite switching time.

### 4 Results

We carried out the experiment twice with three reflecting mirrors at the farther end. The distance of the farther mirror from the laser was different in each case. As a result, we generated values of delay times for 6 different distances. They are listed in a table below. The mean value of the speed of light turns out to be  $2.98 \times 10^8 \text{ m/s}$ . These are also plotted in the Fig 4. We obtain a good straight line with slope  $3.39 \times 10^{-9} \text{ s/m}$ . Taking the reciprocal of this slope gives us the speed of light to be  $2.95 \times 10^8 \text{ m/s}$ .

The following is our observation table:

Distance (in m)	Time Difference (in ns)
0	0
24.5	80
29	100
49	160
58	200
73.5	240
87	300

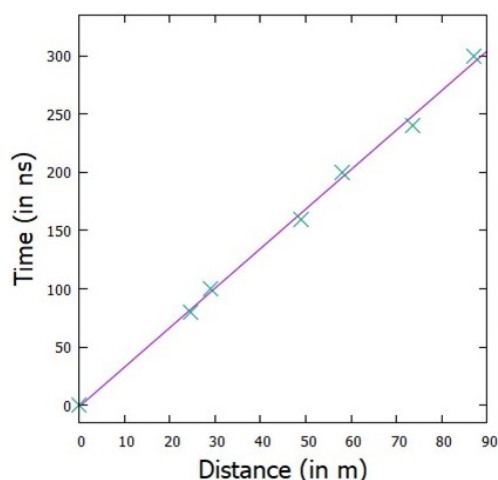


Figure 4: The graph of delay time vs the distance travel

## 5 Concluding remarks

We have demonstrated a simple and direct method for measurement of the speed of light in an undergraduate laboratory. The method that we are proposing is based on the time of flight principle. In this method we divide light into two components using a beam splitter and then one of the beam is made to travel some large distance. The resulting time-delay between the two is recorded. Then the ratio of excess distance to the time lag gives the speed of light. This method is both inexpensive and easy to perform in an undergraduate laboratory. It incorporates some of the basic concepts from electronics and optics as well. The process of setting it up improves the laboratory skills of the student. The experimental set-up and the circuit is so simple that the students can build it from scratch. Thus they would know each and every part of it,

with the working and importance. There is no special equipment required. The cost of components required is less than 500 INR which are reusable in other experiments. It is our experience that the students do experience a thrill when they see the finiteness of the speed of light for themselves for the first time.

## Acknowledgements

We would like to acknowledge the financial support from Department of Biotechnology, India under their Star College Scheme. A major part of this work was carried out as FM's undergraduate project in RJ College. Thanks are also due to several earlier students since 2011 who have rendered their help in the initial stages of this experiment.

## References

- [1] J. Cooke, M. Martin, H. McCartney, and B. Wilf, Direct determination of the speed of light as a general physics laboratory experiment, *Am. J. Phys.* **36**, 847 (1968).
- [2] C. E. Tyler, A pedagogical measurement of the velocity of light, *Am. J. Phys.*, **37**, 1154 (1969)
- [3] J. Rogers, R. McMillan, R. Pickett and R. Anderson, A determination of the speed of light by the phase-shift method, *Am. J. Phys.* **37**, 816 (1969)

- [4] J. Vanderkooy and M. J. Beccario, An inexpensive, accurate laboratory determination of the velocity of light, *Am. J. Phys.* **41**, 272 (1973)
- [5] G. E. Everett and R. L. Wild, Inexpensive time of flight velocity measurements, *Am. J. Phys.* **47**, 426 (1979)
- [6] F.D.Becchetti, K. C. Harvey, B. J. Schwartz and M. L. Shapiro, Time of flight measurement of the speed of light using a laser and a low voltage Pöckelscell modulator, *Am. J. Phys.* **55**, 632(1987)
- [7] J. A. Deblaquiere, K. C. Harvey and A. K. Hemann, Time of flight measurement of the speed of light using an acousto-optic modulator, *Am. J. Phys.* **59**, 443 (1991)
- [8] M. B. James, R. B. Ormond, and A. J. Stasch, Speed of light measurement for the myriad, *Am. J. Phys.* **67**, 8 (1999)
- [9] J. E. Beaver, The speed of light with a shortwave radio, *Phys. Teach.* **38**, 172 (2000)
- [10] K.Aoki and T. Mitsui, A tabletop experiment for the direct measurement of the speed of light, *Am. J. Phys.* **76**, 812(2008).
- [11] E. D. Greaves, A. M. Rodriguez and J. Ruiz-Camacho, A one-way speed of light experiment, *Phys. Teach.* **77**, 894 (2009)
- [12] G. Pegna, An extraordinary tabletop speed of light apparatus, *Am. J. Phys.* **85**, 712 (2017)
- [13] M. Ortiz, A. M. Montecinos, How to measure the speed of light at your university with a dinner budget, *Rev. Bras. Ensino. Fis.* **37**, 1502 (2015)

# Fractals in leaves - An interdisciplinary project for undergraduates

Nishanth P.<sup>1</sup>, Prasanth P.<sup>2</sup>, Reshma P.<sup>3</sup> and Udayanandan K. M.<sup>4</sup>

<sup>1</sup>School of Pure and Applied Physics, Kannur University,  
Payyanur Campus, Payyanur, Kerala - 670 327, India.

mailnishanthp@yahoo.com

<sup>2</sup>Department of Physics, Government Engineering College,  
Thrissur - 680 009, Kerala, India.

prasanthpnair@gmail.com

<sup>3</sup>Department of Physics, S. N. Polytechnic College,  
Kanhangad - 671 315, Kerala, India.

reshmaperayil@gmail.com

<sup>4</sup>Former HoD, Department of Physics, Nehru Arts and Science College,  
Kanhangad, Kerala - 671 314, India.

udayanandan@gmail.com

*Submitted 31-10-2020*

## Abstract

This article proposes an investigatory project for the undergraduates of physical and life science students, on the fractal dimension of leaves. Such a project, we hope, can develop an interdisciplinary approach among science students, since it contains physics, mathematics and plant science. Such studies could create among the physical science students a love and

an awareness about what is happening around them in nature. Doing such projects by the life science students may make them realize that mathematics is an integral part of nature.

---

## 1 Introduction

Fractals are the illustrations of the extent of complexness and the beauty of the symmetry of the structures found in the nature.

Like many structures in our neighbourhood, the shape of leaves has been known to have fractal behaviour [1, 2, 3]. The fractal characters of the leaves have been translated to numerical values with the calculation of the fractal dimension. The estimation of the fractal dimension helps in the identification of the patterns on leaves and this method solves the problems connected with recognition of the structure with rotation or scale change [4]. Many literatures used fractal dimension of leaves for the identification of different features of leaves and the plant in which leaves are contained [5, 6]. The study conducted by Johann Misterio et al. on Norfolk Island Pine leaves, evaluated the change in fractal dimension of leaves with change in their position on the stem. They reported that the stem position influences the structure of leaves and high fractal dimension have been noticed for the leaves in the middle region of the stem [7]. In a paper by Davi Rodrigo Rossatto et al. about the structure on the surface of leaves in the species Melastomataceae, the fractal dimension is used for the identification of the different members [8]. According to them, the difficulties associated with identification due to close resemblance in the texture of some members of the family are overtaken by quantification of the structure with fractal dimension. C. M. Pohontu [9] studied about the structural changes on the plant leaves exposed to toxic substances by the assessment of their fractal dimension. His results showed that the fractal dimension

changes in proportion to the amount of the pollutant. All the above references show that study of fractals in leaves is very useful. We will show that such a study can be conducted by students of any discipline without the use of great laboratories or spending large amount of money. Many articles are available about fractals in nature and related concepts [10, 11], but some readers may not be exposed to this subject. So we give a brief introduction about the fractals in the next section.

## 2 Fractals in nature

### 2.1 What are fractals?

There are many irregular objects that show the patterns similar which are repeated with magnification and such patterns are called fractals. The repeated patterns show the symmetry of the object and this property of the fractals is termed as self similarity. Many natural structures have fractal characteristics and their self similarity is confined to certain range of magnification. But, there are mathematical fractals, like Koch snowflake, which show fractal character even at infinite magnification [12]. A Koch snowflake is formed from a simple equilateral triangle shape, but the final shape has high complexity. This is a general property of any fractal and they have both ordered and random characters. Mandelbrot [13, 14] first proposed the term fractal from a Latin word which means broken and the structure of different objects like clouds, coastlines and

many other natural shapes which are otherwise undetermined with ordinary geometry has been explained in terms of fractals. Let us consider some examples from the na-



Figure 1: The fractal nature of Rose flower



Figure 2: The fractal nature of tree branches

ture which show fractal characters. A. H. Thompson reported that the porous rocks show fractal structure in a magnified view at microscopic scale and the study of their porous structure help to identify the complex nature which leads to the better evaluation of the flow of the fluid in the rock [15]. In a study by M. C. Breslin and J. A. Belward on rainfall in different locations in Queensland, Australia found that there is a statistical symmetry in the monthly variations in rainfall and variations in rainfall over the decades [16]. This indicates that the rainfall over the period has fractal characters. In our body, there are structures which span all over from foot to head like the nerves, the blood vessels which carries the blood and the structure like lungs which forms branches up to small size known as bronchi-

oles, all these are examples of fractals [17]. Our rhythmic beats of heart also has random nature which makes them good fractals and analysis of the fractal behaviour of the heart rate helps in identification of the changes in the heart rate and many disease conditions related with the heart [18]. The Figure 1 shows an example of Rose flower petals and Figure 2 shows a dried tree with branches. Both are fractals. The fractals are found everywhere, not only in the world around us, which we can see directly, but they are seen even at the gigantic scales in the form of galaxies and other structures in space [19]. All these inspire every nature loving person, to make a study of them. In the next section we will discuss how the fractals can be quantified.

### 2.2 Quantifying fractals

The complex nature of the shape of fractals has been quantified with the fractal dimension [20, 21]. We represent the dimension of many familiar objects with integers, like a straight line with dimension one and an image on a paper with dimension two and so on. For complicated structures of fractal, the dimension is a non-integer and it is named as fractal dimension [22]. The basic relation for dimension is [23]

$$n = s^D \tag{1}$$

where  $n$  is the number of similar segments needed to make the whole structure of an object,  $s$  is the scaling factor used to increase the size of an object (if the size of the object is reduced then the scaling factor is  $\frac{1}{s}$ ) and  $D$  is the dimension. Let us find dimension of two objects - line and square in the Figure 3 using the above relation. The line in

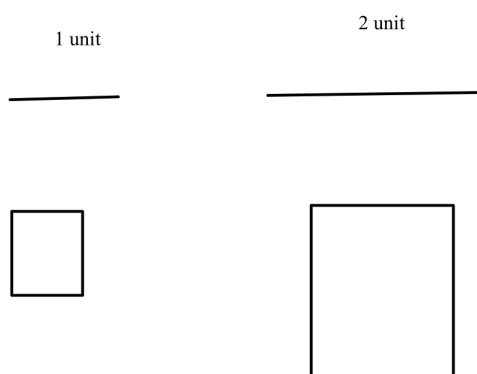


Figure 3: Dimension of basic shapes

LHS has a length of 1 unit (the unit represents the length in centimetre, inch or any

other measurement unit). The length of the second line on RHS is 2 units. From the line at LHS to the line at RHS the scale is doubled and hence  $s = 2$ . The number of line segments in LHS needed to fill the line at RHS is 2 and hence our  $n = 2$ . So we have from above relation

$$2 = 2^D$$

This relation indicates that the dimension of a line is one. In the same way, the side length of the square on RHS is 2 units. This is twice as the side length of the square at LHS (with side length 1 unit). This means the scale change for square is  $s = 2$ . The number of squares (with side length 1 unit) needed to fill the square at RHS is  $n = 4$ . So one can write above relation is

$$4 = 2^D$$

This relation indicates that the exponent has a value of 2 and hence the dimension of square is two. Taking logarithm of Eq (1) on both sides we get

$$D = \frac{\ln n}{\ln s} \tag{2}$$

### 2.3 Fractal dimension for Koch curve

Koch snowflake is a fractal introduced by mathematician H. V. Koch and it is formed in different stages which starts from an equilateral triangle [24]. In the first step, all the sides of the equilateral triangle is divided into 3 equal parts. In next step, at each side, form equilateral triangles with middle portion as base and after this step remove the

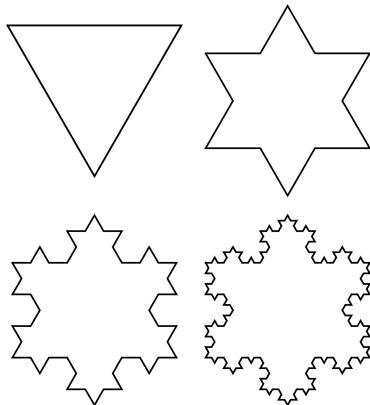


Figure 4: First few levels of Koch curve

base portion of newly formed equilateral triangles. Repeat the entire process again and again to get Koch snowflake at different levels. The Figure 4 shows a Koch snowflake plotted with Mathematica [25]. From the Figure 4, one can find that from the equilateral triangle to the first level, the number of segments in a side is changed to 4. At first level, the length of each line segment is reduced by  $\frac{1}{3}$  of the length of line segment of the equilateral triangle. So, we get  $n = 4$ ,  $s = 3$  and hence the fractal dimension of a Koch snowflake is [26]

$$D = \frac{\ln 4}{\ln 3} = 1.2618$$

### 2.4 Box counting-Theory

There have been many methods used for the calculation of the fractal dimension and out of which the box counting method is the simplest and the most used [27]. In this method, the square boxes of a particular side length are placed under the image of the

fractal as shown in Figure 5. The figure contains a Neem leaf on which square grids are placed. The number of boxes needed to fill

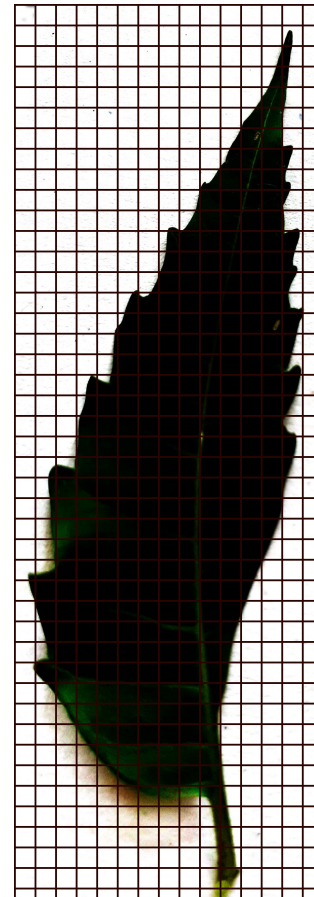


Figure 5: A Neem leaf with grids

the image and length of a side of the square box or grid are the parameters measured for the calculation of the fractal dimension. The process is repeated with boxes of different side length. A log-log plot of inverse of side length and number of boxes is plotted and the slope of the graph gives the required fractal dimension of the object. Since it's a repeated process and the accuracy increases with smallest side length of the boxes, the computer algorithm are used for the calcula-

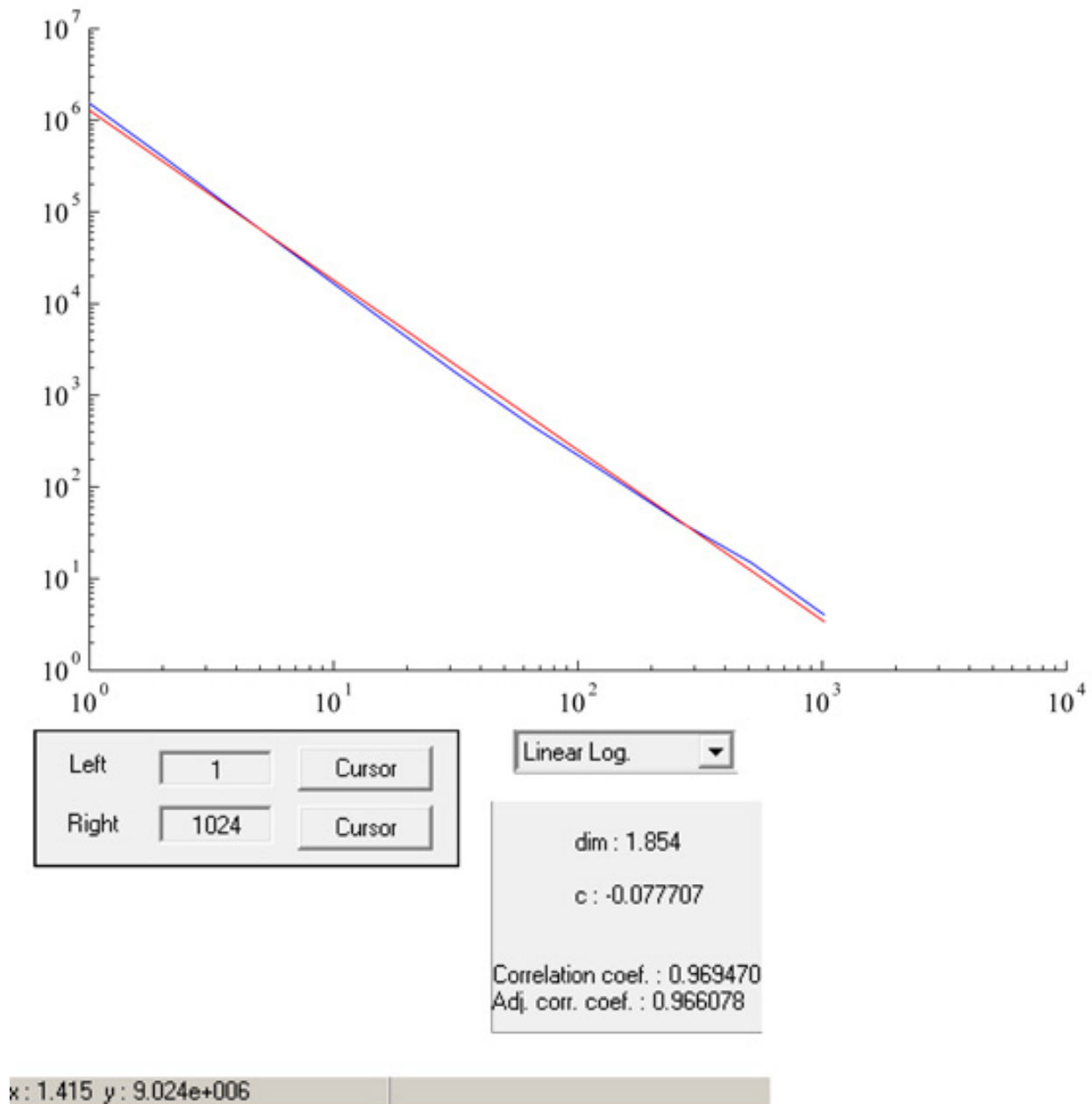


Figure 6: The log - log plot of a sample leaf.

tion of the fractal dimension [28]. Many natural objects exhibit fractal property in certain range and thus, in a log - log plot only linear part is chosen for calculation of fractal dimension with reasonable accuracy [29].

### 2.5 Box counting-Experimental Technique

The images were taken using *Clear scanner* application downloaded from Play store using an android phone. The colour of the im-

ages was removed for analysis (This could be done with any photo editing software). For uniformity of the images, the size (resolution) of samples was set to 300 dpi and final image samples were stored as bitmap files in the computer. The fractal dimensions of the leaves were found using the free software *Fractalyse* available in the internet [30]. For the windows operating system an executable file (.exe) was downloaded from the website home page. The file was double clicked for execution and Ok button was clicked in all the steps till end. The software was opened from start menu after installation. To find fractal dimension, the following steps were executed as

**File** → **Open**

**Analyse** → **Box**

In the Box window the box size was chosen as exponential and the algorithm was chosen as grid type. The estimation window appeared after clicking the Ok button. The estimation window showed the log - log plot for the sample and its dimension. A window of the estimation of the fractal dimension for a sample leaf is shown in the Figure 6. The blue colour line shows the log - log plot and the curve fitting function is shown in the red colour line.

### 3 Fractals in leaves - A study

The fractal dimension and names of all the leaves studied are given in the table given below.

Leaf	Sample1	Sample 2	Sample 3	Sample 4	Mean
Hibiscus	1.802	1.785	1.793	1.743	1.78075
Neem	1.749	1.771	1.766	1.765	1.76275
Tragia involucrata	1.787	1.776	1.798	1.804	1.79125
Pegoda	1.791	1.765	1.854	1.818	1.807

#### 3.1 Observations

The images of all the samples are shown in Figures 7, 8, 9 and 10. Samples of leaves collected from same plants show changes in their geometrical shape due to the changes that takes place to the leaves by physiological or environmental causes [31]. So for each leaf, the fractal dimension changes and to

get more precise value large number of samples are needed. Since it's a study to demonstrate measurement of fractal dimension of leaves, we choose only few samples. If it is an actual project or research more samples will be needed. The following are the observations:

1. Maximum fractal dimension is for Pe-

goda leaves. The mean value is 1.807. The high fractal dimension of the leaves indicate the complexness in their structure and the Pegoda leaves has maximum complexity in its leaf structure. The complexity in the leaf structure helps the leaves to fulfil their need for light and temperature for their biological processes [32]. The Pegoda leaves have projections on the leaf structure called the lobes. The lobes of Pegoda leaves increase the complexity and help them for the better adaptation with the surrounding conditions. S. Siso et al. studied about complexity in the leaf structure of different leaves in *Quercus* species and found that an increase in the complexity in the structure reduces the resistance to flow of water [33]. This indicates that the complex shape of the leaves of Pegoda is an adaptation for better intake of water.

2. The minimum fractal dimension is for Neem leaves and the mean value is 1.76275. The complexity of Neem leaves is low as they have low fractal dimension. In a study on Black alder leaves, F. sala et al. [34] reported that the fractal dimension of leaves has direct relation with area, width, scanned leaf area and perimeter. These parameters are small in Neem leaves compared with others and hence Neem leaves have low fractal dimension.

3. It is found that the fractal dimension for

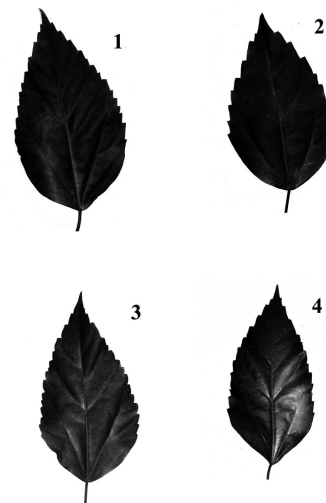


Figure 7: The samples of Hibiscus leaves

each type of leaf remains within a certain range of values.

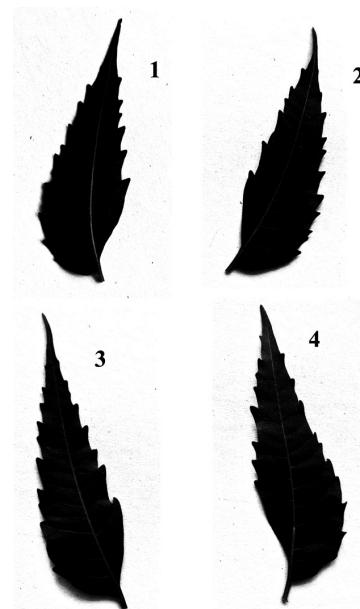


Figure 8: The samples of Neem leaves

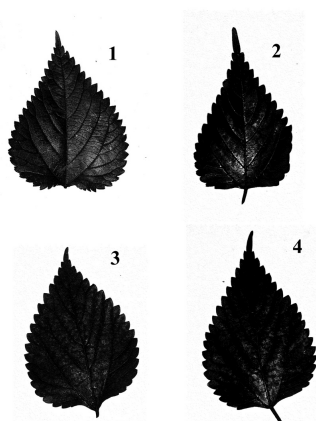


Figure 9: The samples of *Tragia involucrata* leaves

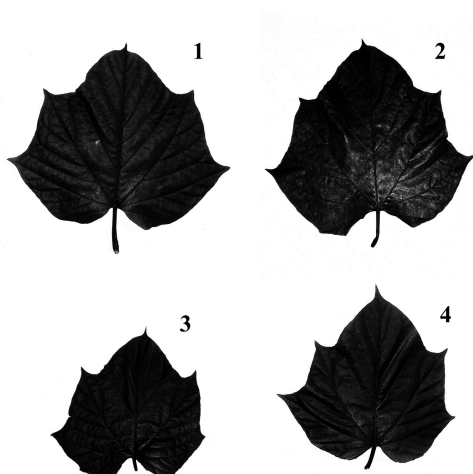


Figure 10: The samples of Pegoda leaves

## 4 Conclusion

We had demonstrated how an interdisciplinary project can be done very easily without much financial liabilities. There is always a complaint that studies are becoming too narrow in the subjects and many are not useful to the society. During the course study it is advisable to give projects of interdisciplinary nature, which will give stu-

dents a respect for subjects of other discipline. During the undergraduate studies it is better to give work of a broader nature and hence the project given in this article we hope, will be one among them in attaining this goal.

## Acknowledgments

One of the authors, Nishanth P. wishes to thank his friends for the help provided during the data collection.

## References

- [1] N. R. Silva, J. B. Florindo, M. C. Gomez, R. M. Kolb & O. M. Bruno (2014). *J. Phys. : Conf. Ser.* 490 (1), 012085.
- [2] W. Borkowski (1999). *Can. J. For. Res.* 29 (9), 1301.
- [3] J. Vlcek & E. Cheung (1986). *Can. J. For. Res.* 16 (1), 124.
- [4] A. R. Backes & O. M. Bruno (2010). *Pattern Recognit. Lett.* 31 (1), 44.
- [5] O. M. Bruno, R. de Oliveira Plotze, M. Falvo & M. de Castro (2008). *Inf. Sci.* 178 (12), 2722.
- [6] J. R. Castrejon Pita, A. Sarmiento Galan & R. Castrejon Garcia (2002). *Fractals*, 10 (04), 429.
- [7] K. Ravindra, R. D. Rivero, H. McCloud, L. Burr-Alexander & N. Ravindra (2007). 2007 ASEE Annual Confer-

- ence & Exposition Proceedings, Honolulu, Hawaii.
- [8] D. R. Rossatto, D. Casanova, R. M. Kolb & O. M. Bruno (2011). *Plant Syst. Evol.* 291 (1-2), 103.
- [9] C. M. Pohonu (2018). *Curr. Trends Nat. Sci.* 7 (13), 244.
- [10] H. Takayasu. *Fractals in the physical sciences*, (Manchester University Press, 1990)
- [11] D. Avnir, O. Biham, D. Lidar & O. Malcai (1998). *Science*, 279 (5347), 39.
- [12] A. Garg, A. Agrawal & A. Negi (2014). *Int. J. Comput. Appl.* 975, 8887.
- [13] L. Debnath (2006). *Int. J. Math. Educ. Sci. Technol.* 37 (1), 29.
- [14] B. B. Mandelbrot (1989). *Proc. R. Soc. Lond. A* 423, 3.
- [15] A. H. Thompson (1991). *Annu. Rev. Earth Planet. Sci.* 19 (1), 237.
- [16] M. C. Breslin & J. A. Belward (1999). *Math. Comput. Simul.* 48 (4-6), 437.
- [17] K. Falconer. *Fractals: A very short introduction*, (Oxford University Press, 2013)
- [18] D. Kumar, S. P. Arjunan & B. Aliahmad. *Fractals: applications in biological Signalling and image processing*, (CRC Press, 2017)
- [19] L. Pietronero (1992). *Physica A*, 191 (1-4), 85.
- [20] K. Zembrowska & M. Kuzma (2002). *Phys. Teach.* 40, 470.
- [21] B. B. Mandelbrot (1985). *Phys. Scr.* 32 (4), 257.
- [22] G. Hartvigsen (2000). *Am. Biol. Teach.* 62 (9), 664.
- [23] S. A. Shirali (2014). *Resonance*, 19 (11), 1000.
- [24] Y. D. Sergeyev (2016). *Comm. Nonlinear Sci. Numer. Simulat.* 31 (1-3), 21.
- [25] S. Wagon. *Mathematica in action: problem solving through visualization and computation*, (Springer Science & Business Media, 2010)
- [26] K. Falconer. *Fractal geometry: mathematical foundations and applications*, (John Wiley & Sons, 2003)
- [27] M. J. Ostwald & J. Vaughan. *The fractal dimension of architecture (Vol. 1)*, (Birkhauser, 2016)
- [28] P. V. S. Souza, R. L. Alves & W. F. Baltazar (2019). *Phys. Teach.* 57 (7), 467.
- [29] S. Mancuso (2002). *Vitis* 41 (3), 137.
- [30] G. Vuidel (2020). *Fractal.yse - Fractal analysis software*. Retrieved 18 October 2020, from <http://www.fractal.yse.org/>

- [31] M. Bayirli, S. Selvi & U. akilcioglu (2014). Bangladesh J. Bot. 43 (3), 267.
- [32] S. Oancea (2008). Lucrari stiintifice Univ de Stiinte Agricole si Medicina Veterinara Iasi Agronomie, 51, 62.
- [33] S. Siso, J. Camarero & E. Gil-Pelegn (2001). Trees 15 (6), 341.
- [34] F. Sala, A. D. Datcu & C. Rujescu (2020). Annals of West University of Timioara, ser. Biology, 23 (1), 73.

# Learning Density Matrix with the help of exercises

A. Reshma. P<sup>1</sup>, B. Prasanth. P<sup>2</sup>, C. Nishanth. P<sup>3</sup> and D. K. M. Udayanandan<sup>4</sup>

<sup>1</sup>Department of Physics, S.N.Polytechnic College, Kanhangad, Kerala.

<sup>2</sup>Department of Physics, Govt. Engineering College, Thrissur, Kerala

<sup>3</sup> School of Pure and Applied Physics, Payyannur, Kerala.

<sup>4</sup>Former H O D, NAS College, Kanhangad, Kerala.

udayanandan@gmail.com

*Submitted on 11-12-2020*

## Abstract

In real situations, the systems that we deal with in quantum statistical mechanics, are mainly mixed systems. We will not be able to write a single state vector for such systems, which makes finding the average thermodynamic properties impossible. In statistical mechanics what we find or measure is the ensemble average of any thermodynamic property. Density matrix comes to rescue or save physicist from this difficult situation. Hence understanding density matrix and its uses will be of great help for students and teachers and this article aims to clarify the doubts faced by the learners of statistical mechanics, while studying density matrices.

this concept are very limited, recently some are available [3, 4] and the topic is also discussed in some papers [5, 6, 7, 8, 9]. Random walks in a crystal lattice, migration in a homogeneous isotropic continuum, thermoactivated transitions between quantum states [6], quantum lattice gas [7] were some of the fields where the work is done. The density matrix formalism also makes it possible to develop a quantum kinetic theory of a many-particle system [8] interacting with a heat reservoir. New theory of superconductivity, the equilibrium states of the interacting particle system are also described using the density matrix [9].

## 1 Introduction

The density matrix was introduced by J. von Neumann [1] and L Landau in 1927 [2] to describe the statistical concepts in quantum mechanics. Even though books dealing with

## 2 Classical Statistical Mechanics

### Ensemble average

Any macroscopic thermodynamic quantity of a system which we wish to find is measured over a finite time, which is very long

compared to the time-scale of motion of the particles of the system. So, the measured quantity is actually a time-averaged quantity. But finding time average is very difficult. J. W. Gibbs[10] proposed an alternative to avoid time averaging in order to obtain equilibrium properties of macroscopic objects. He introduced and developed the concept of ensemble and formulated a theoretical scheme where equilibrium properties of the system can be obtained as an ensemble average. It is as follows[11, 12]. Consider any observable property, say  $X$ . The ensemble average is a simple average over all the members of the ensemble.

$$\langle X \rangle = \lim_{N \rightarrow \infty} \frac{1}{N} \sum_{i=1}^N n_i X_i$$

where  $N$  is the total number and  $n_i$  is the number in the  $i^{th}$  state. This equation can be changed by introducing probability given by

$$p_i = \frac{n_i}{N}$$

Then the average becomes

$$\langle X \rangle = \lim_{N \rightarrow \infty} \sum_{i=1}^N p_i X_i$$

where  $p_i$  is the probability of a member of the ensemble to be in the  $i^{th}$  microscopic state. Our aim is to provide the reader large number of exercises so that a working knowledge is obtained. We will start with the first one.

**Exercise**

Find the average energy of an electron in a magnetic field in canonical ensemble.

Let  $\mu$  be the dipole moment and  $B$  be the magnetic field. Then classical energy is

$$E = -\mu \cdot B$$

For the up and down spin, the energy will be  $E_1 = \mu B$  and  $E_2 = -\mu B$ . Then

$$\langle E \rangle = \frac{e^{-\beta\mu B} \mu B - e^{\beta\mu B} \mu B}{e^{-\beta\mu B} + e^{\beta\mu B}}$$

where  $p_i = \frac{e^{-\beta E_i}}{Q}$

$$\langle E \rangle = -\mu B \tanh \beta\mu B$$

**Exercise**

A collection  $N$  of non-interacting spins  $S_i = \pm 1$ , is kept in an external magnetic field  $B$  at a temperature  $T$ . Find the average spin

$$\langle S_i \rangle = \frac{1 \times e^{\beta\mu B} + -1 \times e^{-\beta\mu B}}{Q}$$

$$\begin{aligned} \langle S_i \rangle &= \left( \frac{e^{\beta\mu B} - e^{-\beta\mu B}}{e^{\beta\mu B} + e^{-\beta\mu B}} \right) \\ &= \tanh \beta\mu B \end{aligned}$$

Thus finding average is not a difficult problem in classical statistical mechanics. Let us now see how we can find average in quantum mechanics.

**3 Quantum Mechanics**

In quantum mechanics(QM) we use a wave function,  $\psi(x)$ , for representing the state of the object. This function contains all information about the physical state of the object.

Usually a particle being in a state described by a superposition or linear sum of all basis solutions. If there are 3 possibilities then the wave function is given by

$$\psi = c_1\phi_1 + c_2\phi_2 + c_3\phi_3$$

So using Dirac notation, the state of a system can be represented by a state function

$$|\psi\rangle = \sum c_n |\phi_n\rangle$$

Then

$$\langle\psi| = \sum c_n^* \langle\phi_n|$$

where  $c_i$ 's are complex coefficients and  $\phi_i$ 's are basis vectors [12]. In quantum physics problems, the vectors can be infinitely large for example, a moving particle can be in an infinite number of states. Handling large arrays of states is not easy using vector notation, so instead of explicitly writing out the whole vector each time, quantum physics usually uses the notation developed by physicist Paul Dirac- the Dirac or bra-ket notation. We will use this notation in our further studies.

### 3.1 Expectation Value and Density matrix

The expectation value of an operator is the average value that you would measure if you perform the measurement many times. When we make a measurement of an observable (represented by an operator) of the system, we observe the time average or equivalently the ensemble average of its value. This average value of observable is

described by the expectation value of the corresponding operator. Now we can define average or expectation value in QM using Dirac notation. For an operator  $\hat{A}$ , the expectation value is

$$\langle\hat{A}\rangle = \langle\psi|\hat{A}|\psi\rangle$$

Let us consider a particle being in a state described by the superposition of two basis vectors  $\phi_1$  and  $\phi_2$ . Consider a state formed by a superposition

$$|\psi\rangle = c_1 |\phi_1\rangle + c_2 |\phi_2\rangle$$

such that  $\sum_i |\phi_i\rangle \langle\phi_i| = 1$

$$\langle\psi| = c_1^* \langle\phi_1| + c_2^* \langle\phi_2|$$

The expectation value of an operator  $\hat{A}$  is

$$\langle\hat{A}\rangle = \langle\psi|\hat{A}|\psi\rangle$$

$$\langle\hat{A}\rangle = \sum_m c_m^* \langle\phi_m| \hat{A} \sum_n c_n |\phi_n\rangle$$

Introducing an identity matrix  $I$

$$\langle\hat{A}\rangle = \sum_m \sum_n c_m^* c_n \langle\phi_m| I \hat{A} |\phi_n\rangle$$

$$\langle\hat{A}\rangle = \sum_m \sum_n c_m^* c_n \langle\phi_m| \sum_n |\phi_n\rangle \langle\phi_n| \hat{A} |\phi_n\rangle$$

$$\langle\hat{A}\rangle = \sum_m \sum_n \langle\phi_m| c_m^* c_n |\phi_m\rangle \langle\phi_n| \hat{A} |\phi_n\rangle$$

Defining density matrix

$$\rho = \sum_m \sum_n c_m^* c_n |\phi_m\rangle \langle\phi_n|$$

we get

$$\langle\hat{A}\rangle = \sum_m \sum_n \langle\phi_m| \rho \hat{A} |\phi_n\rangle$$

If  $m = n$ , then

$$\langle \hat{A} \rangle = \sum_m \langle \phi_m | \rho \hat{A} | \phi_m \rangle = \text{Trace of } (\rho \hat{A})$$

This is how we define the expectation value in quantum mechanics. To make things clear we will do some exercises

**Exercise**

Show that using examples if  $m = n$ , then  $\langle \hat{A} \rangle = \text{Trace of } (\rho \hat{A})$  using an example.

Let  $|\phi_1\rangle = \begin{pmatrix} 0 \\ 1 \end{pmatrix}$  and  $|\phi_2\rangle = \begin{pmatrix} 1 \\ 0 \end{pmatrix}$  and  $\rho \hat{A} = \begin{pmatrix} a_1 & a_2 \\ a_3 & a_4 \end{pmatrix}$ . Then from the definition of expectation value

$$\begin{aligned} \langle \hat{A} \rangle &= \begin{pmatrix} 0 & 1 \end{pmatrix} \begin{pmatrix} a_1 & a_2 \\ a_3 & a_4 \end{pmatrix} \begin{pmatrix} 0 \\ 1 \end{pmatrix} + \\ &\quad \begin{pmatrix} 1 & 0 \end{pmatrix} \begin{pmatrix} a_1 & a_2 \\ a_3 & a_4 \end{pmatrix} \begin{pmatrix} 1 \\ 0 \end{pmatrix} \\ \langle \hat{A} \rangle &= \begin{pmatrix} 0 & 1 \end{pmatrix} \begin{pmatrix} a_2 \\ a_4 \end{pmatrix} + \begin{pmatrix} 1 & 0 \end{pmatrix} \begin{pmatrix} a_1 \\ a_3 \end{pmatrix} \\ &= a_1 + a_4 \\ \langle \hat{A} \rangle &= \text{Tr } \rho \hat{A} \end{aligned}$$

**Exercise**

Let us show that  $\sum_i |\phi_i\rangle \langle \phi_i| = 1$

$$\begin{aligned} &|\phi_1\rangle \langle \phi_1| + |\phi_2\rangle \langle \phi_2| \\ &= \begin{pmatrix} 0 \\ 1 \end{pmatrix} \begin{pmatrix} 0 & 1 \end{pmatrix} + \begin{pmatrix} 1 \\ 0 \end{pmatrix} \begin{pmatrix} 1 & 0 \end{pmatrix} \end{aligned}$$

$$= \begin{pmatrix} 0 & 0 \\ 0 & 1 \end{pmatrix} + \begin{pmatrix} 1 & 0 \\ 0 & 0 \end{pmatrix} = \begin{pmatrix} 1 & 0 \\ 0 & 1 \end{pmatrix}$$

**Examples**

Using the definition of expectation value in quantum mechanics let us find the average spin and the average energy of an electron in a magnetic field. Here the dipole moment becomes a dipole moment operator. So

$$\hat{\mu} = \mu_B \hat{\sigma}$$

where  $\sigma$  represent Pauli spin matrices. Let the applied field be in the z direction. So  $\sigma = \sigma_z = \begin{pmatrix} 1 & 0 \\ 0 & -1 \end{pmatrix}$  which is the Pauli spin matrix. Hence Hamiltonian is

$$\hat{H} = -\mu_B B \hat{\sigma}_z = \begin{pmatrix} -\mu_B B & 0 \\ 0 & \mu_B B \end{pmatrix}$$

Density matrix in canonical ensemble is[10]

$$\hat{\rho} = \frac{e^{-\beta \hat{H}}}{\text{Tr } e^{-\beta \hat{H}}}$$

where  $\text{Tr } e^{-\beta \hat{H}} = e^{-\beta \mu_B B} + e^{\beta \mu_B B}$

$$\hat{\rho} = \frac{1}{\text{Tr } e^{-\beta \hat{H}}} \begin{pmatrix} e^{\beta \mu_B B} & 0 \\ 0 & e^{-\beta \mu_B B} \end{pmatrix}$$

**Exercise**

From the equations for  $\hat{\rho}$  and  $\hat{H}$  we get

$$\hat{\rho} \hat{H} = \frac{1}{\text{Tr } e^{-\beta \hat{H}}} \begin{pmatrix} e^{\beta \mu_B B} & 0 \\ 0 & e^{-\beta \mu_B B} \end{pmatrix} \begin{pmatrix} -\mu_B B & 0 \\ 0 & \mu_B B \end{pmatrix}$$

Multiplying and finding trace we get the average energy

$$\langle E \rangle = -\mu_B B \tanh \beta \mu_B B$$

**Exercise**

Similarly we can find the average spin as below.

$$\hat{\rho}\hat{\sigma} = \frac{1}{\text{Tr } e^{-\beta\hat{H}}} \begin{pmatrix} e^{\beta\mu_B B} & 0 \\ 0 & e^{-\beta\mu_B B} \end{pmatrix} \begin{pmatrix} 1 & 0 \\ 0 & -1 \end{pmatrix}$$

Then we get average spin as

$$\langle S \rangle = \tanh \beta\mu_B B$$

We get the results same as in classical statistical mechanics.. Thus we had shown that the density matrix is a new tool to find the average of any physical quantity in quantum statistical mechanics. Now we will show the most important use of density matrix, differentiating a pure and a mixed state.

**4 Understanding a pure state**

There is some difference in the meaning of pure and mixed systems in physics and daily life. Consider a glass of water ( a pure

state) and some sugar(once again a pure state). If they are completely mixed we get a new pure state called sugar solution. If there is proper superposition we call this state as a pure state. It is a new single entity or mathematically it will have a single eigen value. Instead if we take a glass of water and pour some oil to it. It remains unmixed, and it will never be a single entity. It will have 2 eigen values which will be different. In physics we call such a state as mixed state. The examples we took does not have a one to one correspondence with quantum states and states have different meanings. To have a more understanding on pure states we take some examples. Consider a state

$$|\psi\rangle = c_1 |\phi_1\rangle + c_2 |\phi_2\rangle$$

Let  $|\phi_1\rangle = \begin{pmatrix} 0 \\ 1 \end{pmatrix}$  and  $|\phi_2\rangle = \begin{pmatrix} 1 \\ 0 \end{pmatrix}$

This represents 50% electrons in the one state and 50% electrons in another state.

**Exercise**

Let  $c_1 = \frac{1}{\sqrt{2}}$  and  $c_2 = \frac{1}{\sqrt{2}}$

$$|\psi\rangle = \frac{1}{\sqrt{2}} \begin{pmatrix} 0 \\ 1 \end{pmatrix} + \frac{1}{\sqrt{2}} \begin{pmatrix} 1 \\ 0 \end{pmatrix}$$

$$\begin{aligned} \rho &= c_1^* c_1 |\phi_1\rangle \langle\phi_1| + c_2^* c_1 |\phi_2\rangle \langle\phi_1| + c_1^* c_2 |\phi_1\rangle \langle\phi_2| + c_2^* c_2 |\phi_2\rangle \langle\phi_2| \\ &= \frac{1}{2} \begin{pmatrix} 0 \\ 1 \end{pmatrix} \begin{pmatrix} 0 & 1 \end{pmatrix} + \frac{1}{2} \begin{pmatrix} 1 \\ 0 \end{pmatrix} \begin{pmatrix} 0 & 1 \end{pmatrix} + \frac{1}{2} \begin{pmatrix} 0 \\ 1 \end{pmatrix} \begin{pmatrix} 1 & 0 \end{pmatrix} + \frac{1}{2} \begin{pmatrix} 1 \\ 0 \end{pmatrix} \begin{pmatrix} 1 & 0 \end{pmatrix} \\ &= \frac{1}{2} \begin{pmatrix} 0 & 0 \\ 0 & 1 \end{pmatrix} + \frac{1}{2} \begin{pmatrix} 0 & 1 \\ 0 & 0 \end{pmatrix} + \frac{1}{2} \begin{pmatrix} 0 & 0 \\ 1 & 0 \end{pmatrix} + \frac{1}{2} \begin{pmatrix} 1 & 0 \\ 0 & 0 \end{pmatrix} = \begin{pmatrix} \frac{1}{2} & \frac{1}{2} \\ \frac{1}{2} & \frac{1}{2} \end{pmatrix} \end{aligned}$$

$$\text{Tr } \rho = \frac{1}{2} + \frac{1}{2} = 1$$

$$\rho^2 = \begin{pmatrix} \frac{1}{2} & \frac{1}{2} \\ \frac{1}{2} & \frac{1}{2} \end{pmatrix} \begin{pmatrix} \frac{1}{2} & \frac{1}{2} \\ \frac{1}{2} & \frac{1}{2} \end{pmatrix} = \begin{pmatrix} \frac{1}{2} & \frac{1}{2} \\ \frac{1}{2} & \frac{1}{2} \end{pmatrix} = \rho$$

$$\text{Tr } \rho^2 = 1 = \text{Tr } \rho$$

The eigen value equation is

$$\begin{vmatrix} \frac{1}{2} - \lambda & \frac{1}{2} \\ \frac{1}{2} & \frac{1}{2} - \lambda \end{vmatrix} = 0$$

Solving we get,  $\lambda = 0$  or  $\lambda = 1$ .

Now we can find the average spin. We have Pauli matrices  $\sigma_x = \begin{pmatrix} 0 & 1 \\ 1 & 0 \end{pmatrix}$   $\sigma_y = \begin{pmatrix} 0 & -i \\ i & 0 \end{pmatrix}$

and  $\sigma_z = \begin{pmatrix} 1 & 0 \\ 0 & -1 \end{pmatrix}$

$$S_x = \begin{pmatrix} 0 & \frac{\hbar}{2} \\ \frac{\hbar}{2} & 0 \end{pmatrix} \quad S_y = \begin{pmatrix} 0 & -\frac{i\hbar}{2} \\ \frac{i\hbar}{2} & 0 \end{pmatrix} \quad \text{and} \quad S_z = \begin{pmatrix} \frac{\hbar}{2} & 0 \\ 0 & -\frac{\hbar}{2} \end{pmatrix}$$

$$\langle S_x \rangle = \text{Tr } \rho S_x$$

$$\begin{aligned} \langle S_x \rangle &= \text{Tr} \left[ \begin{pmatrix} \frac{1}{2} & \frac{1}{2} \\ \frac{1}{2} & \frac{1}{2} \end{pmatrix} \begin{pmatrix} 0 & \frac{\hbar}{2} \\ \frac{\hbar}{2} & 0 \end{pmatrix} \right] \\ &= \text{Tr} \begin{pmatrix} \frac{\hbar}{4} & \frac{\hbar}{4} \\ \frac{\hbar}{4} & \frac{\hbar}{4} \end{pmatrix} = \frac{\hbar}{2} \end{aligned}$$

$$\langle S_y \rangle = \text{Tr } \rho S_y$$

$$\begin{aligned} \langle S_y \rangle &= \text{Tr} \left[ \begin{pmatrix} \frac{1}{2} & \frac{1}{2} \\ \frac{1}{2} & \frac{1}{2} \end{pmatrix} \begin{pmatrix} 0 & -\frac{i\hbar}{2} \\ \frac{i\hbar}{2} & 0 \end{pmatrix} \right] \\ &= \text{Tr} \begin{pmatrix} \frac{i\hbar}{4} & -\frac{i\hbar}{4} \\ \frac{i\hbar}{4} & -\frac{i\hbar}{4} \end{pmatrix} = 0 \end{aligned}$$

Even though the electrons have 2 types of orientation the effective spin is in one direction and hence eigen value is 1. This is characteristic of a pure state. One more example we will work with a different composition.

**Exercise**

Let  $c_1 = \sqrt{\frac{2}{3}}$  and  $c_2 = \sqrt{\frac{1}{3}}$

$$|\psi\rangle = \sqrt{\frac{2}{3}} \begin{pmatrix} 0 \\ 1 \end{pmatrix} + \sqrt{\frac{1}{3}} \begin{pmatrix} 1 \\ 0 \end{pmatrix}$$

$$\begin{aligned} \rho &= c_1^* c_1 |\phi_1\rangle \langle \phi_1| + c_2^* c_1 |\phi_2\rangle \langle \phi_1| + c_1^* c_2 |\phi_1\rangle \langle \phi_2| + c_2^* c_2 |\phi_2\rangle \langle \phi_2| \\ &= \frac{2}{3} \begin{pmatrix} 0 \\ 1 \end{pmatrix} \begin{pmatrix} 0 & 1 \end{pmatrix} + \frac{\sqrt{2}}{3} \begin{pmatrix} 1 \\ 0 \end{pmatrix} \begin{pmatrix} 0 & 1 \end{pmatrix} + \frac{\sqrt{2}}{3} \begin{pmatrix} 0 \\ 1 \end{pmatrix} \begin{pmatrix} 1 & 0 \end{pmatrix} + \frac{1}{3} \begin{pmatrix} 1 \\ 0 \end{pmatrix} \begin{pmatrix} 1 & 0 \end{pmatrix} \\ &= \frac{2}{3} \begin{pmatrix} 0 & 0 \\ 0 & 1 \end{pmatrix} + \frac{\sqrt{2}}{3} \begin{pmatrix} 0 & 1 \\ 0 & 0 \end{pmatrix} + \frac{\sqrt{2}}{3} \begin{pmatrix} 0 & 0 \\ 1 & 0 \end{pmatrix} + \frac{1}{3} \begin{pmatrix} 1 & 0 \\ 0 & 0 \end{pmatrix} = \begin{pmatrix} \frac{2}{3} & \frac{\sqrt{2}}{3} \\ \frac{\sqrt{2}}{3} & \frac{1}{3} \end{pmatrix} \end{aligned}$$

$$\text{Tr } \rho = \frac{2}{3} + \frac{1}{3} = 1$$

$$\rho^2 = \begin{pmatrix} \frac{2}{3} & \frac{\sqrt{2}}{3} \\ \frac{\sqrt{2}}{3} & \frac{1}{3} \end{pmatrix} \begin{pmatrix} \frac{2}{3} & \frac{\sqrt{2}}{3} \\ \frac{\sqrt{2}}{3} & \frac{1}{3} \end{pmatrix} = \begin{pmatrix} \frac{6}{9} & \frac{3\sqrt{2}}{9} \\ \frac{3\sqrt{2}}{9} & \frac{3}{9} \end{pmatrix}$$

$$\text{Tr } \rho^2 = 1$$

The eigen value equation is

$$\begin{vmatrix} \frac{2}{3} - \lambda & \frac{\sqrt{2}}{3} \\ \frac{\sqrt{2}}{3} & \frac{1}{3} - \lambda \end{vmatrix} = 0$$

Solving we get,  $\lambda = 0$  or  $\lambda = 1$ .

$$\begin{aligned} \langle S_x \rangle &= \text{Tr} \left[ \begin{pmatrix} \frac{2}{3} & \frac{\sqrt{2}}{3} \\ \frac{\sqrt{2}}{3} & \frac{1}{3} \end{pmatrix} \begin{pmatrix} 0 & \frac{\hbar}{2} \\ \frac{\hbar}{2} & 0 \end{pmatrix} \right] \\ &= \text{Tr} \begin{pmatrix} \frac{\sqrt{2}\hbar}{6} & \frac{2\hbar}{6} \\ \frac{\hbar}{6} & \frac{\sqrt{2}\hbar}{6} \end{pmatrix} = \frac{\sqrt{2}\hbar}{3} \end{aligned}$$

$$\begin{aligned} \langle S_y \rangle &= \text{Tr} \left[ \begin{pmatrix} \frac{2}{3} & \frac{\sqrt{2}}{3} \\ \frac{\sqrt{2}}{3} & \frac{1}{3} \end{pmatrix} \begin{pmatrix} 0 & -\frac{i\hbar}{2} \\ \frac{i\hbar}{2} & 0 \end{pmatrix} \right] \\ &= \text{Tr} \begin{pmatrix} \frac{\sqrt{2}i\hbar}{6} & -\frac{2i\hbar}{6} \\ \frac{i\hbar}{6} & -\frac{\sqrt{2}i\hbar}{6} \end{pmatrix} = 0 \end{aligned}$$

The results are same as in first example. Now we can give the properties of a pure state as below.

**Observations**

In all cases we can see that

$$\text{Tr } \rho = 1$$

$$\text{Tr } \rho^2 = 1$$

$$\text{Eigen value} = 1$$

Average spin is along one direction.

**5 Mixed states**

Now we will do same type of exercises for mixed states.

**Exercise**

Let  $|\psi\rangle = |0\rangle + |1\rangle$

$$\rho = |\psi\rangle\langle\psi| = (|0\rangle + |1\rangle)(\langle 0| + \langle 1|)$$

$$\rho = |0\rangle\langle 0| + |0\rangle\langle 1| + |1\rangle\langle 0| + |1\rangle\langle 1|$$

$$\rho = \begin{pmatrix} 1 & 1 \\ 1 & 1 \end{pmatrix}$$

$$\text{Tr } \rho = 1 + 1 = 2$$

This is not a pure state and is not physically acceptable. Some text books gives examples for state vector for mixed state like above. But we can see that total probability is greater than 1. This shows that we cannot write a single vector for a mixed state, but we can only define density matrix for a mixed state. The form of density matrix for a mixed state is

$$\rho = p_1 |0\rangle\langle 0| + p_2 |1\rangle\langle 1|$$

for the chosen basis vectors. For general case

$$\rho = p_1 |\phi_1\rangle\langle\phi_1| + p_2 |\phi_2\rangle\langle\phi_2|$$

$$\rho = p |\phi_1\rangle\langle\phi_1| + (1 - p) |\phi_2\rangle\langle\phi_2|$$

The density matrices are chosen such that there is no superposition and each part remains independent.

**Exercise**

Consider a case  $\rho = \frac{1}{2} |0\rangle\langle 0| + \frac{1}{2} |1\rangle\langle 1|$

Therefore,

$$\rho = \begin{pmatrix} \frac{1}{2} & 0 \\ 0 & \frac{1}{2} \end{pmatrix}$$

$$\text{Tr } \rho = \frac{1}{2} + \frac{1}{2} = 1$$

$$\rho^2 = \begin{pmatrix} \frac{1}{2} & 0 \\ 0 & \frac{1}{2} \end{pmatrix} \begin{pmatrix} \frac{1}{2} & 0 \\ 0 & \frac{1}{2} \end{pmatrix} = \begin{pmatrix} \frac{1}{4} & 0 \\ 0 & \frac{1}{4} \end{pmatrix}$$

$$\text{Tr } \rho^2 = \frac{1}{4} + \frac{1}{4} < 1$$

The eigen value equation is

$$\begin{vmatrix} \frac{1}{2} - \lambda & 0 \\ 0 & \frac{1}{2} - \lambda \end{vmatrix} = 0$$

Solving we get,  $\lambda_1 = \frac{1}{2}$   $\lambda_2 = \frac{1}{2}$

$$\begin{aligned} \langle S_x \rangle &= \text{Tr} \left[ \begin{pmatrix} \frac{1}{2} & 0 \\ 0 & \frac{1}{2} \end{pmatrix} \begin{pmatrix} 0 & \frac{\hbar}{2} \\ \frac{\hbar}{2} & 0 \end{pmatrix} \right] \\ &= \text{Tr} \begin{pmatrix} 0 & \frac{\hbar}{4} \\ \frac{\hbar}{4} & 0 \end{pmatrix} = 0 \end{aligned}$$

$$\begin{aligned} \langle S_y \rangle &= \text{Tr} \left[ \begin{pmatrix} \frac{1}{2} & 0 \\ 0 & \frac{1}{2} \end{pmatrix} \begin{pmatrix} 0 & -\frac{i\hbar}{2} \\ \frac{i\hbar}{2} & 0 \end{pmatrix} \right] \\ &= \text{Tr} \begin{pmatrix} 0 & -\frac{i\hbar}{4} \\ \frac{i\hbar}{4} & 0 \end{pmatrix} = 0 \end{aligned}$$

**Exercise**

Consider another case ,  $\rho = \frac{3}{4} |0\rangle\langle 0| + \frac{1}{4} |1\rangle\langle 1|$

$$\rho = \begin{pmatrix} \frac{3}{4} & 0 \\ 0 & \frac{1}{4} \end{pmatrix}$$

$$\text{Tr } \rho = \frac{3}{4} + \frac{1}{4} = 1$$

$$\rho^2 = \begin{pmatrix} \frac{3}{4} & 0 \\ 0 & \frac{1}{4} \end{pmatrix} \begin{pmatrix} \frac{3}{4} & 0 \\ 0 & \frac{1}{4} \end{pmatrix} = \begin{pmatrix} \frac{9}{16} & 0 \\ 0 & \frac{1}{16} \end{pmatrix}$$

$$\text{Tr } \rho^2 = \frac{9}{16} + \frac{1}{16} < 1$$

The eigen value equation is

$$\begin{vmatrix} \frac{3}{4} - \lambda & 0 \\ 0 & \frac{1}{4} - \lambda \end{vmatrix} = 0$$

Solving we get,  $\lambda_1 = \frac{3}{4}$   $\lambda_2 = \frac{1}{4}$

$$\begin{aligned} \langle S_x \rangle &= \text{Tr} \left[ \begin{pmatrix} 0 & \frac{\hbar}{2} \\ \frac{\hbar}{2} & 0 \end{pmatrix} \begin{pmatrix} \frac{3}{4} & 0 \\ 0 & \frac{1}{4} \end{pmatrix} \right] \\ &= \text{Tr} \begin{pmatrix} 0 & \frac{\hbar}{8} \\ \frac{3\hbar}{8} & 0 \end{pmatrix} = 0 \end{aligned}$$

$$\begin{aligned} \langle S_y \rangle &= \text{Tr} \left[ \begin{pmatrix} 0 & -\frac{i\hbar}{2} \\ \frac{i\hbar}{2} & 0 \end{pmatrix} \begin{pmatrix} \frac{3}{4} & 0 \\ 0 & \frac{1}{4} \end{pmatrix} \right] \\ &= \text{Tr} \begin{pmatrix} 0 & -\frac{i\hbar}{8} \\ \frac{3i\hbar}{8} & 0 \end{pmatrix} = 0 \end{aligned}$$

**Observations**

In all physical cases for mixed systems we can see that

$$\text{Tr } \rho = 1$$

$$\text{Tr } \rho^2 < 1$$

Eigen values  $\neq 1$

Average spin along any direction is = 0.

Thus for mixed states we will never get a single eigen value and there will no effective or average value.

**6 Conclusions**

In this article we tried to give a clear difference between pure and mixed systems. There is no superposition in mixed systems. We had used large number of exercises to make clarity on density matrix, pure state and mixed state. Density matrix happens to be a hard nut to crack for both students and teachers. We hope our article will help them to learn it in a better way.

**References**

- [1] J. von Neumann. Mathematical Basis of Quantum Mechanics, (Nauka, Moscow, 1964)
- [2] L. Landau(1927). Das Dmpfungsproblem in der Wellenmechanik, Z. Phys. 45, 430441
- [3] K. Blum. Density Matrix Theory and Application, (Plenum Press, New York, 1981)
- [4] B. V. Bondarev. Density Matrix Method in Quantum Cooperative Process Theory, (Sputnik, Moscow, 2013)
- [5] Y. R. Shen(1967). Phys.Rev. 155, 921
- [6] B. V. Bondarev(1991). Physica.A 176, 366

- [7] B. V. Bondarev(1992). *Physica.A* 184, 205
- [8] B. V. Bondarev(1992). *Physica.A* 183, 159
- [9] B. V. Bondarev(1994). *Theor.Mat.Fiz.* 100, 33
- [10] Gibbs, Josiah Willard. *Principles in Statistical Mechanics*, (New York: Charles Scribner's Sons, 1902)
- [11] K. Huang. *Introduction to Statistical Physics*, (Chapman and Hall/CRC 2009)
- [12] R. K. Pathria and P. D. Beale. *Statistical Mechanics*, (Butterworth 2009)

# Simulation of Vibrational Spectrum of Diatomic Molecules Using Morse Potential by Matrix Methods in Gnumeric Worksheet

O.S.K.S Sastri<sup>1</sup>, Aditi Sharma, Shikha Awasthi, Anil Khachi and Lalit Kumar

Department of Physical and Astronomical Sciences  
Central University of Himachal Pradesh, HP 176215, Bharat(India)

<sup>1</sup>sastri.osks@gmail.com

*Submitted 18-09-2020*

## Abstract

The vibrational energy levels of a non-homogeneous diatomic molecule are obtained by solving Time Independent Schrodinger equation (TISE) by choosing Morse potential. Here, we solve this problem using matrix method based numerical technique. The central idea is to embed the Morse potential within an infinite square well potential whose wave functions are chosen as the basis to obtain the H-matrix. The numerical method is implemented in free open source software (FOSS) Gnumeric, a worksheet environment. Relationships, between model parameters of Morse potential and parameter data available from NIST, have been obtained using analytical expressions resulting from solution of TISE using Nikiforov-Uvarov (NU) method. Energy eigenvalues of diatomic molecule HCl are obtained to determine its vibrational

frequencies to an accuracy  $\leq 0.21\%$ . Finally, the fundamental vibrational frequency of various diatomic molecules such as HBr, HI, HF, CO and NO, are determined and have been found to be matching with expected values to an accuracy of  $\leq 0.03\%$ .

**Keywords:** Vibrational Spectra, Diatomic molecules, Morse potential, Matrix method, Gnumeric Worksheet

## 1 Introduction

Numerical methods to solve physics problems adds a third dimension to doing and learning physics alongside theoretical modeling and experimental observations. UGC curriculum for B.Sc.(Hons) in Physics [1] has taken the bold step of introducing simulation problems in various courses such as quantum mechanics (QM), statistical physics and all mathematical physics courses. Previously, we have performed cer-

tain simulations for teaching and learning fundamental concepts in statistical physics using worksheets [2] and Scilab programming environment [3, 4]. Here, we look at the suggested lab for QM, that involves solving the TISE for Hydrogen atom Coulomb potential, Yukawa-type screened Coulomb potential, anharmonic oscillator and Morse potentials. Typically the numerical methods employed to solve these potentials involves either Runge-Kutta or Numerov methods. Marsiglio et. al have introduced the idea of using 1-D particle in a box wavefunctions to be employed as a basis for solving TISE using matrix methods for HO[5] and extended it to study central potentials[6]. Our PER group has applied this method for solving Woods-Saxon potential to obtain single-particle energies of magic nuclei within the shell model across the periodic table[7]. Another interesting implementation from a pedagogical perspective is the use of worksheet environment for solving the hamiltonian matrix for its eigenvalues and eigenfunctions. We have used Gnumeric software (FOSS) for solving harmonic oscillator (HO), Anharmonic oscillator (AHO) and quartic oscillators (QO) and obtained their energy levels and wavefunctions[8].

Just as experimental labs require a process to ensure appropriate learning and development of skill sets, similarly a simulation activity should be implemented with a systematic step by step approach for it to be effective. We have suggested such an approach for performing simulations through

a previous paper[9] in this journal by solving the square well potential. In this paper, the solution of TISE for Morse potential using matrix methods based on Fourier basis using Gnumeric worksheet environment is discussed.

In this article, our foremost step is to discuss how to model a non-homogeneous diatomic molecule using four stage process proposed by Hestenes.[10] Then, the numerical method chosen to solve Schrodinger equation is elaborated along with system preparation in appropriate set of units and discretising the variables involved by uniformly sampling them within the region of interest (ROI). Further, we briefly discuss the algorithm for implementation which is tested for obtaining the vibrational frequency of HCl using harmonic oscillator potential in Gnumeric. Finally, results are simulated for obtaining the first five vibrational frequencies of HCl and fundamental frequencies of various other diatomic non-homogeneous molecules.

## 2 Modelling theory of diatomic molecule undergoing vibration and rotation

### A. Description stage

- **Object description:**

- **Object type:** A linear non-homogeneous diatomic molecule.
- **Object composition:** Classically, such a molecule (for eg. HCl) is

composed of two ions, of which, one is highly electro-negative (Cl) than the other (H) and they form a bond to complete their respective outer shell configurations to attain stability. The resultant molecule has a permanent dipole moment.

In quantum domain, we treat them simply as two atoms that together have smaller energy than their respective rest mass energies, which binds them together.

– **Object variables:**

- \* Size of two atoms, specified by their radii,  $R_A$  and  $R_B$ .
- \* In atoms A and B, there are nuclei  $N_A$  &  $N_B$  having masses  $m_A$  &  $m_B$ , with positive charges  $Z_A$  &  $Z_B$ , respectively and electrons( $e^-$ ) with same values of negative charges.

• **Interaction description:**

- **Type of Interaction:** Both the atoms are executing vibrational and rotational motion, even as the diatomic molecule as a whole is undergoing translational motion.
- **Interaction agent:** Classically, a molecule with permanent dipole moment  $\bar{\mu}_N$  has an electromagnetic character. Since  $\bar{\mu}_N$  changes with respect to time, as its individual ions vibrate about an equilibrium distance and the

molecule executes rotation in a direction perpendicular to bond axis, it interacts with the incoming electromagnetic(EM) radiation.[16]

**Quantum perspective:** The two atoms are having positive nuclei with electrons surrounding them in orbits. One needs to consider all possible electromagnetic interactions i.e the  $e^- - e^-$ ,  $N_A - N_B$  repulsion and  $e^- - N_A$  &  $e^- - N_B$  attraction. As the masses involved are too small, the gravitational interaction could be neglected.

**Born-Oppenheimer Approximation:** Masses of nuclei are relatively very large (an order of  $10^3$  or more) as compared to mass of electron. So, kinetic energy of nuclei can be considered to be negligible in comparison to that of electrons. This is also called clamped nuclei approximation, by which the nuclear co-ordinates are considered to not change and become parameters for determining the minimum energy for the  $e^-$  density. Mathematically this approximation allows decoupling of electron and nuclear motion in the sense that total energy is written as sum of nuclear and electronic energies and total wavefunction as product of individual wavefunctions.[11]

– **Interaction variables:**

- \* Equilibrium bond length,  $R_e$ .
- \* Bond strength,  $k$  reflects the vibrational frequency of molecule.
- \* Dissociation energy of molecule,  $D_e$ .
- \* Rotational frequency,  $\nu_e$  of molecule resulting from centrifugal force.

- **Process description:**

- **Reference system:** Two-body system is replaced with one-body system by making a transformation from  $(\bar{R}_A, \bar{R}_B)$  to  $(\bar{R}_{CM}, \bar{R})$ . While translational motion results from Center of Mass co-ordinate  $\bar{R}_{CM}$ , variation of relative position vector  $\bar{R}$  describes the internal motion of nuclei resulting in both vibrational and rotational degrees of freedom. As electromagnetic force is purely a function of relative distance  $R$ , the problem could be treated as that of a central force having spherical symmetry. Hence, the ideal choice of reference system would be spherical polar co-ordinates  $(R, \theta, \phi)$ .
- **State variables:** The quantum mechanical state of the resultant one body system would be  $\Psi(R, \theta, \phi)$  separable into  $\chi_{vib}(R)\chi_{rot}(\theta, \phi)$  with corresponding vibrational and rotational energies  $E_{vib}$  and  $E_{rot}$  respectively.

### Formulation Stage:

- **Interaction law:** The three electromagnetic interactions can be modelled mathematically as:

- **$e^- - e^-$  repulsion:** If there are  $N$  electrons in the two nuclei comprising the diatomic molecule, then the repulsive potential is given by

$$V_{e^- - e^-} = \sum_{i=1}^{N-1} \sum_{j=i+1}^N \frac{e^2}{4\pi\epsilon_0 r_{ij}} \quad (1)$$

where  $r_{ij} = |\bar{r}_i - \bar{r}_j|$  is the distance between  $i^{th} e^-$  and  $j^{th} e^-$ .

- **$N_A - N_B$  repulsion:** The repulsive interaction between the two positively charged nuclei with charges  $Z_A$  and  $Z_B$  is given by

$$V_{N-N} = \frac{Z_A Z_B e^2}{4\pi\epsilon_0 R_{AB}} \quad (2)$$

where  $R_{AB} = |\bar{R}_A - \bar{R}_B|$

- **$e^- - N$  attraction:** Each of the  $N e^-$ s experience attractive potential due to the two nuclei  $N_A$  and  $N_B$  and total interaction is given by

$$V_{e^- - N} = \sum_{i=1}^N \sum_{j=A,B} \frac{-Z_j e^2}{4\pi\epsilon_0 |\bar{r}_i - \bar{R}_j|} \quad (3)$$

and is dependent on the distance between  $i^{th} e^-$  and  $j^{th}$  nuclei.

- **Dynamical law:** The motion at microscopic level is governed by

Time-dependent Schrodinger equation(TDSE)

$$i\hbar \frac{\partial \Psi(\bar{r}_i, \bar{R}_j, t)}{\partial t} = H\Psi(\bar{r}_i, \bar{R}_j, t) \quad (4)$$

where  $\Psi(\bar{r}_i, \bar{R}_j, t)$  is state wave-function of two-body system with  $\bar{r}_i$  and  $\bar{R}_j$  denoting the position vectors of  $i^{th}e^-$  and  $j^{th}$  nucleus respectively.

Using separation of variables technique,  $\Psi(\bar{r}_i, \bar{R}_j, t) = \Psi(\bar{r}_i, \bar{R}_j)T(t)$ , we obtain TISE as

$$H\Psi(\bar{r}_i, \bar{R}_j) = E\Psi(\bar{r}_i, \bar{R}_j) \quad (5)$$

and  $T(t) = e^{-iEt/\hbar}$

The hamiltonian for a diatomic molecule is given by

$$H = \left( -\frac{\hbar^2}{2m_A} \frac{\partial^2}{\partial \bar{R}_A^2} - \frac{\hbar^2}{2m_B} \frac{\partial^2}{\partial \bar{R}_B^2} \right) + \left( -\frac{\hbar^2}{2m_e} \sum_{i=1}^N \frac{\partial^2}{\partial \bar{r}_i^2} \right) + V_{N-N} + V_{e-N} + V_{e-e} \quad (6)$$

Using BO-approximation, we can express the wavefunction as product of  $e^-$  and nuclear wavefunctions as

$$\Psi(\bar{r}_i, \bar{R}_A, \bar{R}_B) = \phi_e(\bar{r}_i; \bar{R}_A, \bar{R}_B)\chi_N(\bar{R}_A, \bar{R}_B) \quad (7)$$

While the electronic wavefunction only varies with  $\bar{r}_i$ , it has parametric dependence on the nuclear co-ordinates  $\bar{R}_A$  and  $\bar{R}_B$ . Substituting in eq (5) and applying separation of variables tech-

nique, we get TISE for the electrons as

$$-\frac{\hbar^2}{2m_e} \sum_{i=1}^N \frac{\partial^2 \phi_e}{\partial \bar{r}_i^2} + [V_{e-N} + V_{e-e} + V_{NN}(R_{AB})]\phi_e = E_e \phi_e \quad (8)$$

and the TISE for nuclear vibrational and rotational motion as

$$\left( -\frac{\hbar^2}{2m_A} \frac{\partial^2}{\partial \bar{R}_A^2} - \frac{\hbar^2}{2m_B} \frac{\partial^2}{\partial \bar{R}_B^2} + U_e(R_{AB}) \right) \chi_N(\bar{R}_A, \bar{R}_B) = E \chi_N(\bar{R}_A, \bar{R}_B) \quad (9)$$

The nuclear motion happens in the electronic potential energy  $U_e(R_{AB})$ , which is obtained by determining ground state value  $E_e(\bar{r}_i; \bar{R}_A, \bar{R}_B)$  for different inter-nuclear distances  $R_{AB}$  using eq.(2). From here onwards, we drop subscript AB and write  $R_{AB}$  as simply R. The electronic potential energy curve attains a minima at an inter-nuclear distance  $R = R_e$ , called as equilibrium bond length. Now, for small variations in 'R' about  $R_e$ , the potential can be expanded in Taylor series as

$$U_e(R) = U_e(R_e) + \left( \frac{dU_e}{dR} \right)_{R=R_e} (R - R_e) + \frac{1}{2} \left( \frac{d^2U_e}{dR^2} \right)_{R=R_e} (R - R_e)^2 + \dots \quad (10)$$

Now,  $U_e(R_e)$  is only a constant and it has an effect of shifting all energy levels by a certain value. This value is chosen as reference potential and can be set to

zero. Since, potential has local minima at  $R = R_e$ , it's first derivative  $\frac{dU_e}{dR} = 0$ . Therefore, we obtain the HO approximation, by assuming all terms higher than second order to be negligible.

$$U_e(R) \approx \frac{1}{2}k(R - R_e)^2 = V_{HO}(R) \quad (11)$$

where  $k = \left(\frac{d^2U_e}{dR^2}\right)_{R=R_e}$  is a constant that reflects the bond strength. Generally, this is the form chosen for the potential in the first iteration while modeling vibrational motion of a diatomic molecule. But, the results do not match to a very good accuracy with this approximation and also only a single frequency is obtained that corresponds to the fundamental line in the actual vibrational spectrum, which has overtones as well. Hence, one needs to consider more terms in Taylor series. This was achieved by Morse who has proposed a potential of the form [12]

$$U_e(R) = D_e \left( e^{-2\alpha x} - 2e^{-\alpha x} \right) = V_M(R) \quad (12)$$

where  $x = \frac{(R-R_e)}{R_e}$  and  $\alpha = bR_e$ . The constant  $D_e$  is called dissociation energy of the molecule and typically reflects the depth of the attractive potential and  $\alpha$  describes the shape of the curve as it moves away from harmonicity and hence is termed as anharmonicity constant and is a characteristic that is different for various molecules. This is the potential using which the nuclear TISE, given by eq.(9),

can be solved for obtaining the vibrational and rotational wavefunctions and their corresponding energies  $E_{vib}$  and  $E_{rot}$  that specify the state of the system, which is fundamental goal of this paper.

### Transformation from Two Body to One-Body System:

Making the transformation from  $(\bar{R}_A, \bar{R}_B)$  to  $(\bar{R}_{CM}, \bar{R})$  gives TISE satisfied by reduced mass ' $\mu_N$ ' for relative position vector  $\bar{R}$  of the diatomic molecule as

$$\left[ \frac{-\hbar^2}{2\mu_N} \frac{\partial^2}{\partial \bar{R}^2} + U_e(R) \right] \chi_N(\bar{R}) = E \chi_N(\bar{R}) \quad (13)$$

### BO approximation to decouple vibrational and rotational motion:

From experimental data, we find that the rotational energy is three orders of magnitude less than that of vibrational energy. So, BO-approximation proposes to treat them as independent of each other. That is, total energy is given by  $E = E_{vib} + E_{rot}$  and  $\chi(\bar{R})$  can be written as a product of vibrational and rotational wavefunctions.

$$\chi(\bar{R}) = \chi_{vib}(R) \chi_{rot}(\theta, \phi) \quad (14)$$

Applying separation of variables technique[13], we obtain radial equation as

$$\left[ \frac{-\hbar^2}{2\mu_N} \left( \frac{1}{R^2} \frac{d}{dR} R^2 \frac{d}{dR} - \frac{J(J+1)}{R^2} \right) + U_e(R) \right] \chi_{vib}(R) = E \chi_{vib}(R) \quad (15)$$

where  $J$  is total angular momentum quantum number arising from  $\theta$  equation. Choosing  $\chi_{vib}(R) = S(R)/R$ , we obtain

$$\frac{d^2S(R)}{dR^2} + \frac{2\mu_N}{\hbar^2} \left[ E - U_e(R) - \frac{J(J+1)\hbar^2}{2\mu_N R^2} \right] S(R) = 0 \quad (16)$$

So, an effective vibrational potential can be defined as  $U_{eff}(R) = U_e(R) + \frac{J(J+1)\hbar^2}{2\mu_N R^2}$ , in which second term represents centrifugal potential that gives rise to rotational levels of the molecule. Here, we focus only on vibrational spectra of diatomic molecule, by considering  $J = 0$  case.

#### Ramification Stage:

Our aim in this paper is to numerically solve TISE in eq.(16), using Morse potential in eq.(12). This requires model parameters  $D_e$ ,  $b$  and  $R_e$ . In NIST chemistry webbook, compiled by Huber & Herzberg, spectroscopic information on diatomic molecules that are given by taking into account both theoretical and experimental studies. Theoretically, formula utilized to calculate term values by considering anharmonic oscillator model (Morse potential) is[16]

$$\varepsilon(v, J) = \omega_e \left( v + \frac{1}{2} \right) - \omega_e x_e \left( v + \frac{1}{2} \right)^2 \quad (17)$$

The data comprises of molecular constants for various molecular states. But, no information is given on model parameters for Morse potential. Rather, constants like  $\omega_e$ ,  $\omega_e x_e$ ,  $R_e$  and others are given. To obtain

the relationships between required model parameters  $D_e$  and  $b$  in terms of the available parameters  $\omega_e$  and  $\omega_e x_e$  in NIST, we had to take recourse to analytical solution of formulated mathematical model in eq.(16). Methods like Nikiforov- Uvarov (NU)[14] and asymptotic iteration (AIM)[15] are employed to solve TISE for rotating Morse potential under Pekeris approximation to obtain analytical expressions for energy eigenvalues and corresponding eigenfunctions. Here, we consider only non-rotating part of the Morse potential solution obtained by NU method[14]. The reduced energy expression ( $E_n$ ) for determining energies is

$$E_n = -\frac{\hbar^2 a^2}{2\mu_N} \left[ \frac{\epsilon_2}{2\sqrt{\epsilon_3}} - \left( n + \frac{1}{2} \right) \right]^2 \quad (18)$$

where

$$\frac{\epsilon_2}{2\sqrt{\epsilon_3}} = \frac{2\mu_N D_e}{b^2 \hbar^2 \sqrt{\epsilon_3}}$$

and

$$\sqrt{\epsilon_3} = \frac{2\mu_N R_e^2 D_e}{\hbar^2 b^2 R_e^2}$$

The model parameters ( $D_e$  and  $b$ ) are solved for, in terms of  $\omega_e$  and  $\omega_e x_e$ , and satisfy the following relations:

$$D_e = \frac{\omega_e^2}{4\omega_e x_e} \quad (19)$$

and

$$b = \sqrt{\frac{2\mu_N \omega_e x_e}{\hbar^2}} \quad (20)$$

While  $D_e$  is in eV and  $b$  is in  $\text{\AA}^{-1}$ , the parameters,  $\omega_e$  and  $\omega_e x_e$  are in  $cm^{-1}$ . One can use

the following conversion relation between  $cm^{-1}$  and  $eV$  [17]:

$$1cm^{-1} = 1.2397 \times 10^{-4}eV \quad (21)$$

#### Emergent Properties:

**Selection rules** The transitions between various vibrational energy levels satisfy [16]

$$\Delta v = \pm 1, \pm 2, \pm 3, \dots \quad (22)$$

**Vibrational Spectrum:** The analytical expressions for vibrational frequencies corresponding to absorption are given by [18]

$$\bar{\nu}_{0 \rightarrow n} = \bar{\omega}_e(n - n(n+1)x_e)cm^{-1}$$

**Validation stage:** From molecular data for various diatomic molecules compiled by Huber & Herzberg [20],  $D_e$ ,  $b$  are determined using Eqs. (19) and (20) for six diatomic heterogeneous molecules to four decimal places. These calculated values along with  $R_e$  data are compiled in Table 1. Now, using these parameters in numerical

Table 1: Model parameters for Morse Potential deduced from NIST data

Molecules	$D_e(eV)$	$b(\text{\AA}^{-1})$	$R_e(\text{\AA})$
HCl	5.2491	1.7518	1.2745
HF	6.0882	2.2232	0.9169
HBr	4.8096	1.6339	1.4144
HI	4.1681	1.5333	1.6092
CO	10.9807	2.3246	1.1283
NO	7.9842	2.4966	1.1508

matrix method algorithm, energy eigenvalues for these molecules are obtained. The frequencies obtained from these energies on simulation are to be validated with experimental values.

## 3 Preparation of system for numerical solution

### 3.1 Choice of numerical technique

TISE is often solved using Runge-Kutta method, central divided difference and Numerov methods. In this paper, we focus on matrix diagonalization technique suggested by Marsiglio [5, 19] which is fast, highly efficient and gives accurate results as compared with the mentioned methods.

**Matrix method:** In this approach, the potential of interest  $U_e(R)$  is embedded within an infinite square well potential  $[0, a_0]$ , where  $a_0$  is the width chosen to be certain cut-off radius for central potentials. This is equivalent to writing eq. (16) as

$$\left[ \frac{-\hbar^2}{2\mu_N} \frac{d^2}{dR^2} + V_{inf}(R) + U_{eff}(R) \right] S(R) = ES(R) \quad (23)$$

which can be rewritten as

$$\left[ H_0 + U_{eff}(R) \right] S(R) = ES(R) \quad (24)$$

where  $H_0$  is the hamiltonian of the infinite square well potential, whose eigen values are given by

$$E_n^{inf} = \frac{n^2 \pi^2 \hbar^2}{2\mu_N a_0^2} = n^2 E_1^{inf} \quad (25)$$

with corresponding eigen functions as

$$\phi_n(R) = \sqrt{\frac{2}{a_0}} \sin\left(\frac{n\pi R}{a_0}\right) \quad (26)$$

Expanding radial wavefunction  $S(R)$  in terms of infinite square well eigenfunctions

as the choice of basis functions  $\phi_n(R)$ , we have

$$S(R) = \sum_{n=0}^{\infty} c_n \phi_n(R) = \sqrt{\frac{2}{a_0}} \sum_{n=0}^{\infty} c_n \sin\left(\frac{n\pi R}{a_0}\right) \quad (27)$$

where,  $c_n$  are coefficients that need to be determined. Multiply eq.(24) by  $\phi_m^*(R)$  and integrating over 0 to  $a_0$ , and substituting the expansion from eq.(27), one obtains

$$\begin{aligned} \int_0^{a_0} \left( \phi_m^*(R) [H_0 + U_e(R)] \sum_{n=1}^{\infty} c_n \phi_n(R) \right) dR \\ = E \int_0^{a_0} \left( \phi_m^*(R) \sum_{n=1}^{\infty} c_n \phi_n(R) \right) dR \end{aligned} \quad (28)$$

Using eigen value equation  $H_0 \phi_n(R) = E_n^{inf} \phi_n(R)$  and orthonormality condition,  $\int_0^{a_0} \phi_m^*(R) \phi_n(R) dR = 1$ , it reduces to

$$E_m^{inf} c_m + \sum_{n=0}^{\infty} V_{mn} c_n = E c_m \quad (29)$$

or

$$\sum_{n=1}^{\infty} H_{mn} c_n = E c_m \quad \text{for } m = 1, 2, 3, \dots \quad (30)$$

where  $H_{nm}$  is an infinite dimensional square symmetric matrix and  $V_{mn}$  is given by

$$V_{mn} = \int_0^{a_0} \phi_m^*(R) U_e(R) \phi_n(R) dR \quad (31)$$

We need to choose a finite number of basis functions, say  $N_0$  for solving the problem numerically. The parameters  $a_0$  and  $N_0$  introduced into the technique are related to the algorithm and are adjusted to ensure convergence to expected results from experiment.

### 3.2 Rephrasing of units

We will begin by choosing an appropriate set of units so as to avoid large round-off errors while doing computations which could arise due to very large or very small numbers in the numerical problem being solved. In atomic and molecular physics, energy is measured in hartree or eV, distances in nm or Å and frequencies in wavenumbers as  $\text{cm}^{-1}$ . Here, we prefer to opt unit of energy as eV and distance as Å for numerical calculations.

**Rephrasing of ground state energy term in eV:**  $E_1^{inf}$  is modified as

$$E_1^{inf} = \frac{\pi^2 \hbar^2}{2\mu_N a_0^2} = \frac{\pi^2 (\hbar c)^2}{2(\mu_N c^2) a_0^2 \times 10^6} eV \quad (32)$$

where  $\mu_N$  is reduced mass of diatomic molecule expressed in  $eV/c^2$  and  $\hbar c = 1973.29 eV \text{Å}$ .

### 3.3 Discretizing continuous variable

For doing simulation in computers, it is essential to discretize continuous variable  $R$  with appropriate step-size and restrict it to a finite region of interest  $[0, a_0]$ .

## 4 Implementation of Numerical Method:

### 4.1 Algorithm

1. **Initialisation:** The object variable such as masses of atoms in the diatomic molecule are taken from standard

databases and the reduced mass is determined. The interaction variables are the model parameters for a particular molecule as per those obtained using theoretical considerations and presented in Table 1. Other initialisations include the conversion factors that are required for calculations.

- Potential definition:** The HO potential is chosen to be embedded within an infinite square well potential of width  $a_0$ , and is given by

$$V_{HO}(R) = \frac{1}{2}k(R - R_e)^2 \quad (33)$$

and including anharmonicity as in Morse potential, is written as

$$V_M(R) = D_e \left[ e^{-2\alpha\left(\frac{R-R_e}{R_e}\right)} - 2e^{-\alpha\left(\frac{R-R_e}{R_e}\right)} \right] \quad (34)$$

- Defining  $H_{mn}$  matrix:** In matrix method, hamiltonian matrix ( $H_{mn}$ ) defined in eq.(30) will be a square symmetric matrix consisting of diagonal and non-diagonal elements respectively. Now, for both HO and Morse potential ( $J = 0$ ), integrals can be obtained analytically.

The hamiltonian matrix for **HO potential** is given as eq.(35)

$$H_{mm}^{HO} = \begin{cases} \frac{m^2\pi^2\hbar^2}{2\mu_N a_0^2} + \frac{ka_0^2}{2} \left( \frac{1}{12} - \frac{2}{(2m\pi)^2} \right), & \text{for } m = n \\ \frac{ka_0^2}{2} \left[ \left( \frac{2(-1)^{n-m}\pi+1}{((n-m)\pi)^2} \right) - \left( \frac{2(-1)^{n+m}\pi+1}{((n+m)\pi)^2} \right) \right], & \text{for } m \neq n \end{cases}$$

and for **Morse potential** as eq.(36)

$$H_{mn} = \begin{cases} m^2 E_1^{inf} + \frac{De}{a_0} \left[ \left( \frac{\exp(2bR_e) - \exp(-2b(a_0 - R_e))}{2b} \right) + 2 \left( \frac{\exp(-b(a_0 - R_e)) - \exp(bR_e)}{b} \right) - \frac{a_0^2 b}{2} \left( \frac{\exp(2bR_e) - \exp(-2b(a_0 - x_0))}{a_0^2 b^2 + m^2 \pi^2} \right) + 2a_0^2 b \left( \frac{\exp(bR_e) - \exp(-b(a_0 - R_e))}{a_0^2 b^2 + 4m^2 \pi^2} \right) \right], & \text{for } m = n \\ \frac{De}{a_0} \left[ 2a_0^2 b \left( \frac{\exp(2bR_e) - (-1)^{n-m} \exp(-2b(a_0 - R_e))}{4a_0^2 b^2 + (n-m)^2 \pi^2} \right) - 2a_0^2 b \left( \frac{\exp(2bR_e) - (-1)^{n+m} \exp(-2b(a_0 - R_e))}{4a_0^2 b^2 + (n+m)^2 \pi^2} \right) - 2a_0^2 b \left( \frac{\exp(bR_e) - (-1)^{n-m} \exp(-b(a_0 - R_e))}{a_0^2 b^2 + (n-m)^2 \pi^2} \right) + 2a_0^2 b \left( \frac{\exp(bR_e) - (-1)^{n+m} \exp(-b(a_0 - R_e))}{a_0^2 b^2 + (n+m)^2 \pi^2} \right) \right], & \text{for } m \neq n \end{cases}$$

- Obtaining eigen values:** In Gnumeric, ‘eigen’ command can be used to obtain energy eigenvalues and their corresponding eigen-vectors for a symmetric matrix.

#### 4.2 Implementation in Gnumeric:

The steps for implementing a general HO potential have been elucidated in the Appendix in [8]. A similar procedure has been followed to set up the simulation for HO potential for HCl molecule and has been used as known problem to test the correctness of the implementation.

#### 4.3 Testing the correctness using HO potential for HCl molecule:

First initialise reduced mass  $\mu_N = 0.9796 * 931.49410 * 10^6 eV/c^2$  and  $k = 32.2252 eV$

for HCl molecule and set factor  $\hbar c = 1973.29 eV \text{ \AA}$ . Then, the numerical algorithm parameters infinite well width  $a_0$  and number of basis functions  $N_0$  need to be varied so as to obtain convergence of simulation results to those of expected values. The energies of HO potential for HCl molecule are obtained and their difference gives its vibrational frequency. For this, we begin with  $a_0 = 4 \text{ \AA}$  and  $N_0 = 20$ . Using these, energy values are determined in eV but these have to be converted into wavenumbers by dividing each of them with a factor of  $hc = 1239.8419 \times 10^{-7} eV - cm$ . Taking the difference of values by using transition rule, the vibration frequency  $\bar{\omega}_{HO}$  is calculated to be  $3357.1566 cm^{-1}$ . But, this value is in large deviation to the expected value of  $2886 cm^{-1}$ [18]. So,  $N_0$  is increased further in steps of 10, so as to obtain convergence in energy values. Beyond  $N_0 = 70$ , it has been observed that there has been no further change in the first six energy eigenvalues upto four decimal places. Hence, for  $N_0 = 70$  and  $a_0 = 4 \text{ \AA}$ , the vibrational frequency of HCl is obtained as  $\bar{\omega}_{HO} = 2990.9418 cm^{-1}$ , which is closer to reported value, i.e  $2885.9 cm^{-1}$  with 3.64% error. This confirms that the implementation correctly obtains the solutions of TISE using matrix methods approach and is ready for simulating for other variations in H-matrix elements.

## 5 Simulation and Discussion of Results:

### 5.1 Study of HCl using Morse potential:

In order to study the vibration spectra of HCl molecule by considering Morse potential, the H-matrix elements are generated in Gnumeric, by using eq.(36). The model parameters given in Table 1 are initialised. Now, on plotting Morse function, it is observed that the potential gets saturated after  $4 \text{ \AA}$  ). Hence,  $a_0$  is chosen as 4 and similar to the test case, for  $N_0 \geq 70$ , the first six energy values (in eV) have been found to converge to four decimal places (as shown in column 3 of Table 2). Analytical energy values are also obtained using NU method expression in eq.(18), which are tabulated in column 2. It can be seen that both analytical and numerical results agree exactly upto four decimal places. After converting these value into wavenumbers, fundamental vibration frequency and first four overtones (column 4) are calculated by using selection rules and are compared with those observed (given in column 1) and % errors are determined (in column 5). One can observe that maximum error obtained is only 0.21%. One can also observe that while the HO model predicts only the fundamental frequency, the anharmonic oscillator model with Morse potential gives the experimentally observed overtones as well. Further, the fundamental frequency in this case is merely having an error of 0.03% as compared to 3.64% in HO case, confirming both higher accuracy and better

Table 2: HCl vibration spectra obtained from matrix method (MM) by calculating parameter values from NIST database[20] and choosing algorithmic parameter values as  $a_0 = 4\text{\AA}$  and  $N_0 = 70$ .

$n$	$\bar{\nu}_{0 \rightarrow n}^{exp.} (cm^{-1})$	Energy values(eV)		$\epsilon_{v'', J''=0} (cm^{-1})$	$\bar{\nu}_{0 \rightarrow n}^{MM} (cm^{-1})$	% error
		$E_{anal.}^{NU}$	$E_{sim}^{MM}$			
1	2886	-5.0653	-5.0653	-40854.7725	2885	0.03
2	5668	-4.7077	-4.7077	-37969.8378	5664	0.07
3	8347	-4.3631	-4.3631	-35190.5255	8338	0.11
4	10923	-4.0316	-4.0316	-32516.8354	10906	0.16
5	13396	-3.7132	-3.7132	-29948.7677	13368	0.21
		-3.4079	-3.4079	-27486.3224		

predictive capability of the AHO (based on Morse potential) model.

## 5.2 Simulation for other diatomic molecules

We obtain fundamental vibration frequency of other diatomic heterogeneous molecules such as HF, HBr, HI, CO and NO respectively. Now, we need to only change the model parameters in the initialisation step and rest of the implementation remains unchanged. Utilising the model parameters tabulated in Table 1, first two energy values for each of the molecules have been determined with same choice of  $a_0$  and  $N_0$ . The energy values are also determined using analytical expression of eq.(18) and are once again observed to match with the simulated to four decimal places. Using these energy values, fundamental vibration frequency for each of the molecules considered is determined and is compared with experimentally

observed value [20] along with corresponding % error. All these data are presented in Table. 3 and one can observe that error is  $\leq 0.03\%$ .

## 6 Conclusion

In this paper, the vibrational spectra of non-homogeneous diatomic molecules have been modeled using Morse potential and the resulting TISE has been solved using matrix methods technique with sine wavefunctions of infinite square well potential chosen as basis. The model Morse potential parameters  $D_e$  and  $b$  are deduced from  $\omega_e$  and  $\omega_e x_e$  available from NIST. The numerically simulated energy eigenvalues have been found to be exactly matching to four decimal places with the analytical solutions obtained from the solution of TISE using NU method. It has been conclusively seen that the fundamental frequency of HCl molecule

Table 3: Fundamental vibration frequencies calculated for five diatomic molecules.

Molecules	E(eV)	$\epsilon_{v'',j''=0}(cm^{-1})$	$\bar{\nu}_{0 \rightarrow 1}^{sim}(cm^{-1})$	$\bar{\nu}_{0 \rightarrow 1}^{exp}(cm^{-1})$	%error
HF	-5.9038	-47617.1531	2906.39	2906.67	0.01
	-5.5434	-44710.7979			
HBr	-4.6476	-37485.4414	2558.26	2558.54	0.01
	-4.3304	-62051.9472			
HI	-4.0262	-32473.5460	2229.44	2229.72	0.01
	-3.7498	-30244.1038			
CO	-10.8466	-87483.8618	2142.98	2143.24	0.01
	-10.5809	-92782.7550			
NO	-7.8666	-63448.5817	1875.57	1876.05	0.03
	-7.6341	-61573.0120			

obtained from HO potential is far less accurate as compared to that obtained from AHO modeled using Morse potential. Further, the fundamental frequencies of various other diatomic molecules studied have also given results matching with experimental values to less than 0.03%. To establish numerical simulation procedure as an independent methodology to solve physics problems without recourse to analytical solutions, it is required to optimize the model parameters directly from the algorithm by matching the simulated results with the experimental values by reducing the  $\chi^2$  values. Such a procedure using variational Monte-Carlo (VMC) approach is being attempted.

## References

- [1] [https://www.ugc.ac.in/pdfnews/7870779\\_B.SC.PROGRAM-PHYSICS.pdf](https://www.ugc.ac.in/pdfnews/7870779_B.SC.PROGRAM-PHYSICS.pdf).
- [2] Sharda, V., Sastri, O. S. K. S., Bhardwaj, J., & Jha, A. K. (2016), "A computer simulation using spreadsheets for learning concept of steady-state equilibrium", *Physics Education* 51, no. 2, (2016): 025007.
- [3] Sharda, V., Bhardwaj, J., Sastri, O. S. K. S., & Jha, A. "A. Learning to Construct Boltzmann Distribution Concept: Using Computer Simulation Activity", *International Education Conference, Learning Technology in Education*, (2015): 367-374.
- [4] Aditya, Abhishek, Ravikanth and Sastri O.S.K.S, "Computer Simulation Approach to Teaching Fundamental Ideas

- in *Statistical Physics*", THE BEDE ATHENAEUM 3, no. 1, (2012): 1-5.
- [5] Marsiglio F., "The Harmonic Oscillator in Quantum Mechanics: A third way", *American Association of Physics Teachers* 77, no. 3, (2009): 253-258.
- [6] Jugdutt B.A. and Marsiglio F., "Solving for three-dimensional central potentials using numerical matrix methods", *American Association of Physics Teachers* 81, no. 5, (2013): 345-346.
- [7] Aditi Sharma et al., "Simulation study of nuclear shell model using sine basis", *American Journal of Physics* 88 (2020): 576-585.
- [8] Aditi Sharma and O. S. K. S. Sastri, "Numerical simulation of quantum anharmonic oscillator, embedded within an infinite square well potential, by matrix methods using gnumeric spreadsheet", *European Journal of Physics* (2020):1-20.
- [9] O. S. K. S. Sastri et al, "Numerical solution of square well potential with matrix method using worksheets", *Phys. Educ* 36 (2019): 1-14.
- [10] David Hestenes, "Toward a modeling theory of physics instruction", *American Journal of Physics* 55, no. 5, (1987): 440-454.
- [11] Struve, Walter S. *Fundamentals of molecular spectroscopy*. New York: Wiley, 1989.
- [12] Philip M. Morse, "Diatomic molecules according to the wave mechanics. II. Vibrational levels," *Physical review* 34.1 (1929): 57.
- [13] Ghatak, Ajoy K., and S. Lokanathan. *Quantum mechanics: theory and applications*. Macmillan, 2004.
- [14] Cuneyt Berkdemir and Jianguang Han, "Rotational correction on the Morse potential through the Pekeris approximation and Nikiforov-Uvarov method," *arXiv preprint quant-ph/0502182* (2005).
- [15] O. Bayrak, and I. Boztosun, "Arbitrary-state solutions of the rotating Morse potential by the asymptotic iteration method," *Journal of Physics A: Mathematical and General* 39.22 (2006): 6955-6964.
- [16] Colin N. Banwell and M. McCash Elaine, *Fundamentals of molecular spectroscopy*, New York: McGraw-Hill, 1994.
- [17] <https://www.nist.gov/pml/atomic-spectroscopy-compendium-basic-ideas-atomic-spectroscopy-0>.
- [18] [https://chem.libretexts.org/Courses/University\\_of\\_California\\_Davis/UCD\\_Chem\\_110A%3A\\_Physical\\_Chemistry\\_\\_I/UCD\\_Chem\\_110A%3A\\_Physical\\_Chemistry\\_I\\_\(Larsen\)/Lectures/14%3A\\_Harmonic\\_Oscillators\\_and\\_IR\\_Spectroscopy](https://chem.libretexts.org/Courses/University_of_California_Davis/UCD_Chem_110A%3A_Physical_Chemistry__I/UCD_Chem_110A%3A_Physical_Chemistry_I_(Larsen)/Lectures/14%3A_Harmonic_Oscillators_and_IR_Spectroscopy)

- [19] Pavelich, R. L., and Frank Marsiglio. "The Kronig-Penney model extended to arbitrary potentials via numerical matrix mechanics." *American Journal of Physics* 83.9 (2015): 773-781.
- [20] K. P. Huber and G. Herzberg, "IV, Constants of Diatomic Molecules, Molecular Spectra and Molecular Structure," (1979).

# Some issues in teaching Landau diamagnetism

Reshma. P<sup>1</sup>, Prasanth. P<sup>2</sup>, Sreeraj. P<sup>3</sup> and K. M. Udayanandan<sup>4</sup>

<sup>1</sup> S.N.Polytechnic College, Kanhangad, Kerala, India.

<sup>2</sup> Govt. Engineering College, Thrissur, Kerala, India.

<sup>3</sup> Sree Narayana College, Vadakara, Kerala, India.

<sup>4</sup>Former H O D, NAS College, Kanhangad, Kerala, India.

udayanandan@gmail.com

*Submitted on 17-10-2020*

## Abstract

Teachers and students of statistical mechanics have to teach and study Landau diamagnetism with a cloud of doubts, since there are a large number of gaps in understanding it. Everyone know it is a quantum problem, but what many teach is the classical statistical mechanics results. We here define the limits of classical and quantum conditions with reference to Landau diamagnetism and explain when it is a quantum statistics problem and when it is a quantum mechanics problem.

## 1 Introduction

Diamagnetism is a material property that characterizes the response of electrons to an applied magnetic field. Diamagnetic system exhibits a negative magnetic susceptibility, the benchmark of diamagnetism. The experimental studies of Faraday and Curie [1] on weakly magnetic substance

remained completely unexplained up to the end of 19th century. The understanding of magnetism and the historical context of Tyndall's diamagnetic investigations [2] "The magneto-optic properties of crystals, and the relation of magnetism and diamagnetism to molecular arrangement", was a great contribution to the experimental part of understanding diamagnetism. In 1905 Paul Langevin [3] presented a microscopic theory of diamagnetism based on Lorentz theory of the electron, using classical physics. In 1919 J. H. van Leeuwen [4] proved something which Bohr[5] had anticipated in his PhD thesis in 1911: the impossibility of finding the magnetism of matter exclusively based on classical mechanics. Leeuwen demonstrated that when classical Boltzmann statistics is applied to any dynamical system, the susceptibility is zero. The gradual development of the new quantum ideas, eventually leading to quantum mechanics, the development

of quantum statistics and the discovery of the electrons magnetic moment and spin, resulted in a dramatically new treatment of the physics of diamagnetism[6].

## 2 Landau diamagnetism-an introduction

In 1930 Landau [7],[8] showed that when an electron is subjected to an external magnetic field, then its orbital motion is quantized whereas its axial motion along the magnetic field is not quantized. When the Schrodinger equation for electrons confined in a box and placed in a magnetic field directed along z direction, was solved by Landau, the energy obtained was

$$\epsilon_{j,p_z} = \left( j + \frac{1}{2} \right) \hbar\omega + \frac{p_z^2}{2m}$$

where  $\omega = \frac{eB}{m}$  is the angular frequency of the circular motion,  $p_z$  is the momentum in the z direction, B is the magnetic field, m is the mass and e is the charge of the electron, j is the quantum number with values 0, 1, 2, 3,.....Here the circular motion is quantized, where as the linear motion is continuous. Each energy level has a degeneracy

$$g_j = L_x L_y \frac{eB}{h}$$

where  $L_x$  and  $L_y$  are the length and breadth of the confined box and h is the Planck's constant. Using this energy and degeneracy Landau was able to explain the reason for negative susceptibility. A detailed explanation will be done in the coming sections.

## 3 Bohr- van Leeuwen theorem

In 1932, Van Vleck in a book "The Theory of Electric and Magnetic Susceptibilities" [9] formulated and expanded the findings of both Bohr and J. H. van Leeuwen, after which their findings were popularly known as Bohr- van Leeuwen theorem. This theorem could be stated as "Magnetism is strictly a quantum mechanical effect. Classically there cannot be either dia, para or collective magnetism". According to the theorem, classical charged particles moving in a constant magnetic field show zero magnetization in thermal equilibrium. We will give a brief demonstration of this. This theorem can be proved, if we can show that even when an external field is switched on,  $Q_N$ , the partition function for N particles, does not depend on this field.

Consider a solid consisting of identical atoms in thermal equilibrium to which a magnetic field is applied. Magnetization is given by [8]

$$M = \frac{1}{\beta} \left( \frac{\partial}{\partial B} \ln Q_N \right)_{V,T} \tag{1}$$

The equation for partition function  $Q_N$  can be written as,

$$Q_N = \frac{\int \int \int dx_1 \dots \dots dx_{3N} dp_1 \dots \dots dp_{3N} e^{-\beta H}}{N! h^{3N}} \tag{2}$$

where N is the number of electrons per ion. For convenience, we write

$$Q_N = \frac{Q_N^*}{N! h^{3N}} \tag{3}$$

where

$$Q_N^* = \int \int \int dx_1 \dots dx_{3N} dp_1 \dots dp_{3N} e^{-\beta H} \tag{4}$$

The Hamiltonian of an electron in a magnetic field is

$$H = \frac{1}{2m} (p + eA)^2 - e\phi \tag{5}$$

When there is no electric field, the above equation becomes,

$$H = \frac{1}{2m} (p + eA)^2 \tag{6}$$

So, in the presence of a magnetic field, Hamiltonian has the general form,

$$H = \frac{1}{2m} \sum_{i=1}^{3N} (p_i + eA_i)^2 \tag{7}$$

Let us substitute the value of  $H$  in Eqn (4) for  $Q_N^*$ . Here momentum integration runs from  $-\infty$  to  $+\infty$ , as it is one dimensional. The momentum integral could be calculated by substituting  $p_i + eA_i = u_i$ , which gives

$$dp_i = du_i$$

. Therefore,

$$Q_N^* = V \int_{-\infty}^{+\infty} \dots \int_{-\infty}^{+\infty} du_1 \dots du_{3N} e^{-\frac{\beta}{2m} \sum_{i=1}^{3N} u_i^2} \tag{8}$$

where  $V$  is the spatial volume.

Then on integrating

$$Q_N^* = V \left( \frac{2m\pi}{\beta} \right)^{\frac{3N}{2}}$$

From above equation, it is clear that  $Q_N^*$

is independent of applied magnetic field. So the average magnetization obtained from Eqn.(1) vanishes in all cases.

$$M = 0 \tag{9}$$

Thus in the frame work of classical statistical mechanics, there would be no magnetism. This is in agreement with Bohr- von Leeuwen theorem. In Langevin magnetism, the angular momentum of the molecule is restricted to a particular value, which is a great restriction as far as electrons are concerned. Now we will find out how Landau calculated susceptibility.

#### 4 Landau's diamagnetism(LD) for all temperature

We here give a simple and an alternate method to obtain the Landau susceptibility. The logarithm of the grand partition function is given by[8]

$$\ln Z = \sum_{j,p_z} g_j \ln(1 + ze^{-\beta \epsilon_j p_z})$$

where  $\epsilon_j$  is a function of both  $j$  and  $p_z$  and  $z$  is the fugacity.

We have,

$$\ln(1 + x) = \sum_{l=1}^{\infty} (-1)^{(l-1)} \frac{x^l}{l}$$

Substituting

$$\ln \mathcal{Z} = \sum_{j,p} L_x L_y \frac{eB}{h} \sum_{l=1}^{\infty} (-1)^{(l-1)} \frac{z^l}{l} e^{-\beta l \left( (j+\frac{1}{2})\hbar\omega + \frac{p_z^2}{2m} \right)}$$

Using Euler's summation formula

$$\sum_{j=0}^{\infty} f\left(j + \frac{1}{2}\right) = \int_0^{\infty} f(x) dx + \frac{1}{24} f'(0)$$

we get

$$\ln \mathcal{Z} = \frac{VeB}{h^2} \left( \frac{2\pi m}{\beta} \right)^{\frac{1}{2}} f_{\frac{3}{2}}(z) \left[ \int_0^{\infty} e^{-\beta x \hbar \omega l} dx + \frac{1}{24} (-\beta \hbar \omega l) \right]$$

We have  $\omega = \frac{Be}{m}$  and Bohr magneton  $\mu_{eff} = \frac{eh}{4\pi m}$  and changing the variable  $x$  to  $x' = Bx$ , we get

$$\ln \mathcal{Z} = \frac{Ve}{h^2} \left( \frac{2\pi m}{\beta} \right)^{\frac{1}{2}} f_{\frac{3}{2}}(z) \int_0^{\infty} e^{-2\beta \mu_{eff} x' l} dx' - \frac{VeB}{h^2} \left( \frac{2\pi m}{\beta} \right)^{\frac{1}{2}} f_{\frac{1}{2}}(z) \frac{\beta \mu_{eff} B}{12}$$

The first part of this equation is independent of B and hence does not contribute to M. Taking the second part only

$$M = - \frac{BV (2\pi m)^{\frac{3}{2}} \mu_{eff}^2 f_{\frac{1}{2}}(z)}{3h^3 \beta^{\frac{1}{2}}}$$

Hence diamagnetic susceptibility is given by

$$\chi = \frac{M}{B} = -V \frac{(2\pi m)^{\frac{3}{2}} \mu_{eff}^2 f_{\frac{1}{2}}(z)}{3h^3 \beta^{\frac{1}{2}}}$$

#### 4.1 $\chi$ for low temperature

At low temperature

$$f_{\frac{1}{2}}(z) = \frac{2}{\sqrt{\pi}} (\ln z)^{\frac{1}{2}}$$

So

$$\chi = - \frac{(2\pi m)^{\frac{3}{2}} \mu_{eff}^2}{3h^3} \frac{2}{\sqrt{\pi}} (\beta^{-1} \ln z)^{\frac{1}{2}}$$

#### 4.2 $\chi$ for 0 kelvin

Here at  $T = 0$ ,  $\mu = \varepsilon_F$ , Since  $\beta^{-1} \ln z = \varepsilon_F$ , then,

$$\chi_0 = - \frac{2\pi (2m)^{\frac{3}{2}} \mu_{eff}^2 \varepsilon_F^{\frac{1}{2}}}{3h^3} = - \frac{1}{2} \frac{n \mu_{eff}^2}{\varepsilon_F}$$

0 kelvin magnetic susceptibility is temperature independent.

#### 4.3 $\chi$ for high temperature

At high temperature

$$f_{\frac{1}{2}}(z) = z$$

$$\chi = \frac{-(2\pi m)^{\frac{3}{2}} z \mu_{eff}^2}{3h^3 \beta^{\frac{1}{2}}} = -\frac{\mu_{eff}^2 n}{3kT}$$

At high temperature the susceptibility is depending on both temperature and number density ( $n$ ). These are the results of Landau's calculations. In Bohr magneton we have Planck's constant and hence even at high temperature, susceptibility value is a quantum contribution or the results are due to quantum mechanics. At low temperature the results are due to both quantum mechanics and quantum statistics.

## 5 Landau Diamagnetism in some popular textbooks

Many popular textbooks give the derivation and explanation for LD in different ways. Let us take textbooks with names A, B, C and D. We wish not to create an embarrassment to authors and hence the name of the authors are not given. All are popular textbooks. Given below is a brief description about what is given in these textbooks regarding diamagnetic susceptibility.

### 5.1 A

In this diamagnetism is considered as an idealized problem of a spin less electron gas in an external magnetic field. Here to calculate the magnetization only the high temperature limit in the classical domain is taken. Then the magnetic susceptibility is found as

$$\chi = -\frac{\mu_{eff}^2 n}{3kT}$$

### 5.2 B

B discusses the same at high temperature first considering the condition  $z \ll 1$  and reaches the same expression as above. Then does the problem at all temperatures and solves using Euler's summation formula. Hence obtain the results given in 4.1, 4.2 and 4.3.

### 5.3 C

In C the limit  $z \ll 1$  is considered and the high temperature result is obtained.

### 5.4 D

Here, Euler's summation formula is taken to evaluate the logarithm of the partition function. For  $z \gg 1$  and  $T = 0K$  the same results are obtained as above. For  $z \ll 1$  the expression for magnetization is written in terms of Langevin function.

## 6 Issues while teaching LD

In general we can see that many text books give extra importance to high temperature  $\chi$  and explain high temperature diamagnetism by taking the condition that  $z \ll 1$  without proving it. Besides there is no coherence in what to teach about LD. Some issues faced are

1. For an ideal gas the condition  $z \ll 1$  is valid, but we cannot say that this condition is valid for LD which has both quantum and classical energy.

2. In text books it is not mentioned at what temperature, the high temperature condition is valid
3. Many text books does not point out that

$$\lambda = -\frac{C}{T}$$

is a quantum effect

4. At what temperature in diamagnetic materials quantum statistics will come into play? This is not discussed.

These questions are to be answered in class rooms. Only then students can understand LD properly. In the coming sections we try to explain these issues and are trying to resolve it.

### What is Quantum statistics and when does it work for LD?

Where do we need to worry about quantum statistics and when will the classical statistics work? A good illustration is provided by an ideal gas, so let's consider an ideal system with momentum  $p$ , then de Broglie thermal wavelength

$$\lambda = \frac{h}{\sqrt{2\pi mkT}}$$

,where  $h$  is Planck's constant. For an ideal gas, if the volume per particle is comparable to this quantum volume, then quantum statistics come into play.

When the volume per particle is much larger than quantum volume, then we can use classical description. So we have,

$$\frac{V}{N} \gg V_Q$$

$$\frac{N}{V}\lambda^3 \ll 1 \text{ Classical statistics}$$

other wise it will be a quantum system. So

$$\frac{N}{V}\lambda^3 \gg 1$$

$$\frac{N}{V}\lambda^3 \approx 1$$

$$\frac{N}{V}\lambda^3 = 1$$

all represent quantum systems. Then criterion for quantum /classical statistics depends upon the (number)density and temperature.

So let us check this for copper a typical diamagnetic substance. In case of copper, density of free electrons is  $8.5 \times 10^{28}/m^3$ . We have

$$k = 1.380649 \times 10^{-23} \text{ J/K}$$

$$h = 6.626 \times 10^{-34} \text{ Js}$$

$$m = 9.109 \times 10^{-31} \text{ kg}$$

Consider the equation

$$\frac{N}{V}\lambda^3 = \frac{N}{V} \frac{h^3}{(2\pi mkT)^{3/2}}$$

The table below list out the values of different temperature and corresponding  $\frac{N}{V}\lambda^3$ .

Temperature	100K	200K	300K	500K
$\frac{N}{V}\lambda^3$	$3.520 \times 10^4$	$1.244 \times 10^4$	$6.774 \times 10^3$	$3.148 \times 10^3$
Temperature	$10^4$ K	$10^5$ K	$10^6$ K	$10^7$ K
$\frac{N}{V}\lambda^3$	$3.520 \times 10^1$	1.113	$3.520 \times 10^{-2}$	$1.113 \times 10^{-3}$

Thus we can see that even at room temperature the diamagnetism is a quantum phenomenon. The de Broglie thermal wavelength of electron will be about 15 times greater than that of separation distance and hence there can be a substantial overlap of the wave functions. Thus only at or above  $10^7$  K LD become a classical problem. This can happen only in places like core of the sun. This shows that  $\chi = -\frac{C}{T}$  is not a quantum

statistics problem, but it a quantum mechanics problem. This result is mainly due to the quantum energy and degeneracy agreeing with B L theorem.

### 7 Can we take fugacity $z \ll 1$ for high temperature LD

Considering the series expansion in logarithm of grand partition function we get,

$$\ln \mathcal{Z} = \sum_{j=0}^{\infty} \frac{L_x L_y eB}{h} z e^{-\beta(j+\frac{1}{2})\hbar\omega} e^{-\beta\frac{p_z^2}{2m}} + \frac{1}{2} \sum_{j=0}^{\infty} \frac{L_x L_y eB}{h} z e^{-2\beta(j+\frac{1}{2})\hbar\omega} e^{-2\beta\frac{p_z^2}{2m}}$$

$$+ \frac{1}{3} \sum_{j=0}^{\infty} \frac{L_x L_y eB}{h} z e^{-3\beta(j+\frac{1}{2})\hbar\omega} e^{-3\beta\frac{p_z^2}{2m}} + \frac{1}{4} \sum_{j=0}^{\infty} \frac{L_x L_y eB}{h} z e^{-4\beta(j+\frac{1}{2})\hbar\omega} e^{-4\beta\frac{p_z^2}{2m}}$$

Since  $p_z$  is continuous, summation can be replaced by integration and carrying out same procedure as before we have,

$$\ln \mathcal{Z} = \sum_{l=1}^{\infty} (-1)^{l-1} \frac{VeB}{lh^2} z^l \frac{1}{2 \sinh(l\beta\mu_{eff}B)} \left(\frac{2\pi m}{l\beta}\right)^{1/2}$$

obtain,

Number of particles is given by the equation,  $N = z \frac{\partial}{\partial z} \ln \mathcal{Z}$

Substituting for  $\ln \mathcal{Z}$  and differentiating we

$$N = \sum_{l=0}^{\infty} (-1)^{l-1} \frac{VeBz^l}{h^2 2 \sinh(l\beta\mu_{eff}B)} \left(\frac{2\pi m}{l\beta}\right)^{1/2}$$

Using the result for  $\lambda$  and  $\mu_{eff}$ , the above equation becomes,

$$\frac{N\lambda^3}{V} = \sum_{l=0}^{\infty} (-1)^{l-1} l^{-1/2} z^l \frac{\beta\mu_{eff}B}{\sinh(l\beta\mu_{eff}B)}$$

This equation is of the form,  $\frac{N\lambda^3}{V} = \sum_{l=0}^{\infty} a_l z^l$  where  $a_l$  is,

$$a_l = (-1)^{l-1} l^{-1/2} \frac{\beta\mu_{eff}B}{\sinh(l\beta\mu_{eff}B)}$$

By series inversion we can write,

$$z = \sum_{l=1}^{\infty} b_l \left(\frac{N\lambda^3}{V}\right)^l = b_1 \left(\frac{N\lambda^3}{V}\right)^1 + b_2 \left(\frac{N\lambda^3}{V}\right)^2 + \dots \text{and } b_2 = \frac{1}{\sqrt{2}} \frac{1}{(\beta\mu_{eff}B)^2} \frac{(\sinh(\beta\mu_{eff}B))^3}{\sinh(2\beta\mu_{eff}B)}$$

The relation between the coefficients is given by,  $b_1 = \frac{1}{a_1}$  and  $b_2 = \frac{-a_2}{a_1^3}$  From equa-

Therefore fugacity becomes,

$$z = \frac{\sinh(\beta\mu_{eff}B)}{\beta\mu_{eff}B} \left(\frac{N\lambda^3}{V}\right)^1 + \frac{1}{\sqrt{2}} \frac{1}{(\beta\mu_{eff}B)^2} \frac{(\sinh(\beta\mu_{eff}B))^3}{\sinh(2\beta\mu_{eff}B)} \left(\frac{N\lambda^3}{V}\right)^2 + \dots$$

At high temperature  $n\lambda^3$  is very very small. So we need to consider only first term which comes to ideal gas condition at high temperature. From the first term we can make sure that only at temperature of the order of  $10^7$  K, fugacity is much less than 1.

tion of  $a_l$  we get,

$$a_1 = \frac{\beta\mu_{eff}B}{\sinh(\beta\mu_{eff}B)}$$

and

$$a_2 = -\frac{1}{\sqrt{2}} \frac{\beta\mu_{eff}B}{\sinh(2\beta\mu_{eff}B)}$$

Using these results we obtain,

$$b_1 = \frac{\sinh(\beta\mu_{eff}B)}{\beta\mu_{eff}B}$$

## 8 Justifying that the relation

$\chi = -\frac{C}{T}$  is a classical statistical mechanics result

If we can get the same result we obtained using grand canonical ensemble, by canonical ensemble we can confirm that it is a classical result. In canonical ensemble, the partition function

$$Q = \sum e^{-\beta\epsilon}$$

where  $\varepsilon$  is the energy and  $\beta = \frac{1}{kT}$ . The single particle partition function

$$Q_1 = \sum_j \sum_{p_z} g_j e^{-\beta \left( (j+\frac{1}{2})\hbar\omega + \frac{p_z^2}{2m} \right)}$$

Hence applying earlier calculations, we get

$$Q_1 = \frac{V}{\lambda^3} \frac{\beta\mu_{eff}B}{\sinh(\beta\mu_{eff}B)}$$

Considering N particle system if it is classical system we can take

$$Q_N = \frac{1}{N!} Q_1^N$$

If there is an overlapping of wave functions, which is a quantum statistics effect, we are not allowed to use this expression. So

$$Q_N = \frac{1}{N!} \left( \frac{V}{\lambda^3} \frac{\beta\mu_{eff}B}{\sinh(\beta\mu_{eff}B)} \right)^N$$

Magnetization,

$$M = \frac{N}{\beta} \left[ \frac{\beta\mu_{eff}}{\beta\mu_{eff}B} - \frac{\beta\mu_{eff} \cosh(\beta\mu_{eff}B)}{\sinh(\beta\mu_{eff}B)} \right]$$

Considering the steps as before we obtain diamagnetic susceptibility for high temperature as

$$\chi = \frac{M}{B} = \frac{-N\mu_{eff}^2}{3kT}$$

## 9 Conclusions

We make a critical analysis of the teaching and understanding of Landau diamagnetism. Many textbooks, compared to Pauli paramagnetism or Debye specific heat,

is not presenting all temperature diamagnetism and then to low and high temperature effects. Instead many present high temperature diamagnetism directly (which is not at all a practical result) creating an air of misunderstanding. Some authors of this article and many like us, we hope have experienced this issue while teaching LD, and we wish this article will help them to resolve their issues.

## References

- [1] A. W. Hirshfeld. The electric life of Michael Faraday, (Walker and company, 2006)
- [2] Ronald Jackson(2015). Annals of science 72, 435-439
- [3] P. Langevin(1905). J. Phys. Theor. Appl. 4(1), 678693
- [4] J. H. van Leeuwen(1921). J. Phys (Paris) 2, 361
- [5] J. R. Nielsen. Early Work (1905-1911) Niels Bohr : Collected Works Volume 1, (North- Holland Publishing Company, 1972)
- [6] S. Dattagupta, A. M. Jayannavar and N. Kumar(2001). Current Science 80, 861
- [7] Landau L. D.(1930). Z.Phys. 64, 629637
- [8] Kerson Huang. Statistical Mechanics, (John Wiley and Sons, 1963)

- [9] J. H. Van Vleck. The Theory of Electric and Magnetic Susceptibilities, (Clarendon Press, 1932)

---

# Designing of Digital Processing System Using ADS1115 and Arduinouno

Sreenath Nair, Snehal Vataliya, Devansh Desai and P. D. Lele

Department of Physics, School of Sciences,  
Gujarat University, Ahmedabad-380009, India.

snmnsree64@gmail.com

*Submitted 06-05-2020*

## Abstract

In this paper, analog-to-digital converter ADS1115 is used with Arduino UNO and different analog application. The ADS1115 is an external digital analog device that we are able to connect with a processor like Arduino to calculate analog signals. Here ADS1115 uses Sigma Delta method for conversion. Sigma Delta ADC is widely used in communication system, professional audio systems and high precision measurement systems. The ADS1115 provides 16-bit precision at 860 samples/second over I2C interface/protocol. The chip can be configured as 4 single-ended input channels, or two differential channels. We like this ADC because it can run from 2V to 5V power, can measure a large range of signals and it is very easy to use. The advantage of using ADS1115 is to get better precision, additionally to releasing the processor from this burden and also in certain cases it has the possibility of measuring negative voltages. Our aim is to provide students with a better understanding of ADC with 16 bit accuracy with optimum use of arduino for the future projects. The results show the real time data in form of graphical outputs with every different variable.

---

## Introduction

Technology and the digital revolution can disrupt conventional models and bring benefits to the

common man in many ways. Digitization, when implemented accurately, will show patterns of benefits with respect to cost and efficiency. It is often said that digital information is transforming the way we learn, the way we communicate, even the way we think. In the digital world, all knowledge is divided into two parts. The binary strings of 0s and 1s that make up the crucial part of data, allow information to be fruitful and multiply, and allow people to create, change, and share information in ways that appear to be innovative. Our objective is to investigate different application of analog devices that can work simultaneously and give us better and accurate results can match or exceed the performance while requiring relatively modest digital hardware resources for implementation. The work shows how a student can be taught how to use Arduino and the accuracy we get with higher bit ADC. One reason to use a high-resolution digitizer is to measure small signals. Resolution determines the precision of a measurement. The greater the resolution, more precise the measurement values.

An ADC changes over a continuous-time and continuous-amplitude analog signal to a discrete-time and discrete-amplitude digital signal. The transformation includes quantization of the given signal, so it essentially presents a limited quantity of noise. Besides, rather than ceaselessly performing conversion, an ADC does the change periodically, sampling the given signal, restricting

the suitable bandwidth of the information signal. ADCs are classified according to conversion technique. Based on Conversion methodology common types of converters are Flash or Direct conversion or Simultaneous Conversion Technique, Counter type ADC, Successive Approximation ADC, Integrating type of ADC (Single Slope, Dual Slope and Multi slope ADCs), Sigma- delta ADC, Simple Counter ADC, Sectional Counter ADC. All this techniques have advantages as well as disadvantages.

In present scenario Arduino is being used extensively in microcontroller programming among other things due to its user friendly nature, like any microcontroller an arduino is a circuit board with chip that can be programmed to do numerous number of tasks, it sends information from the computer programme to the Arduino microcontroller and finally to the specific circuit or machine with multiple circuits in order to execute the specific command. An arduino can help us to read information from input devices such as e.g. Sensors, Antenna, Trimmer (potentiometer) etc. ... and can also send information to output devices such as LED, Speakers, LCD Screen, DC motor etc. ... [8]

ADCs can fluctuate incredibly between various microcontrollers ADC utilizes the analog voltage to energize an internal capacitor and afterward measure the time it takes to discharge over an internal resistor. The microcontroller screens the quantity of clock cycles that go before the capacitor is discharged. This number of cycles is the number that is returned once the ADC is

finished. Number is written in a particular register or memory region, and ends up accessible to microcontroller's ALU. The converters find more applications as an intermediate device to change over the signals from analog to digital value, displays yield on LCD through a microcontroller. The goal of an A/D converter is to determine the output corresponding to an analog signal. Another experiment which can be studied using sensors and arduino is hysteresis. The output of a sensor may be different for a given input, depending on whether the input is increasing or decreasing. This phenomenon is known as hysteresis and can be described as the difference in output between the rising and falling output values for a given input. Hysteresis commonly occurs when a sensing technique relies on the stressing of a particular material. It is a method where the electrical readings vary contingent upon how quick or moderate the sensor is being given the input. At the point when a sensor has high hysteresis, the electrical readings will vary considerably under a similar input, making the estimations untrustworthy.

### **ADS1115**

The ADS1115 device is a precision, low-power, 16-bit, I<sup>2</sup>C-compatible, analog-to-digital converters (ADCs) offered in an ultra-small, leadless. The device incorporates a low-drift voltage reference and an oscillator <sup>[6]</sup>.

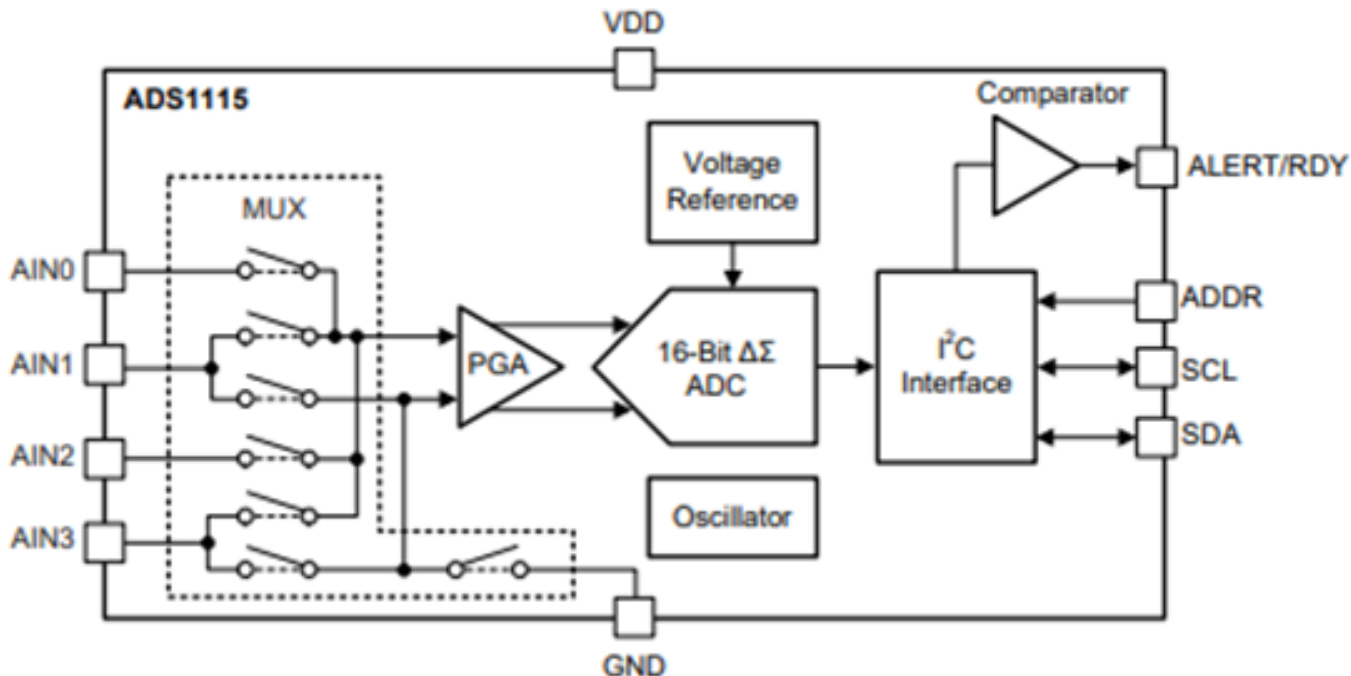


**Fig1: Internal Diagram for ADS1115** [6]

ADS1115 also includes a programmable gain amplifier, up to x16, to help boost up smaller single/differential signals to the full range. The chip is fairly small so it comes on a breakout board with ferrites to keep the AVDD and AGND quiet. Interfacing is done via I2C. The Chip convey through an I2C interface. I2C is a

two-wire open-drain interface that underpins different gadgets and master on a single bus. Devices on the I2C transport just drive the transport lines low by associating them to ground; the gadgets never drive the transport lines high. Rather, the transport wires are pulled high by pullup resistors, so the transport wires are in every case high when no gadget is driving them low.

### Working Principle

The working principle of this work describes the functionality of the components and their output simultaneously. The block diagram is shown in Fig. 2. Firstly, all the components are started by supplying the required power of +5v. We have used here an NTC thermistor which uses the resistance properties of ceramic/metal composites to measure the temperature. Another sensor that is being used is LDR (Light dependent resistor). When light falls i.e. when the photons fall on the device, the electrons in the valence band of the semiconductor material are excited to the

conduction band. These photons in the incident light should have energy greater than the bandgap of the semiconductor material to make the electrons jump from the valence band to the conduction band. The natural light intensity may vary from time to time [5]. Here the experiment has been designed keeping in mind the best way to calculate the reliability of LDR. The circuit is connected as shown in the figure. Here arduino cannot output the analog value directly but it can approximate the analog signals by rapidly turning the voltage ON and OFF. Here all the pins are

capable of Pulse width Modulation [8]. With the help of variable resistor we are changing the voltage which changes the intensity of LED light. With respect to change in the intensity the LDR value changes which give us the Hysteresis graph. Another analog device that is being used in the Sound sensor. This module features a sensitive microphone for detecting sound. It features both a

digital and an analog output. The analog pin outputs a real-time voltage signal of the microphone. The digital pin can output either a high or low signal indicating when sound intensity has reached a certain threshold. The sensitivity threshold can be adjusted via the potentiometer on the sensor [3]

### Architecture Design

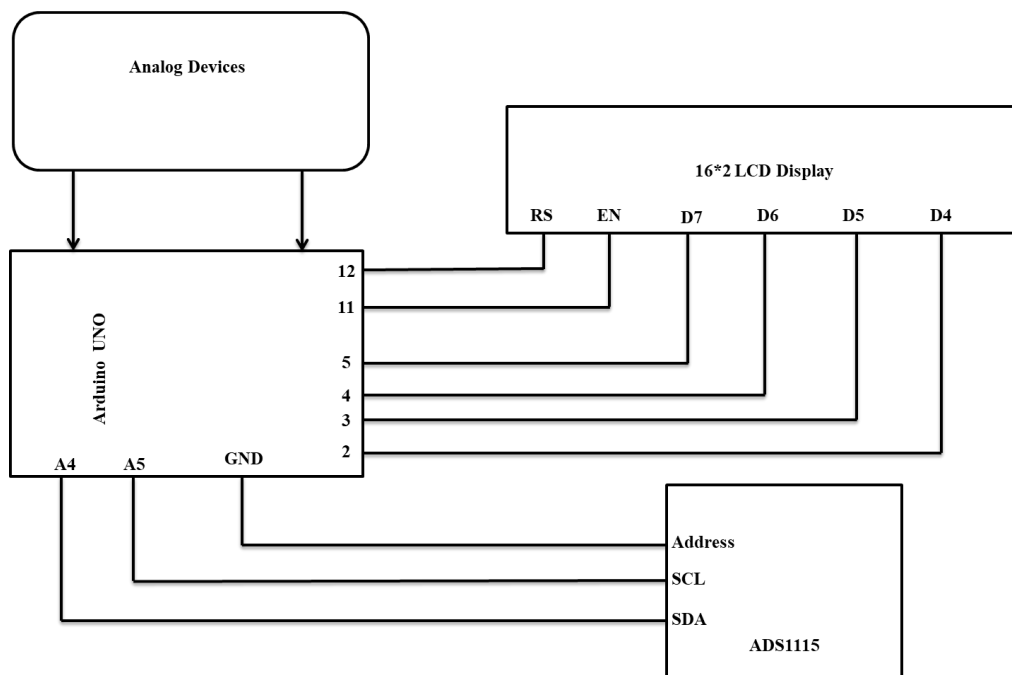


Fig 2: Block diagram

Arduino is connected to all the components. The sensors are connected to the analog input of the Arduino. It is also connected to the 16x2 LCD and the PC. The outputs can be seen in the serial monitor section of arduino program. The LCD is connected to the digital pins D5- D2 and RS and E pin are connected to 12 and 11 pins respectively. And the back-light control is connected to digital pin 13. The rest other pins are connected to the GND. ADS1115 is connected to A4, A5, GND points.

The working model is shown in Fig.3

### Experimental Setup

Here as shown in the figure Arduino is connected with ADS115. Analog to digital conversion module has 6 input ports. The number of the port varies with your ARDUINO model but the coding remains the same. The analog reading in the analog inputs is converted into corresponding 10bit (0-1023). The developers have made such an option that you can print anything and see it on the Serial monitor. Here A0 is used for Voltage measurement, A1 is used for Temperature, A2 is



**Fig 3: Circuit hardware**

used for Sound and A3 used as light intensity measurement. The analog input lines are connected with SCL and SDA. SDA carries data; SCL provides the clock. All data are transmitted across the I2C bus in groups of eight bits. To send a bit on the I2C bus, drive the SDA line to the appropriate level while SCL is low (a low on SDA indicates the bit is zero; a high indicates the bit is one). After the SDA line normalizes, the SCL line is brought high, then low. This pulse on SCL clocks the SDA bit into the receiver shift register [6]. Here the microcontroller uses delta Sigma analog to digital converter. Delta-sigma ( $\Delta\Sigma$ ) analog-to-digital converters (ADCs) are based on the principle of oversampling. The input signal of a  $\Delta\Sigma$  ADC is sampled at a high frequency (modulator frequency) and subsequently filtered and decimated in the digital domain to yield a conversion result at the respective output data rate. Now for better understanding of the experiment

we have used certain analog devices. The concepts of simplicity, ability to use noise and almost unlimited resolution makes Sigma-Delta ADCs user friendly. When it comes to applications, SARs tend to be more popular for work that requires a high sampling rate and low-to-moderate resolution. Sigma-Deltas tend to be more popular for experiments that can tolerate a lower sampling rate but need higher resolution [7]. ARDUINO developers have made such an option that you can print anything and see it on the Serial monitor.

### Results and discussion

We got the simulation results shown in fig 4 which is the real time graphical representation of the analog signals converted into digital signals with respect to change in time, and table 1 shows digital value for given analog devices. Here table 2 has been added which shows the ratio of

increment in the LED brightness with respect to the increase in voltage and vice versa. Fig 5 shows the graph of hysteresis curve. When it is applied to an electronic circuit, the voltage rises towards the trigger voltage, and actually gets slightly above the point where the output should change state. Once it does trigger, the effect is instant, and the voltage now has to be reduced to some value below the trigger voltage before the output will change state again. The amount of hysteresis you actually need is determined by the likelihood of small fluctuations at or around the threshold voltage. No switching system should ever be used without hysteresis, because there will be a point where the relay chatters. This is a condition where the contacts are making and breaking rapidly - usually at 50 or 60Hz due to mains noise pickup <sup>[9]</sup>. Accuracy is one of the most basic components to think about when determining an ADC for test and measurement applications. Shockingly, it's frequently mistaken for resolution, and in spite of the fact that related

they are particularly unique. At the point when you compose a measured value worth utilizing significant digits notation, the quantity of significant digits is identified with the uncertainty of the estimation. The more digits after the decimal point, the less uncertainty. As appeared in the graph the Arduino Serial Plotter takes approaching serial data over the USB association and can graph the data along the X/Y out on to the Serial Monitor. The vertical Y-axis auto changes itself as the estimation of the output increase or decrease, and the X-axis is a fixed 100 point axis with each tick of the axis equivalent to an executed `Serial.println()` command. At the end of the day the plot is refreshed along the X-axis axis, beyond simply observing numbers being let every time the `Serial.println()` is refreshed with another data. While displaying numerous waveforms, every different variable/value/parameter is displayed utilizing an alternate color like demonstrated in the graph

Sr. No	Voltage (Reference)	Channel 1 (Voltage)	Channel 2 (Temperature)	Channel 3 (Sound)	Channel 4 (LDR)
1	2.51 V	2.5115625 V	22.5825004 0C	2.2895624 dB	2.9094373 lux
2	1.97 V	1.9786874 V	22.5768756 0C	1.7414999 dB	2.9101875 lux
3	1.90 V	1.9801875 V	18.9468746 0C	2.2434375 dB	2.8501874 lux
4	1.97 V	1.9788750 V	20.3437500 0C	2.2464375 dB	1.4968124 lux
5	1.97 V	1.9788750 V	19.9462509 0C	2.2556250 dB	1.6496249 lux
6	1.98 V	1.9803750 V	19.2806243 0C	2.2813124 dB	2.8282499 lux
7	1.98 V	1.9800000 V	22.5637493 0C	2.2580626 dB	2.7601873 lux

**Table1: Values of different Analog Devices**

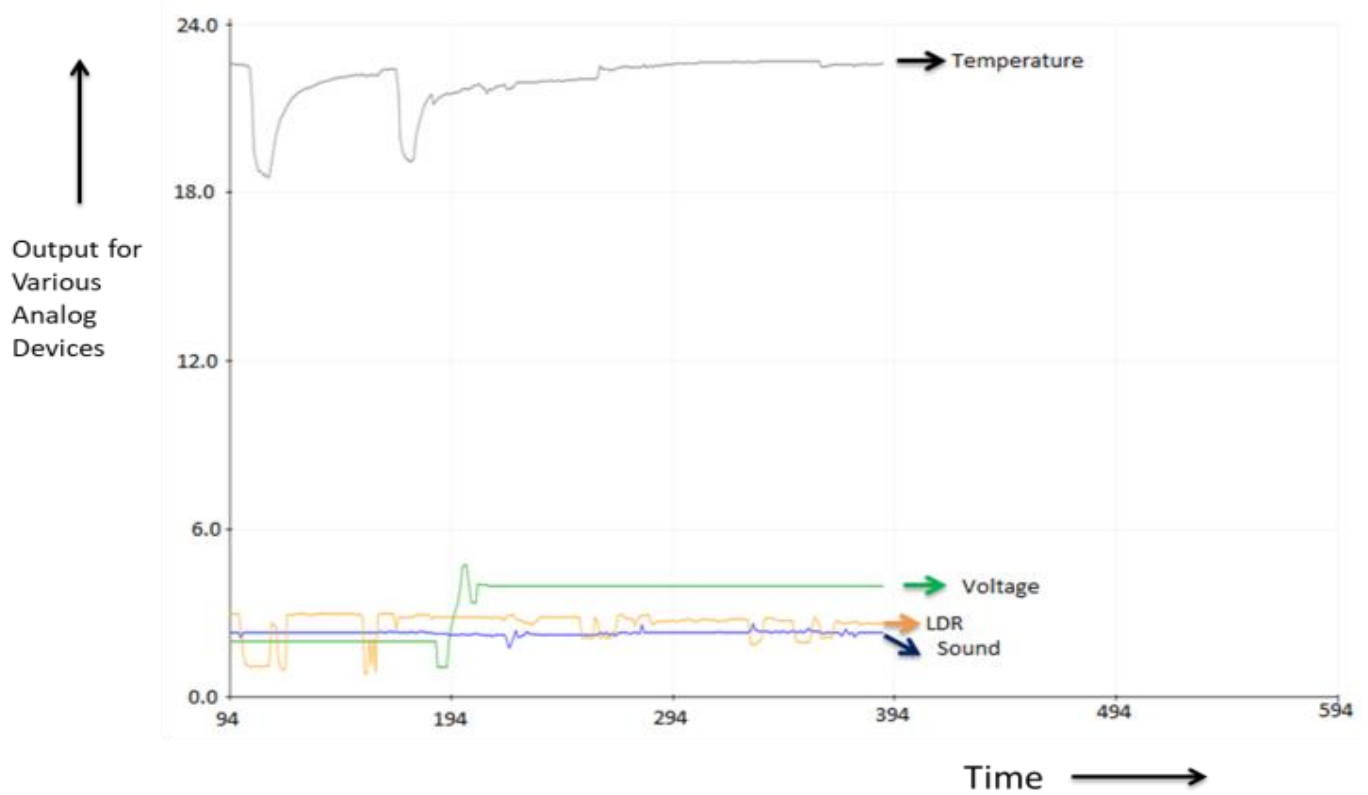


**Fig 4: Real time Graphical representation of Variations of different Analog devices**

Sr. No	LED Brightness	LDR Voltage
1	0%	0
2	4%	0.14
3	3%	0.26
4	5%	0.46
5	9%	0.74
6	12%	0.95
7	16%	1.2
8	20%	1.42
9	22%	1.56
10	27%	1.85
11	31%	2.09
12	35%	2.3
13	40%	2.54
14	44%	2.76
15	47%	2.94
16	52%	3.22
17	58%	3.51
18	63%	3.73
19	68%	3.98
20	74%	4.26
21	78%	4.45
22	84%	4.79
23	89%	4.99
24	91%	5
25	92%	5
26	92%	5
27	92%	5

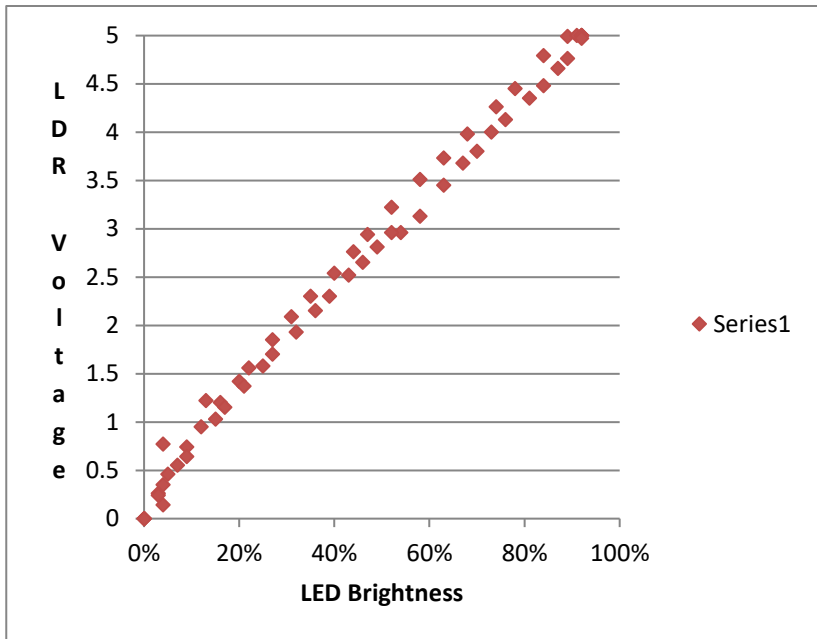


Fig 5: Hysteresis Curve of LED brightness vs LDR Voltage

Table 2: Variation of Brightness w.r.t Voltage

## Conclusions

This whole project revolves around a little board. In short, it is an Analog-to-Digital Converter (ADC) with 16-bits of resolution with a Programmable Gain Amplifier (PGA). ADC is the key design Block in present day microelectronics digital correspondence framework [2]. Arduino has internal ADCs. On the Arduino Uno, Mini and Nano models, we have 6 ADC of 10 bits. As we require more resolution we prefer ADS1115 along with Arduino. For microcontrollers without an analog-to-digital converter or when you want a higher-precision ADC, the ADS1115 provides 16-bit precision at 860 samples/second over I<sup>2</sup>C interface/protocol. The chip can be configured as 4 single-ended input channels, or two differential channels. This model gives students a chance to understand the real time data for all available analog devices with 16 bit accuracy. This model is cost effective and can be reprogrammed with other devices. This gives us a wide range of variation of data using the same device. Reasonable integration in lab works the virtual and real techniques is contributing to deeper understanding of the studied issues. The outcomes displayed prove that there is a chance of growing such models on the base of AVR technologies. To summarize; this paper demonstrates audrino uno processor advanced technology and uses sigma delta advanced ADC with very high precession and resolution. The basis of experiment is to show how

real time fast data analysis is done in a few direct applications in physics laboratory. This experiment will go a long way to improve and increase understanding of physics laboratory experimental applications. We like this ADC because it can run from 2V to 5V power/logic, can measure a large range of signals and its super easy to use.

## Acknowledgement

The Physics Department Gujarat University has received grants under DST-FIST and DRS-SAP programs. The funding agencies are gratefully acknowledged. Authors are also thankful to Prof. P. N. Gajjar, Head of Physics department for providing necessary facilities.

## References:

- [1] AleksandrVostrukhin and Elena Vakhtina “STUDYING DIGITAL SIGNAL PROCESSING ON ARDUINO BASED PLATFORM” ENGINEERING FOR RURAL DEVELOPMENT, Jelgava, 25.-27, May-2016.
- [2] Madhusudan Singh Solanki and Prof. PriyanshuPandey “Review Article of basic ADC design and issue of old Algorithm” International Journal of Scientific research and Engineering Trends, Volume 4, Issue1, Jan-Feb 2018.
- [3]<https://www.wiltronics.com.au/product/9225/audio-sensor-high-sensitivity/>
- [4] KarthikKrishnamurthi, Suraj= Thapa, Lokesh Kothari, ArunPrakash, “Arduino Based Weather

Monitoring System”, International Journal of Engineering Research and General Science Volume 3, Issue 2, March-April, 2015, ISSN 2091-2730

[5] Texas Instruments, “ADS111x Ultra-Small, Low-Power, I2C-Compatible, 860-SPS, 16-Bit ADCs With Internal Reference, Oscillator, and Programmable Comparator,” ADS1113, ADS1114, ADS1115 datasheet, May 2009 [Revised Jan. 2018].

[6] <https://www.analogictips.com/considerations-choosing-sigma-delta-adc-vs-sar-vs-pipeline/>

[7] Yusuf AbdullahiBadamasi, “The Working Principle Of An Arduino.”, IEEE, 2014, ISSN 2091-2730

[8]<https://www.bwp.io/Arduino-Workshops/coding-and-sensors/hysteresis/>

[9] <https://sound-au.com/project131.htm>

---

---

## **Govind Swarup (1929 – 2020)**

### **The dominant force in Radio Astronomy in India since early sixties.**

V Balasubramanian<sup>1</sup> and S Ananthakrishnan<sup>2</sup>

<sup>1</sup> (Formerly) Head, Radio Astronomy Centre,  
NCRA-TIFR, Udhagamandalam – 643001, India

vbalu\_ot@rediffmail.com

<sup>2</sup> Adjunct Professor, Electronic Science Dept.,  
Savitribai Phule Pune University, Pune – 411007, India

subra.anan@gmail.com

**Govind Swarup** was a pioneer in the Indian science scene since the early 1960's. On an invitation to join the Tata Institute of Fundamental Research, Mumbai (TIFR) from Prof Homi Bhabha to four Indian radio astronomers from USA and elsewhere, he alone readily joined in 1963. Following his mentor's advice, he proceeded to build a strong radio astronomy group in TIFR. At the outset, Govind Swarup's main effort was to build a fully steerable radio telescope of large collecting area indigenously by adopting an innovative design and to use it ingeniously for carrying out a survey of weak radio sources at cosmological distances. This resulted in the construction of the large cylindrical radio telescope at Ooty (Fig. 2), popularly known as the Ooty Radio Telescope (ORT) in 1970, and its use for lunar occultation (LO) observations of radio sources at a high angular resolution of 1 arc second. The ORT was used for studies of pulsars and also for observations of compact extragalactic radio sources and the solar wind using the technique of interplanetary scintillations (IPS). Apart from making the Indian astronomers prominent globally, Govind Swarup guided them

and led them from the front in indigenously building world class instruments such as the Giant Metrewave Radio Telescope (GMRT) near Pune. The GMRT (Fig. 3) is used by astronomers from a few dozen countries of the world. From ORT in 1970 to GMRT in 2002, the uniqueness of the growth trajectory of radio astronomy was that it was accompanied by an impressive growth of indigenous technology of antennas and associated electronics for use in space communication, defence, meteorology and several other applications. Inevitably it was accompanied by a corresponding growth in our country's skilled human resource in these areas.

Govind was fortunate to grow up in a relatively wealthy home and to attend good schools. His college education was in the University of Allahabad where he finished his M.Sc. in physics in 1950. He was taught by illustrious and inspiring teachers such as K.S.Krishnan and B.N.Srivastava. After his M.Sc., he again joined K.S.Krishnan who by now was the founder director of the prestigious National Physical Laboratory (NPL), New Delhi. Krishnan asked young Govind to build electronics

at 10 GHz for studying electron spin resonance in the field of quantum magnetism. It was a tall order for a fresh graduate from college. But Govind finished the project successfully in about 18 months by using components from obsolete equipments of World War II surplus which had been procured by NPL at a very low cost [1]. Krishnan had a broad range of interests spanning several branches of science apart from quantum magnetism and was used to keeping himself well informed about the advances in these fields. In 1952 he attended the General Assembly of the International Radio Scientific Union (URSI) in Sydney. He became aware of the impressive progress taking place in radio astronomy. Sensing the great potential of radio astronomy in advancing the frontiers of knowledge about the large variety of objects in the universe, Krishnan planned to start a small group of academics in NPL to work on radio astronomy.

Pioneers in radio astronomy had learnt that the celestial radio sources 'visible' to them were different, unlike stars and galaxies observed by optical telescopes. The stars could not be detected by their small radio telescopes. The exception was the Sun. It was found to be emitting copiously and steadily, but occasionally in bursts of short durations of seconds to hours. The source regions of the radio bursts were suspected to be associated with the optically visible sunspots and solar flares from very small regions on the Sun. It was also realized that stars are at much farther distance and could not have been detected even if their emission is higher than that of the Sun due to their distance. For such detections, radio telescopes had to be much bigger so as to provide a finer angular resolution and sensitivity. A fundamental law of the physics of diffraction stipulates that the field of view or the resolving power  $\theta$  of a telescope is given by  $\theta \approx \lambda / d$  radians, where  $\lambda$  is the wavelength of the signal and  $d$  is the size of the aperture of the telescope. This needs radio telescope antennas of several kilometers in

size to achieve the resolving power of optical telescopes with aperture sizes of a few centimeters. Designing and constructing single radio antennas of such a large size was not feasible. Paraboloidal reflector antennas of a few meter diameter could be economically mass produced in those days. These were popularly known as the 'dish antennas'. The Australian radio astronomers developed the technology of two element radio interferometers (analogous to optical interferometers) and multiple antenna arrays (such as Christiansen's Cross and the Mills cross) to achieve a fine resolving power along with improved sensitivity for this type of radio telescopes. It required combining the signals received from individual elements of the array in the proper phase precisely. (To understand the importance of phase in such technology, please refer to [2,3]). The emission of radio waves by most celestial objects occurs at all wavelengths as a continuous spectrum. There are a few exceptions such as the spectral line emission by atomic hydrogen at 21 cm wavelength. Also most sources emitted at a steady intensity over a wide frequency band without detectable variations from one day to another day. This property of celestial radio sources was utilized to improve the sensitivity of radio telescopes by increasing the bandwidth of the electronic receivers behind the radio telescope antennas. Further improvement in sensitivity is achieved in the case of steady sources by increasing the integration times of the receivers to several seconds or a minute.

Govind Swarup's interest in radio astronomy started as he listened to the lectures by Krishnan about the impressive work being done by the Australian group under the leadership of J.L.Pawsey in the Commonwealth Scientific and Industrial Research Organization (CSIRO), Sydney. Krishnan sent Govind, under a Colombo Plan fellowship in 1952 to Australia for two years to learn about the new field of radio astronomy. By 1950 the Australian radio astronomers had done

pioneering work in solar radio astronomy, and were busy with the development of specialized technologies of antennas, phased antenna arrays and improved electronic receivers to process the signal received from celestial radio sources. Govind joined experienced Australian researchers such as J.L. Pawsey, W.N. Christiansen, J.P. Wild, B.Y. Mills and J.G. Bolton.



Fig. 1. S Ananthakrishnan (left) with Prof Govind Swarup, March 2019 (Courtesy: Mrs Bina Swarup)

He gained invaluable experimental skills in Australia in setting up phased antenna arrays such as Christiansen's Cross and the Mills Cross. Such array radio telescopes were an economical way of achieving high angular resolution at radio wavelengths of tens of centimeters to a few meters. In addition to instrument building skills, Govind gained firsthand knowledge about the characteristics of radio emissions from the Sun. On returning to NPL, India, Govind Swarup with support from Prof. K S Krishnan attempted to set up a small radio telescope for studies on the Sun. As these efforts over a period of two years did not

yield any tangible result, he moved to Harvard University's radio observatory at Fort Davis in USA in 1956 and carried out radio observations of the Sun. The features of the Sun's radio emission in its quiescent state were studied. Govind developed a gyro-radiation model to explain the radio emission. Apart from this study of the Quiet Sun, he discovered a new type of solar radio burst called the U burst while at the Harvard observatory.

His next move was to Stanford to pursue work for his Ph.D. under Prof. Ron Bracewell (the author of the well-known book on Fourier Transforms and their applications). A major part of his doctoral work was the construction of the Stanford Solar Spectroheliograph operating at  $\lambda = 10.7$  cm. This work involved setting up two linear arrays of 16 antennas each; over base line lengths of 114m, the two baselines being mutually perpendicular. The individual antennas of the arrays were 3m diameter paraboloidal dishes which were on polar mounts and connected by a common drive shaft for steering them together in order to track any celestial source. The signals from individual antennas were carried to a central receiver after subjecting them to a complex network of variable phase delays and switching circuits. The net result was equivalent to rapidly scanning the Sun's disc simultaneously with several radio telescopes, each with an angular resolution of 3 arc minutes. Hence one could observe active emission regions on the sun such as sunspots and solar flares, and also study their transient and dynamic characteristics. The Stanford Heliograph was used for several years for producing daily maps of the radio sun at 10 cm.

For satisfactory performance of the heliograph it is imperative that the signals from the elements of the two arrays be combined with the correct phase to a high level of precision (on the order  $3^\circ$  to  $5^\circ$ ) and also necessary that phase stability be maintained all through the observing period of

several hours. A sensitive phase measurement and monitoring system was developed by Swarup and Yang for the heliograph, which was used later by many arrays around the world.

With the high sensitivity of the Stanford spectroheliograph it was possible to observe a few other radio sources than the Sun. The sensitivity and resolving power were augmented by adding two dishes, and along with the arrays it formed the Stanford Compound interferometer. In 1963, using the above Interferometer at 3.3 GHz, Govind showed that Cygnus-A radio source has a weak middle component connecting the two lobes of the double radio galaxy. It had a steep spectrum; the authors suggested interpreting such spectral features of the 'bridge' to gain better insight regarding the age and magnetic-field strength of radio galaxies. Such bridges were used to understand the structure and evolution of double radio galaxies using better resolution instruments later.

**TIFR:**

Govind came on to the Indian scene at a unique time. India was emerging from its backwardness in science over the previous several decades of colonial rule. Our indigenous ability to set up technologically complex instruments by small scientific groups in the universities was in an elementary state. The students from colleges mostly specialised in working on theoretical projects. The Indian atomic energy program was in its early days, and the space program was nascent. However rapid progress was taking place in both of these programs which were directly under the Prime Minister's Office. Homi Bhabha who founded the TIFR in 1945 was also the Chairman of the Atomic Energy Establishment Trombay (AEET). (The AEET was renamed Bhabha Atomic Research Centre (BARC) later). Homi Bhabha was aware of the need to develop indigenous scientific and engineering manpower for success in the atomic energy program and had established the AEET

Training School. This training school took in fresh graduates and post graduates in engineering and physical sciences from Indian universities and colleges, after interviews to identify the candidates with the right aptitude and capability to undertake research. They were given a yearlong training and then absorbed in the various R and D departments of AEET. In the late nineteen fifties and early sixties TIFR had started a few research projects in high energy cosmic ray studies which involved the development of new instruments and new technologies for the observation and measurement of several components of cosmic rays. The reference here is to the development of high-altitude balloons, nuclear emulsions, cloud chambers and other detectors. A sizeable number of young graduates had joined these projects after passing through the AEET Training School.

Govind joined TIFR on April 2, 1963. Those were the heydays of Dr Bhabha. As recounted by Govind, he was sitting in the TIFR Library looking over the beautiful lawns leading to the Arabian sea and browsing through papers, when he chanced upon a paper by Cyril Hazard who reported "observations of a lunar occultation (LO) of the radio source 3C273 made with the 64-m Parkes Radio Telescope". The LO technique relies on using the Moon as a tool to discover weak and distant radio sources. The apparent movement of the Moon as observed from the Earth against the sky background is slower compared to that of a star or radio source. Hence a celestial star or radio source can get eclipsed by the Moon. This phenomenon is referred to as the lunar occultation of celestial radio sources. Therefore, by tracking the Moon using a radio telescope, one gets a weak signal combined with noise from the sky background, since the Moon does not emit much radio radiation. When a radio source overtakes the Moon, being in the same path, the signal suddenly reduces due to the 'immersion' of the radio source behind the Moon. As we all know, a relative decrease of the signal is easier to recognise

compared to the signal itself. Since the Moon has no atmosphere, its limb edge is sharp and that creates a knife-edge diffraction pattern of intensity when a plane wavefront of radio waves from a radio source of compact angular size falls on the Moon as the source gets occulted by the Moon's edge. This pattern of intensity is incident on the radio telescope based on the earth. If the angular size of the radio source were a second of arc or less, the diffraction pattern would show fringes before the intensity decreases while the source gets eclipsed by the moon as well as when it 'emerges' from behind the Moon. For a larger source size, the diffraction fringes wash out and the intensity of the radio source would decrease or increase smoothly without showing any fringe structure. Hence LO observations enable measurements of the angular sizes of sources as small as a second of arc without the need for the radio telescope antenna to have an intrinsic resolving power (as shown earlier to be  $\theta = \lambda/d$ ) of  $\sim 1$  arc second. This is the prime advantage of the technique of lunar occultation of radio sources. Hence, all that one needs is a large collecting area for the antenna to provide a high gain and the ability to track the source. This is the principle of the LO method. Govind, who knew about the LO method apparently got the idea that if he could build a large low cost steerable parabolic cylindrical telescope and put it on a North-South slope whose axis is made parallel to the axis of the Earth, then he could track the Moon from its rise to its set. It was a brilliant idea and when he explained the idea to Prof. M G K Menon and then to Prof. Bhabha, the latter, after questioning him for nearly 2 hours, told him to go ahead and start the project! As is well known, Bhabha was a visionary and wasted little time on paper work, project reports, etc. He told Govind to start collecting a team of bright young graduates and get to work. Thus was born the idea of building the Ooty Radio Telescope (Fig 2), an excellent working instrument built indigenously at low cost, which was finally commissioned in February 1970 and

works till date at a single frequency of 327 MHz ( $\lambda = 92$  cm). The key to this indigenously built telescope was a highly energetic young team that he collected and guided during the first 5 years. It included his erstwhile colleagues from NPL, N V G Sarma and M N Joshi and a bunch of youngsters, most of them freshly minted from the BARC training school. A few others joined as 'JRFs' and were called 'Visiting Members'! Under the guidance of Govind and along with Sarma and Mohan Joshi, this young team learnt a lot of new technology (detailed in a recent 'Resonance' article (March 2021)) and managed to build a major chunk of electronic and electrical sub-systems within the TIFR laboratory in Mumbai. Even now, it is a wonder to those remaining team members, as to how this small group, whose ages ranged between 23 and 30 and a few above that, could manage to build such a massive instrument within 5 years completely indigenously. They were of course, aided by consulting engineers, industry, and technical staff. However, as explained earlier, everyone involved was new to building such a fine instrument, which required an excellent understanding of both basic physics and technology [4].

Observations using the Ooty Radio Telescope (ORT) (Fig. 2) were the first to discover hundreds of new radio sources at the far distant universe by comparing their position with the optical catalogue and identifying them. The radio source data helped Govind and (late) Vijay Kapahi report that angular sizes were correlated with their flux density as  $\theta \propto S^{1/2}$  [5] and that "the angular size data provide independent evidence of evolution in source properties with epoch and that it does not support a steady-state model" [6]. This was an independent supporting evidence for the Big Bang cosmology and earned the authors and the Ooty telescope a global name. Many more discoveries were made using the LO observations, which are too many to mention. The telescope was also used for the discovery of a few Pulsars. Before

significant progress could be made, an accident due to a mechanical failure on the telescope caused a significant delay of nearly two years. Undaunted, under the energetic guidance of Govind Swarup, the team went back to work and refurbished the instrument to make it far more robust and it has stood the test of time for over 5 decades. However, a lot of momentum was lost in making new Pulsar discoveries because the field had moved at a much higher pace. Nevertheless, Ooty has produced some excellent work on Pulsars in the 1970's and later. Similarly, the instrument was used for studying very compact extragalactic radio sources using the intervening solar wind, which is nothing but the expansion of the solar corona – this is called the Interplanetary medium. It was shown by Prof. Anthony Hewish that when radio waves travel from very far away and pass through the solar wind medium, they produce random diffraction on the ground, which can be seen by a radio telescope. The ORT proved to be a very suitable instrument for this purpose and many excellent papers based on the Interplanetary Scintillation (IPS) of radio sources have been produced by a number of research workers including one of the authors (SA). The telescope was also used for the discovery of cometary scintillation when a compact radio source passes very close to the nucleus and plasma density fluctuations are observed. ORT was also used in 1983 for the first successful transcontinental Very Long Baseline Interferometry (VLBI) at 327 MHz with several other telescopes in Europe. This technique is the same as the one used for imaging a 'blackhole' recently at mm wavelengths, using the Event Horizon Telescope.

Govind did not rest on his laurels with the success of ORT. Firstly, he made the team add a few small steerable cylindrical parabolas (100 m x 15 m) to the ORT mostly on its western side and completed the Ooty Synthesis Radio Telescope. This worked for a few years and helped everyone understand

how signals are to be correlated in an interferometric mode. In the meantime, he went ahead and made a plan to install a very large cylindrical parabola (2 km x 50 m) that provides a 100,000 m<sup>2</sup> of physical area on the equator; but this had to be in a different country, so he located sites in Kenya and Indonesia. However, the respective governments were not ready for such massive projects and he had to give up.



Fig. 2. Ooty Radio Telescope looking to the west. First light on February 18, 1970 (Courtesy: NCRA Archives)

Then he started working with the group members to make a frontline instrument within India itself which would have multi-frequency capability. In 1984, he hit on the idea of making a large number of cylindrical parabolas in a Y array pattern. However, international colleagues strongly advised him that these should be regularly steerable parabolic dishes that can use the existing software and hardware techniques to make rapid progress. Thus, was born the Giant Metrewave Radio Telescope (GMRT), which was built during 1987 – 2000. GMRT as it operates today is a very modern instrument with very sophisticated electronics. Searching for a proper site to locate the GMRT was tedious owing to the constraints of low limits on radio frequency interference (RFI)

and wind velocity, scanty rains and an approachable city nearby to house its staff and to get good human resources. A good compromise was reached in its present site close to Khodad village, near Narayangaon town, which is about 80 km from the city of Pune and 130 km from the bustling city of Mumbai, from which it is protected by a series of hills for reducing RFI. An area of about 30 km diameter was made a radio quiet zone by the state Government.

GMRT consists of 30 parabolic dish antennas of a novel concept nick-named SMART (Stretched Mesh Attached to Rope Truss) [7]. The dishes are made of 16 parabolic frames connected together by circular rim truss structures to provide structural stiffness and connected in the centre to a circular steel hub (Fig 3). Between the frames, instead of the standard backup structure, a series of rope trusses made from thin stainless steel (SS) wire ropes, are stretched and tightened using turn buckles to provide structural integrity. Above these an SS mesh is spread which consists of several plain facets which are placed to form the reflecting surface of the dish. This structure is made at the ground level around a concrete tower (Fig 3), lifted up manually using steel ropes and pulleys. This dish structure is then attached to the steerable yoke which is already installed on the top of the tower. Further details on the fabrication and erection of the dishes can be found in [7]. After some initial experience, it took only about 2 hours to raise the structure manually using pulleys and ropes and to rotate it using servo electrical motors, gear boxes, etc. That was how all the 30 GMRT antennas were built in a very economic manner. The dish is steered to different directions and tracks celestial objects using a servo system built at BARC initially and mass produced at the site later.

GMRT, unlike ORT, is a synthesis radio interferometer [7]. What this means is that signals from each telescope are taken to a central point

and correlated between each antenna and all the other antennas one by one.

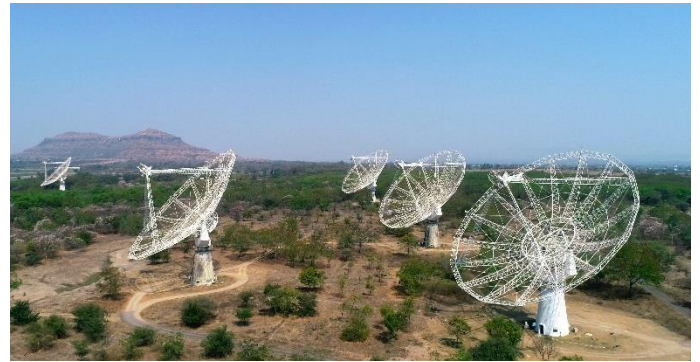


Fig. 3. Five of the 30 GMRT antenna array tracking. First light in 1999 (Courtesy: NCRA Archives)

Thus, if one has 3 telescopes in an interferometer system, then one can have 3 baselines, but for a 4-element system, there will be six baselines and for an N antenna system, there will be  $N(N-1)/2$  baselines. Thus, for a 30-antenna system, there will be 435 instantaneous baseline correlations, that is Fourier components. As the antennas track a radio source, there will be thousands of such correlations that provide high to low resolution information on the object being tracked, using which a synthesised image of the object can be formed.

Although GMRT array saw its first light in 1999, it took some more years to debug all the hardware and software gaps and it was only partially operational till 2001. In 2002, it was dedicated to the scientific world by the Chairman of the TIFR council, Shri. Ratan Tata. It became one among a few powerful synthesis radio telescopes in the world at frequencies below 1450 MHz. Since then, it has been fully operational. Many outstanding results have been produced in a wide area of astrophysical research such as in the areas of solar system physics, galactic objects like Pulsars, Supernovae, the centre of our Milkyway Galaxy and extragalactic objects. About 1000 scientific papers have been published till now. In the last several years, the GMRT hardware and software

systems have been upgraded to significantly improve its sensitivity and upgrade it again into a front ranking instrument in the world [8]. It is now a 'path finder' for the next generation array called the Square Kilometre Array (SKA) in Australia and South Africa in which the GMRT team is playing an important role.

Govind Swarup won many accolades and awards, among them being elected as a Fellow of the Royal Society and all the major science academies of India and far more. However, it was a pleasant news recently to learn of the IEEE milestone award for the GMRT observatory, only the third such award after the two given for the scientific works of Sir J C Bose and Sir C V Raman. It is an honour to all the tireless works by scientists, engineers and all the supporting staff over the last several decades under the able leadership of Prof. Govind Swarup. Had he been alive for another 3 months, he would have proudly savoured this moment.

## References

1. Srinivasan G, Current Science, **109**, 618–630, 2015
2. Nityananda R, Resonance, July, 645 - 657, 2017
3. Chengalur JN, Resonance, February, 165 – 183, 2018
4. Swarup G, Sarma N V G, Joshi M N, Kapahi V K, Bagri D S, Damle S H, Ananthakrishnan S, Balasubramanian V, Bhave SS and Sinha RP, Nature Phys. Science, **230**, 185, 1971.
5. Swarup G, Mon. Not. R. astr. Soc., **172**, 501, 1975.
6. Kapahi Vijay K, Mon. Not. R. astr. Soc., **172**, 513, 1975.
7. Swarup G, Ananthakrishnan S, Kapahi V K, Rao A P, Subrahmanya C R and Kulkarni V K, Current Science, **60**, 95, 1991.
8. Gupta Y, et al., Current Science, **113 (4)**, 707, 2017.